Nitrogenase-like Biosynthesis of (Bacterio)chlorophylls

Von der Fakultät für Lebenswissenschaften

der Technischen Universität Carolo-Wilhelmina zu Braunschweig

zur Erlangung des Grades

eines Doktors der Naturwissenschaften

(Dr. rer. nat.)

genehmigte

Dissertation

von Jan Jasper

aus Oldenburg (Oldb.)

1. Referent: Professor Dr. Dieter Jahn
2. Referentin: Professorin Dr. Gunhild Layer
eingereicht am: 24.06.2021
mündliche Prüfung (Disputation) am: 13.09.2021

Druckjahr 2021

Veröffentlichungen der Dissertation

Teilergebnisse aus dieser Arbeit wurden mit Genehmigung der Fakultät für Lebenswissenschaften, vertreten durch den Mentor der Arbeit in folgenden Beiträgen vorab veröffentlicht:

Publikationen

Jasper, **J.**, Ramos, J. V., Trncik, C., Jahn, D., Einsle, O., Layer, G. and Moser, J. (2020) "Chimeric Interaction of Nitrogenase-Like Reductases with the MoFe Protein of Nitrogenase", *ChemBioChem*, 21, pp. 1733 –1741.

Jasper, **J.**, Ramos, J. V., Trncik, C., Jahn, D., Einsle, O., Layer, G. and Moser, J. (2020) Front Cover: "Chimeric Interaction of Nitrogenase-Like Reductases with the MoFe Protein of Nitrogenase", *ChemBioChem*, 21, pp. 1664.

Moser, J., **Jasper**, **J.**, Ramos, J. V., Sowa, S. T. and Layer, G. (2019) "Expression, Purification, and Activity Analysis of Chlorophyllide Oxidoreductase and Ni^{2+}-Sirohydrochlorin *a*,*c*-Diamide Reductase", in Hu, Y. (ed.) *Metalloproteins: Methods and Protocols*. Humana Press.

Tagungsbeiträge

Jasper, **J.**, Jahn, D., Moser, J.: Nitrogenase-like Biosynthesis of (Bacterio)chlorophylls

- DFG Priority Program 1927 Iron-Sulfur for Life:
    - Kick-Off Meeting, Potsdam, 2016 (Talk)
    - Summer School, Leipzig, 2017 (Poster)
    - 2nd Progress Meeting, Potsdam, 2018 (Poster + Talk)
    - Summer School, Freiburg, 2018 (Poster)
    - Autumn School, Erkner, 2019 (Poster)
- VAAM Jahrestagung, Wolfsburg, 2018 (Poster)

Jasper, **J.**, Jahn, D., Moser, J.: Towards an alternative Nitrogenase Reductase, MOTEC Satellite Meeting "FeS for Life", Potsdam, 2019 (Poster)

Table of contents

Abbreviations

ALA	5-aminolevulinic acid
Amp^R	Ampicillin resistance
AMP-PNP	β,γ-imidoadenosine 5'-triphosphate
Bchl	Bacteriochlorophyll
Bchlide	3-vinyl bacteriochlorophyllide *a*
Bchlide *g*	Bacteriochlorophyllide *g*
BSA	Bovine serum albumin
Chl	Chlorophyll
Chlide	Chlorophyllide *a*
Cm^R	Chloramphenicol resistance
COR	Chlorophyllide *a* oxidoreductase
dH_2O	Deionized water
DPOR	Dark-operative protochlorophyllide oxidoreductase
DT	Sodium dithionite
DTT	1,4-Dithio-D,L-threitol
EPR	Electron paramagnetic resonance
GPC	Gel permeation chromatography
GST	Glutathione S-transferase
HEPES	4-(2-Hydroxyethyl)-1-piperazine ethanesulfonic acid
IPTG	Isopropyl-β-D-galactopyranoside
Kan^R	Kanamycin resistance
LB	Lysogeny broth
LPOR	Light-dependent protochlorophyllide *a* oxidoreductase
M_r	Relative molecular mass
mcs	Multiple cloning site
MST	Microscale thermophoresis
MV	Methyl viologen
$MV^{+\cdot}$	Methyl viologen cation radical
OD	Optical density
ori	Origin of replication
Pchlide	Protochlorophyllide *a*
PVDF	Polyvinylidene difluoride

rbs	Ribosome binding site
rpm	Rounds per minute
SAM	S-adenosyl-L-methionine
SDS-PAGE	Sodium dodecyl sulfate-polyacrylamide gel electrophoresis
SER	Surface entropy reduction
Tet^R	Tetracycline resistance
TRIS	Tris(hydroxymethyl)aminomethane
Tween 20	Polyoxyethylene (20) sorbitan monolaurate
UV-Vis	Ultraviolet/visible light spectrum
v/v	Volume per volume
w/v	Weight per volume

1. Introduction

1.1 Nitrogen - An essential element of life

Nitrogen is essential for the biosynthesis of key biomolecules of life like nucleic acids or proteins and it is the main life-limiting nutrient on earth. Nitrogen-fixing bacteria (and archaea) are able to convert abundant but unreactive atmospheric dinitrogen gas (N_2 inventory: $3.9 \cdot 10^{21}$ g) into bioavailable ammonium. Most organisms rely on the activity of these rare organisms to supply nitrogen in a more reactive, bioavailable form. In a complex process termed nitrogen cycle, nitrogen-fixing organisms and other groups of versatile microorganisms alter the oxidation state of nitrogen (in the range: -3 to +5) in six distinct processes: Nitrogen fixation, nitrification, denitrification, anammox, assimilation and ammonification. An overall of 14 nitrogen-converting redox reactions have been identified to date, four in the past decade. Thermodynamic models suggest that additional reactions are likely part of the nitrogen cycle (Kuypers *et al*., 2018).

The human impact on the nitrogen cycle has been increasing in recent years. Industrial nitrogen fixation (Haber-Bosch process), fossil fuel consumption and biofuel production have substantially increased the anthropogenic nitrogen flux. The yearly anthropogenic nitrogen fixation flux has been estimated to be higher than the terrestrial and marine biological nitrogen fixation flux, respectively. The resulting problems like nitrogen deposition, acidic deposition, ozone depletion, aquatic eutrophication and biodiversity loss are current research topics aiming to manage the balance of the global nitrogen cycle (Galloway *et al.*, 2008; Gruber and Galloway, 2008; Erisman *et al.*, 2015).

On the other hand, industrial nitrogen fixation *via* the Haber-Bosch process is essential for the production of fertilizers. It has been estimated that the food production of 50 % of the human population relies on the Haber-Bosch process (Erisman *et al.*, 2008) and that 80 % of the nitrogen in the proteins of an average human originates from the Haber-Bosch process (Howarth, 2008). However, this energy- and carbon-intensive process accounts for 1.4 % of the global CO_2 emission and 1 % of the global energy demand. Accordingly, more energy-efficient Haber-Bosch plants are investigated (Capdevila-Cortada, 2019). An exciting alternative is the optimization or manipulation of the biological nitrogen fixation performed by the metalloenzyme nitrogenase (Burén and Rubio, 2018).

1.2 Nitrogenase

Biological nitrogen fixation performed by diazotroph organisms is one of the most complex biochemical reactions. These organisms make use of the metalloenzyme nitrogenase. The most studied nitrogenase is the molybdenum (Mo)-nitrogenase from *Azotobacter vinelandii* (Rutledge and Tezcan, 2020). Since its discovery in 1903 (Vineland, New Jersey), *A. vinelandii* has been a diazotrophic model organism in nitrogenase research for over 100 years (Noar and Bruno-Bárcena, 2018). In addition to the Mo-nitrogenase, alternative nitrogenase enzymes with different metals in the nitrogen reduction site of the catalytic subcomplex are known. These enzymes make use of vanadium (V-nitrogenase) or iron (Fe-nitrogenase) (Eady, 1996). *A. vinelandii* possesses all three nitrogenase variants (Mo-, V- and the Fe-nitrogenase). Therefore, *A. vinelandii* is able to regulate nitrogen fixation based on the available metals (Noar and Bruno-Bárcena, 2018). The Mo-nitrogenase consists of two subcomplexes that form a transient octameric protein complex (Figure 1).

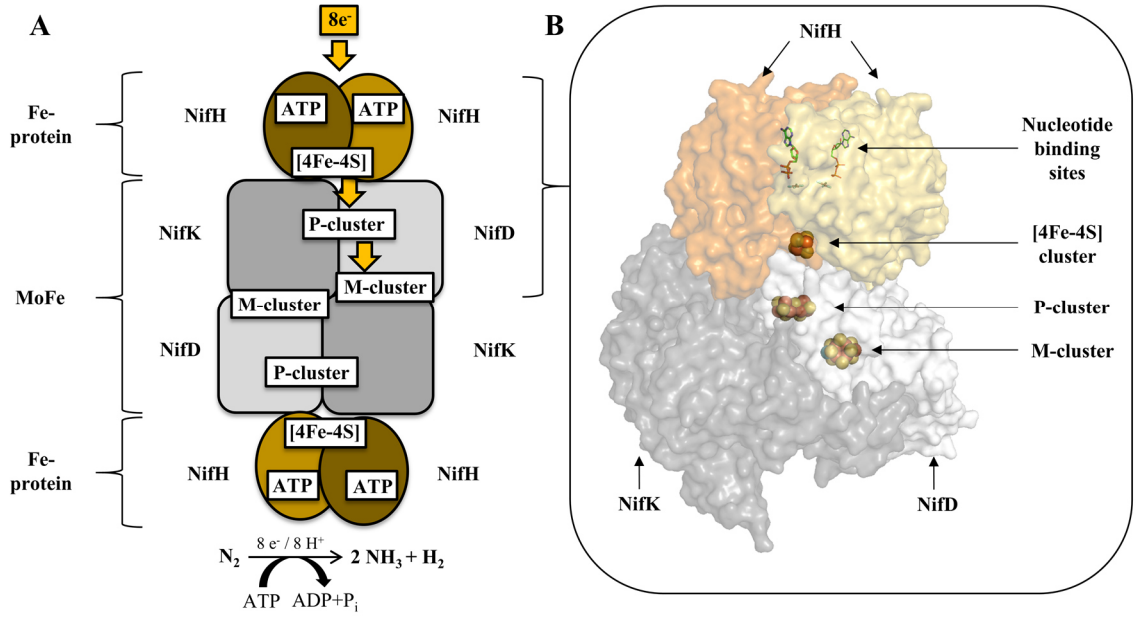

Figure 1: Schematic model of the Mo-nitrogenase from *A. vinelandii*.
Nitrogenase forms a transient octameric protein complex consisting of two $(NifH)_2$ homodimers (Fe-protein) and one $(NifDK)_2$ heterotetramer (MoFe). The inter-subunit [4Fe-4S] cluster of subcomplex $(NifH)_2$, the unique metal cofactors of MoFe (M-cluster and P-cluster) and nucleotide-binding sites of $(NifH)_2$ are indicated. Electrons are transferred in an ATP-dependent manner onto the M-cluster of MoFe (yellow arrows). **A**: Schematic representation of the transient nitrogenase complex. **B**: Protein surface model of nitrogenase. Only one half-octamer is illustrated. The homocitrate moiety of the M-cluster is not shown. The model was generated with PyMOL (Schrödinger LCC, 2021) using the ADP-tetrafluoroaluminate stabilized structure of nitrogenase from *A. vinelandii* (PDB ID: 1M34).

The homodimeric ATP-dependent reductase subcomplex $(NifH)_2$ (also termed Fe-protein) contains a nucleotide-binding site in each NifH subunit and an inter-subunit [4Fe-4S] cluster. The [4Fe-4S] cluster is ligated by two cysteines from each NifH subunit and is positioned close to the protein surface. The charge of the [4Fe-4S] cluster changes between +2 and +1 during the catalytic cycle of nitrogenase. Moreover, an alternative all ferrous state is under debate. However, the physiological and catalytic relevance of this state remains elusive. $(NifH)_2$ is reduced by a flavodoxin or ferredoxin under *in vivo* conditions. Under *in vitro* conditions, the +1 state is commonly generated using sodium dithionite (DT) as a reductant. $(NifH)_2$ couples ATP hydrolysis with conformational changes to facilitate inter-subcomplex electron transfer to the catalytic subcomplex of nitrogenase. Additionally, $(NifH)_2$ is essential for the maturation of the unique cofactors located in the catalytic subcomplex of nitrogenase (Jasniewski *et al.*, 2018).

The catalytic subcomplex of the Mo-nitrogenase is a $(NifDK)_2$ heterotetramer commonly termed molybdenum-iron (MoFe) protein, which houses the complex metallocofactors [8Fe-7S] (P-cluster) and [Mo-7Fe-9S-C-homocitrate] (M-cluster). Subunits NifD and NifK show significant sequence homology, indicating a duplication of a common ancestor gene. Each NifDK dimer of MoFe contains a M- and P-cluster pair. The P-cluster is bridged between the NifD and NifK subunits and ligated by six cysteines and one serine. The M-cluster of MoFe is located in the NifD subunit coordinated by a histidine and cysteine residue. It contains a central carbide (C^{4-}) and an apical Mo coordinated by a homocitrate. The M-cluster functions as N_2 reduction site, whereas the P-cluster acts as an electron-relay between the M-cluster and the reductase subcomplex of nitrogenase (Einsle and Rees, 2020; Rutledge and Tezcan, 2020).

The presence of oxygen can irreversibly inactivate nitrogenase. Therefore, *A. vinelandii* makes use of several strategies to protect the oxygen-sensitive cofactors of nitrogenase. Enzymes like catalase, superoxide dismutase or iron-binding catecholate siderophores are produced under oxidative stress conditions in order to reduce the amount of reactive oxygen species. Furthermore, *A. vinelandii* is able to consume oxygen by an uncoupled respiratory electron transport chain (respiratory protection) and forms alginate capsules depending on the O_2 tension. Another strategy to protect nitrogenase from oxygen is the reversible binding of protein FeSII (Shethna protein) to nitrogenase (Scherings *et al.*, 1983; Dingler and Oelze, 1987; Cornish and Page, 1998; Sabra *et al.*, 2000; Noar and

Bruno-Bárcena, 2018). Phylogenetic analyses suggested that nitrogenase evolved in obligate anaerobic organisms. Thus, nitrogen fixation in the presence of oxygen and the required oxygen protection mechanisms are more recent evolutionary innovations (Boyd and Peters, 2013).

1.3 Catalytic cycle of nitrogenase

The reduction of dinitrogen requires the activation of one of the most stable molecules by the ATP-driven sequential transfer of electrons through complex metal cofactors. In contrast to the industrial alternative, this process is achieved at ambient temperature and pressure. The ATPase $(NifH)_2$ is the reductase subcomplex of nitrogenase and forms a transient complex with MoFe. The association between these subcomplexes initiates a series of events that consecutively accumulate electrons on the MoFe protein.

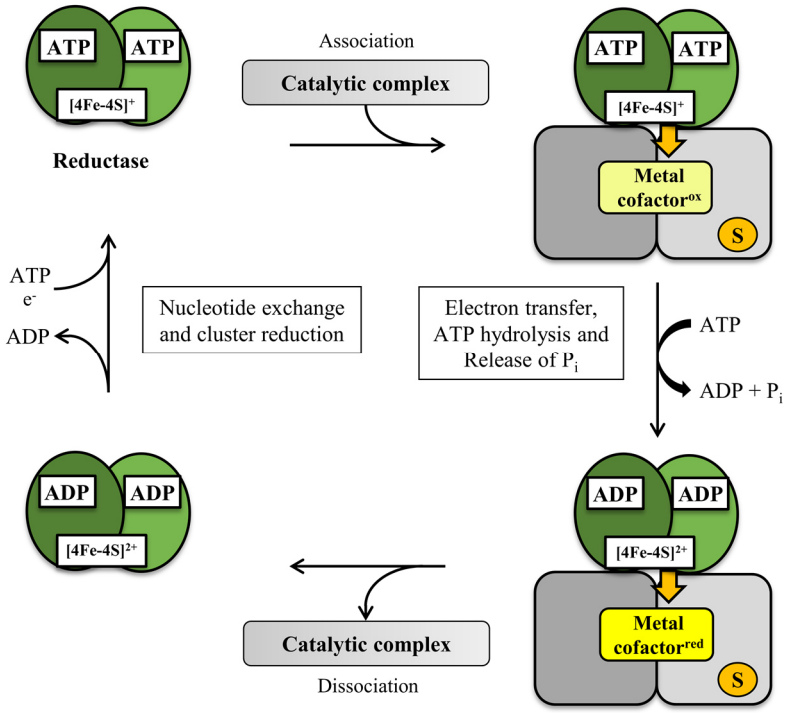

Figure 2: Simplified representation of the catalytic cycle of nitrogenase.
Dynamic interaction and electron transfer between the reductase subcomplex (green) and catalytic subcomplex (grey) are indicated. Electron transfer is facilitated by the association of the ATP-bound reductase with the catalytic subcomplex. Thereby, the oxidized metal cofactor of the catalytic subcomplex is reduced (yellow and bright yellow, respectively) by the $[4Fe\text{-}4S]^{+}$ cluster of the reductase. After electron transfer, ATP hydrolysis and release of P_i, the dissociation of the ADP-bound reductase and catalytic subcomplex is triggered. Nucleotide exchange and reduction of the $[4Fe\text{-}4S]^{2+}$ cluster of the reductase are required for subsequent cycles. Eight consecutive single-electron reductions are required to reduce the substrate (S).

Eight electrons are required for the reduction of one dinitrogen molecule yielding two molecules of ammonia and one molecule of hydrogen. According to current models, two ATP molecules are hydrolyzed to transfer one electron at a time from the reductase subcomplex to the MoFe protein (Seefeldt, Peters, *et al.*, 2018). The dynamic association and dissociation of the nitrogenase subcomplexes is controlled in an ATP-dependent manner and is indicated in the simplified depiction of Figure 2. The ATP-bound reductase subcomplex associates with the catalytic subcomplex, thereby facilitating electron transfer to the metal cofactors of the catalytic subcomplex. Following ATP hydrolysis, electron transfer and release of P_i, the dissociation of the transient complex is triggered. Nucleotide exchange and reduction of the [4Fe-4S] cluster of the reductase are required for subsequent cycles. The exact nature of the conformational control of electron transfer and the order of events (association, dissociation, ATP hydrolysis, P_i release, inter-subcomplex and intra-subcomplex electron transfer in MoFe) have been investigated for over 40 years. However, many ambiguities remain (Rutledge and Tezcan, 2020).

1.4 Nitrogenase maturation

Maturation of the Mo-nitrogenase is a complex process that requires many accessory proteins. Not all proteins and interactions have been assessed to date. Nitrogen fixation genes comprise three structural genes (*nifH, nifD, nifK*) and 49 additional genes involved in cofactor biosynthesis, maturation of MoFe and $(NifH)_2$, O_2 protection, electron transport and regulatory functions. To date, the role of some genes (e.g. *nifT, nafA, nafC*) is still unknown (Burén *et al.*, 2020).

Simplified, the process of nitrogenase maturation is divided into several steps: The maturation of $(NifH)_2$ is facilitated by NifM and the formation of the inter-subunit [4Fe-4S] cluster is performed by NifU and NifS. The maturation of MoFe and *in situ* P-cluster formation from a pair of [4Fe-4S] clusters is performed by NifH, NifZ, NifU, NifS, NifM, NifW and NafH. The *ex situ* M-cluster biosynthesis on the scaffold protein complex NifEN (MoFe homolog) connects multiple maturation pathways (homocitrate biosynthesis, [Fe-S] cluster biosynthesis and Mo pathway) in order to assemble the M-cluster on NifEN. Finally, the M-cluster is inserted into the P-cluster containing MoFe protein (Burén *et al.*, 2020).

The MoFe homolog NifEN is a central platform in the maturation of nitrogenase and can be considered as a simpler version of MoFe. NifEN houses a [4Fe-4S] cluster in the P-cluster position of MoFe. The M-cluster position of MoFe is occupied by a Mo- and homocitrate-free form of the M-cluster (termed L-cluster) (Ribbe, 2015). NifEN is able to form a nitrogenase-like complex with NifH. This complex is not able to reduce nitrogen; however, a reduction of acetylene and azide has been demonstrated (Hu *et al.*, 2009).

The minimal requirements for the maturation of nitrogenase have been demonstrated under *in vitro* conditions. Purified NifH, NifB, NifEN and MoFe (with P-cluster) supplemented with Fe^{2+}, S^{2-}, MoO_4^{2-}, R-homocitrate, S-adenosyl methionine (SAM) and Mg-ATP resulted in a functional nitrogenase under reducing conditions (Curatti *et al.*, 2007). In particular, NifH has a vital role in nitrogenase maturation and activity. It functions as the reductase component for the MoFe protein during nitrogenase catalysis and facilitates the P-cluster formation on MoFe. It is also a Mo and homocitrate insertase during M-cluster formation on NifEN (Jasniewski *et al.*, 2018).

Overall, the maturation of the nitrogenase MoFe protein is orchestrated by a complex network of protein interactions. *A. vinelandii* mutant strains and nitrogenase subcomplex variants have contributed to the investigation of nitrogenase and its maturation over the past decades (Burén *et al.*, 2020; Einsle and Rees, 2020; Rutledge and Tezcan, 2020). Accordingly, further nitrogenase research might benefit from interaction experiments with nitrogenase-like enzymes or engineered protein variants. Engineered organisms with the ability to fix nitrogen are an attractive future perspective of nitrogenase research. Therefore, a detailed understanding of nitrogenase maturation is required. Furthermore, the oxygen sensitivity of nitrogenase has to be considered. The nitrogenase reductase $(NifH)_2$ is a central protein for nitrogenase activity and maturation. The identification or, alternatively, the design of an alternative nitrogenase reductase based on highly homologous nitrogenase-like reductases might provide a useful tool for further nitrogenase research.

1.5 Nitrogenase-like enzymes

Enzymes with homology to nitrogenase are found in the biosynthesis pathways of tetrapyrrole-based compounds (Figure 3). For the biosynthesis of chlorophylls (Chl), the nitrogenase-like enzyme dark-operative protochlorophyllide oxidoreductase (DPOR)

performs the two-electron reduction of the C17-C18 double bond in protochlorophyllide *a* (Pchlide) to chlorophyllide *a* (Chlide) (Figure 3 A). The formation of bacteriochlorophylls (Bchl) requires the subsequent two-electron reduction of the C7-C8 double bond in Chlide to 3-vinyl bacteriochlorophyllide *a* (Bchlide) performed by the enzyme chlorophyllide *a* oxidoreductase (COR) (Figure 3 B).

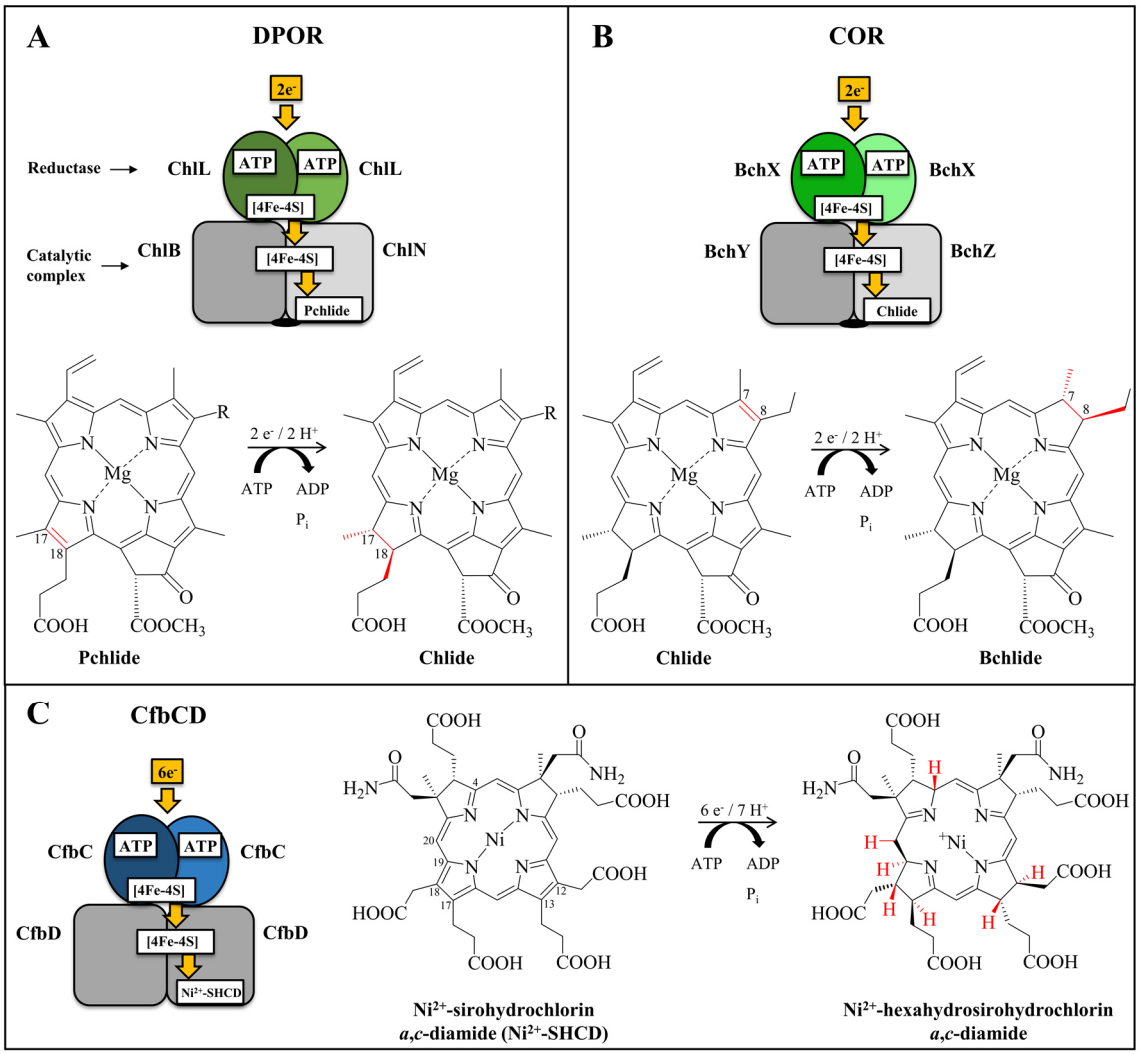

Figure 3: Schematic representation of transient complexes of nitrogenase-like enzymes dark operative protochlorophyllide oxidoreductase (DPOR), chlorophyllide *a* oxidoreductase (COR) and Ni^{2+}-sirohydrochlorin *a*,*c*-diamide reductase (CfbCD).
DPOR (**A**) and COR (**B**) share the octameric protein architecture of nitrogenase. Only one half-octamer is shown and the appropriate twofold symmetry of the overall complex is indicated by a spindle. In contrast, CfbCD (**C**) forms a tetrameric $(CfbCD)_2$ complex. The reductase subcomplexes $(ChlL)_2$, $(BchX)_2$ and $(CfbC)_2$ are highlighted green, bright-green and blue, respectively. Catalytic subcomplexes are depicted grey. Electron transfer through redox-active metallocenters is schematically indicated by yellow arrows. DPOR performs the two-electron reduction of protochlorophyllide *a* (Pchlide) to chlorophyllide *a* (Chlide). R is either ethyl or vinyl. COR catalyzes the two-electron reduction of Chlide to 3-vinyl bacteriochlorophyllide *a* (Bchlide). Reduced bonds are highlighted red. CfbCD drives the six-electron reduction of Ni^{2+}-sirohydrochlorin *a*,*c*-diamide (Ni^{2+}-SHCD) to Ni^{2+}-hexahydrosirohydrochlorin *a*,*c*-diamide. Introduced protons are highlighted red.

A third nitrogenase-like enzyme, termed Ni^{2+}-sirohydrochlorin *a*,*c*-diamide reductase (CfbCD), is involved in the biosynthesis of coenzyme F_{430} (Figure 3 C). This nickel-containing cofactor is used by the enzyme methyl-coenzyme M reductase in methanogenesis. A common feature of the group of nitrogenase-like enzymes is the sophisticated regiospecific and stereospecific reduction of tetrapyrrole compounds. In analogy to nitrogenase, electron transfer *via* metal cofactors is coupled to ATP hydrolysis. However, nitrogenase-like enzymes make use of [4Fe-4S] clusters instead of the unique cofactors of MoFe (Moser and Bröcker, 2011; Moore *et al.*, 2017; Moser *et al.*, 2019). Chimeric enzyme systems composed of COR and DPOR subcomplexes indicated a related docking face and electron transfer in COR and DPOR enzymes from various organisms (Wätzlich *et al.*, 2009).

1.5.1 Dark-operative protochlorophyllide oxidoreductase

X-ray crystal structures of DPOR revealed substantial similarities with the transient octameric structure of nitrogenase. As indicated in Figure 3 A, DPOR comprises the subunits ChlL, ChlN and ChlB that form the homodimeric reductase subcomplex $(ChlL)_2$ and the heterotetrameric catalytic subcomplex $(ChlNB)_2$ (Muraki *et al.*, 2010; Moser *et al.*, 2013). Alternatively, the DPOR subunits of Bchl-synthesizing organisms are termed BchL, BchN and BchB (Suzuki *et al.*, 1997).

The ChlL subunit of DPOR shows a sequence identity of 31-38 % to the NifH subunit of nitrogenase (Wätzlich *et al.*, 2009). DPOR reductase $(ChlL)_2$ has been identified as a dynamic switch protein that links ATP hydrolysis to conformational changes, transient inter-subcomplex interaction and electron transfer to the catalytic subcomplex $(ChlNB)_2$. $(ChlL)_2$ and $(NifH)_2$ share key features like the phosphate-binding P-loop, inter-subcomplex docking regions and switch regions I and II that mediate nucleotide-induced conformational changes (Bröcker *et al.*, 2010; Moser *et al.*, 2013). $(ChlL)_2$ harbors a [4Fe-4S] cluster between the two ChlL subunits. This cluster is symmetrically ligated by two cysteines from each ChlL subunit. As observed for the nitrogenase $(NifH)_2$ reductase, significant structural changes occur in the reductase subcomplex of DPOR during catalysis, including a movement of the surface exposed [4Fe-4S] cluster towards the catalytic subcomplex (Bröcker *et al.*, 2008b; Moser *et al.*, 2013; Einsle and Rees, 2020). Initial steps of the catalytic cycle of DPOR were proposed to resemble nitrogenase catalysis (Figure 2) (Bröcker *et al.*, 2010).

Subunits ChlN and ChlB show a sequence identity of 12-20 % and 14-18 % to the homologous nitrogenase subunits NifD and NifK, respectively (Wätzlich *et al.*, 2009). Each ChlNB heterodimer of the heterotetrameric catalytic subcomplex $(ChlNB)_2$ of DPOR contains a [4Fe-4S] cluster located at the ChlNB interface. This cluster is asymmetrically ligated by three cysteines (from ChlN) and one aspartate (from ChlB). The MoFe protein of nitrogenase harbors the P-cluster in an analogous position and substrate binding in $(ChlNB)_2$ occurs close to the binding site of the M-cluster in MoFe. Moreover, DPOR reduces simple nitrogen-containing artificial substrates like azide and hydrazine, that are also converted by nitrogenase. The reported activities in the presence of artificial substrates are lower in the DPOR system when compared to the holo nitrogenase. However, DPOR and the M-cluster-deficient apo nitrogenase revealed nearly similar activities. These similarities in structure and function clearly indicate an evolutionary link between DPOR and nitrogenase (Moser *et al.*, 2013; Einsle and Rees, 2020).

1.5.2 Chlorophyllide *a* oxidoreductase

To date, no X-ray crystal structure of the nitrogenase-like enzyme COR is available. However, bioinformatic, spectroscopic and biochemical experiments indicate clear similarities to other nitrogenase-like enzymes: As shown in Figure 3 B, COR is composed of subunits BchX, BchY and BchZ that show a sequence identity of 29-36, 13-15 and 11-16 % to the homologous nitrogenase subunits NifH, NifD and NifK, respectively (Wätzlich *et al.*, 2009). Sequence analyses of BchX and NifH indicated that BchX is a dynamic switch protein with a [4Fe-4S] cluster (Burke *et al*., 1993; Wätzlich *et al.*, 2009). Gel filtration experiments revealed a homodimeric $(BchX)_2$ reductase subcomplex and a heterotetrameric $(BchYZ)_2$ catalytic subcomplex for the COR enzyme from *Roseobacter denitrificans*. Furthermore, electron paramagnetic resonance (EPR) spectroscopy revealed a [4Fe-4S] cluster in both subcomplexes of COR from *R. denitrificans*. These results were further supported by mutagenesis experiments that confirmed four cysteine ligands for the [4Fe-4S] cluster in $(BchYZ)_2$ (Kiesel *et al.*, 2015).

The catalyzed reactions of COR are shown in Figure 4. COR catalyzes the C7-C8 double bond reduction in Chlide, resulting in the formation of Bchlide (Figure 4, green). The subsequent activities of BchF and BchC convert the C3 vinyl group of Bchlide to an acetyl group, resulting in the formation of bacteriochlorophyllide *a*.

However, it has been demonstrated that COR enzymes from *Heliobacterium modesticaldum*, *Blastochloris viridis*, *Rhodobacter capsulatus*, *Rhodobacter sphaeroides*, *Rhodopseudomonas palustris*, *Chlorobaculum tepidum* and *Roseiflexus castenholzii* also possess alternative activities. In addition to conventional 8-vinyl reductases (BciA and BciB), COR can function as a third type of 8-vinyl reductase in these organisms (Tsukatani *et al.*, 2013a; Tsukatani *et al.*, 2013b; Harada *et al.*, 2014).

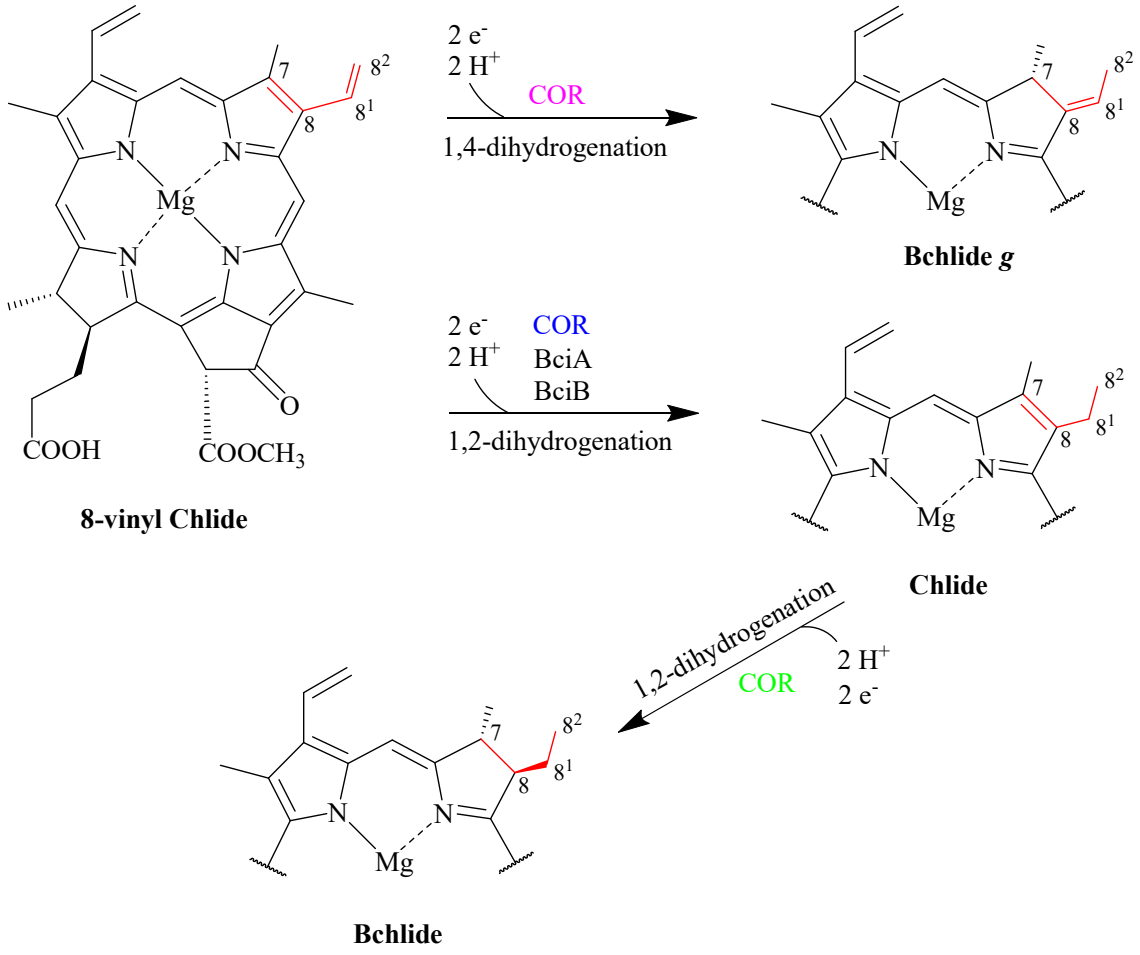

Figure 4: Enzymatic activities of COR.
The reduction of the C7-C8 double bond in chlorophyllide *a* (Chlide) to 3-vinyl bacteriochlorophyllide *a* (Bchlide) is highlighted green. Alternatively, COR functions as 8-vinyl reductase (purple and blue). COR enzymes from *H. modesticaldum* and *B. viridis* (purple) perform a 1,4-dihydrogenation of 8-vinyl Chlide resulting in the formation of bacteriochlorophyllide *g* (Bchlide *g*). 8-vinyl reductases BciA, BciB and COR enzymes from *R. capsulatus*, *R. sphaeroides*, *R. palustris*, *C. tepidum* and *R. castenholzii* drive the 1,2-dihydrogenation of 8-vinyl Chlide to Chlide (blue).

The alternative 8-vinyl reductase activity of COR from *H. modesticaldum* and *B. viridis* allows for the conversion of the 8-vinyl group in Chlide into the 8-ethylidene group, which is found in bacteriochlorophyllide *g* (Bchlide *g*) (Figure 4*,* purple). This reaction can be described as a 1,4-dihydrogenation. The second alternative activity is the 1,2-dihydrogenation of 8-vinyl Chlide that results in the formation of the ethyl group in Chlide (Figure 4, blue). This alternative reaction resembles the typical C7-C8 double bond reduction performed by COR (Figure 4, green) and was demonstrated for *R. capsulatus*, *R. sphaeroides*, *R. palustris*, *C. tepidum* and *R. castenholzii* (Tsukatani *et al.*, 2013a; Tsukatani *et al.*, 2013b; Harada *et al.*, 2014). Interestingly, under in *vitro* conditions the 8-vinyl reductase activity of COR from *R. capsulatus* is preferred when compared to the reduction of the C7-C8 double bond. It was concluded that COR was evolutionary the first 8-vinyl reductase and that other 8-vinyl reductases evolved later (Yamamoto *et al.*, 2020). In organisms lacking the 8-vinyl reductases BciA or BciB (e.g. *R. castenholzii*), the 8-vinyl reductase activity of COR is required to synthesize Bchl *a* (Ito *et al.*, 2008). Overall, the alternative activities of COR are in agreement with related nitrogenase and DPOR enzymes that also show the ability to reduce varying substrates.

1.5.3 Ni^{2+}-sirohydrochlorin *a*,*c*-diamide reductase

Methanogenesis performed by methanogenic archaea (e.g. *Methanosarcina barkeri*) and anaerobic oxidation of methane requires the activity of the coenzyme F_{430} containing methyl-coenzyme M reductase (Wongnate and Ragsdale, 2015; Scott and Cheviron, 2016). The modified tetrapyrrole coenzyme F_{430} (nickel porphinoid) is synthesized from sirohydrochlorin by a series of enzymes termed CfbA-E. CfbCD is a nitrogenase-like two-component system and catalyzes the six electron reduction of Ni^{2+}-sirohydrochlorin *a*,*c*-diamide to Ni^{2+}-hexahydrosirohydrochlorin *a*,*c*-diamide. This reaction involves the addition of seven protons (Figure 3 C).

Unlike nitrogenase or other nitrogenase-like enzymes, CfbCD forms a simpler two-component system containing the homodimeric reductase subcomplex $(CbfC)_2$ and the homodimeric catalytic subcomplex $(CfbD)_2$. Subunits CfbC and CfbD are homologs of NifH and NifD, respectively. EPR spectroscopy revealed a [4Fe-4S] cluster in both subcomplexes of CfbCD.

Moreover, an ATP-dependent electron transfer was proposed for CfbCD. The simpler protein architecture of CfbCD suggests that the ATP coupled reduction of double bonds follows a simpler mechanism when compared to other nitrogenase-like enzymes. The *in vivo* electron source for CfbCD has not been identified yet (Scott and Cheviron, 2016; Moore *et al.*, 2017). Despite the simpler structure of CfbCD, the conservation of cluster ligands, P-loop, inter-subcomplex docking faces and switch regions I and II in CfbC indicates that the catalytic cycle of CfbCD is related to nitrogenase and nitrogenase-like enzymes. Gel filtration experiments suggested the formation of a tetrameric 1:1 complex between $(CfbC)_2$ and $(CfbD)_2$. Interestingly, complex formation was not modulated in the presence of different nucleotides (Jasper *et al.*, 2020).

Phylogenetic analyses suggested CfbD (formerly denoted as NflD) as a basal ancestor of the catalytic subcomplex of nitrogenase and nitrogenase-like enzymes. MoFe, MoFe homolog NifEN and the catalytic subcomplexes of DPOR and COR might have evolved from a single structural protein (CfbD) *via* gene duplication and independent differentiation (Boyd and Peters, 2013).

1.6 Tetrapyrroles

Tetrapyyroles are present in all forms of life and belong to the most abundant compounds on earth. Based on their vital functions in oxygen transport, electron transport, catalysis and photosynthesis, tetrapyrroles were designated “the pigments of life” (Battersby, 2000; Vavilin and Vermaas, 2002).

The core of tetrapyrroles comprises four linked five-membered pyrrole rings. Modifications and a variety of ligands lead to a diverse group of macrocyclic and linear tetrapyrroles. Macrocyclic tetrapyrroles include the porphyrins heme, Chl and Bchl. Heme is most known as a prosthetic group in the oxygen transport protein hemoglobin. Additionally, heme is involved in electron transport (e.g. cytochromes), catalysis and acts as a regulatory molecule and iron supply (Frankenberg *et al.*, 2003; Heinemann *et al*., 2008). Chl and Bchl drive the harvesting of solar energy, charge separation and electron transport during photosynthesis (Masuda, 2008). Porphinoids are more reduced macrocyclic tetrapyrroles like corrinoids (e. g. vitamin B_{12}), siroheme (nitrite and sulfite reductase), coenzyme F_{430} and heme d_1. Bile pigments, phycobilins and tetrapyrrole degradation products are linear tetrapyrroles (collective term: bilins) that are derived from macrocycles. The biosynthesis of tetrapyrroles in eukaryotes is restricted to heme, siroheme, chlorophyll and bilins, whereas prokaryotes can also form the more complex corrinoids, heme d_1 and coenzyme F_{430} (Frankenberg *et al.*, 2003; Heinemann *et al*., 2008; Terry, 2003).

The first step in the biosynthesis of all tetrapyrroles is the formation of 5-aminolevulinic acid (ALA) (Figure 5). In animals, fungi and the α-group of proteobacteria, ALA is synthesized from glycine and succinyl-CoA *via* the ALA-synthase (C4 or Shemin pathway). Most bacteria, all archaea, algae and plants use the C5-pathway for the biosynthesis of ALA from glutamate (glutamyl-tRNA). The subsequent formation of protoporphyrinogen IX from ALA is highly conserved among all organisms. Two ALA molecules are condensed to monopyrrole porphobilinogen. Four porphobilinogen molecules are polymerized and form uroporphyrinogen III *via* isomerization. Uroporphyrinogen III is the last common intermediate for all tetrapyrroles (Figure 5). At this point, the biosynthesis of corrinoids, coenzyme F_{430}, siroheme and heme d_1 branches from the biosynthesis of Chl, Bchl, heme and bilins. Uroporphyrinogen III is further decarboxylated and oxidized to protoporphyrin IX, the branching point of Chl, Bchl and

the classic heme biosynthesis *via* protoporphyrin IX (Papenbrock and Grimm, 2001; Frankenberg *et al.*, 2003; Heinemann *et al*., 2008). Alternative routes for the biosynthesis of heme proceed *via* siroheme (siroheme pathway) or coproporphyrin III (coproporphyrin pathway) (Jahn *et al*., 2021).

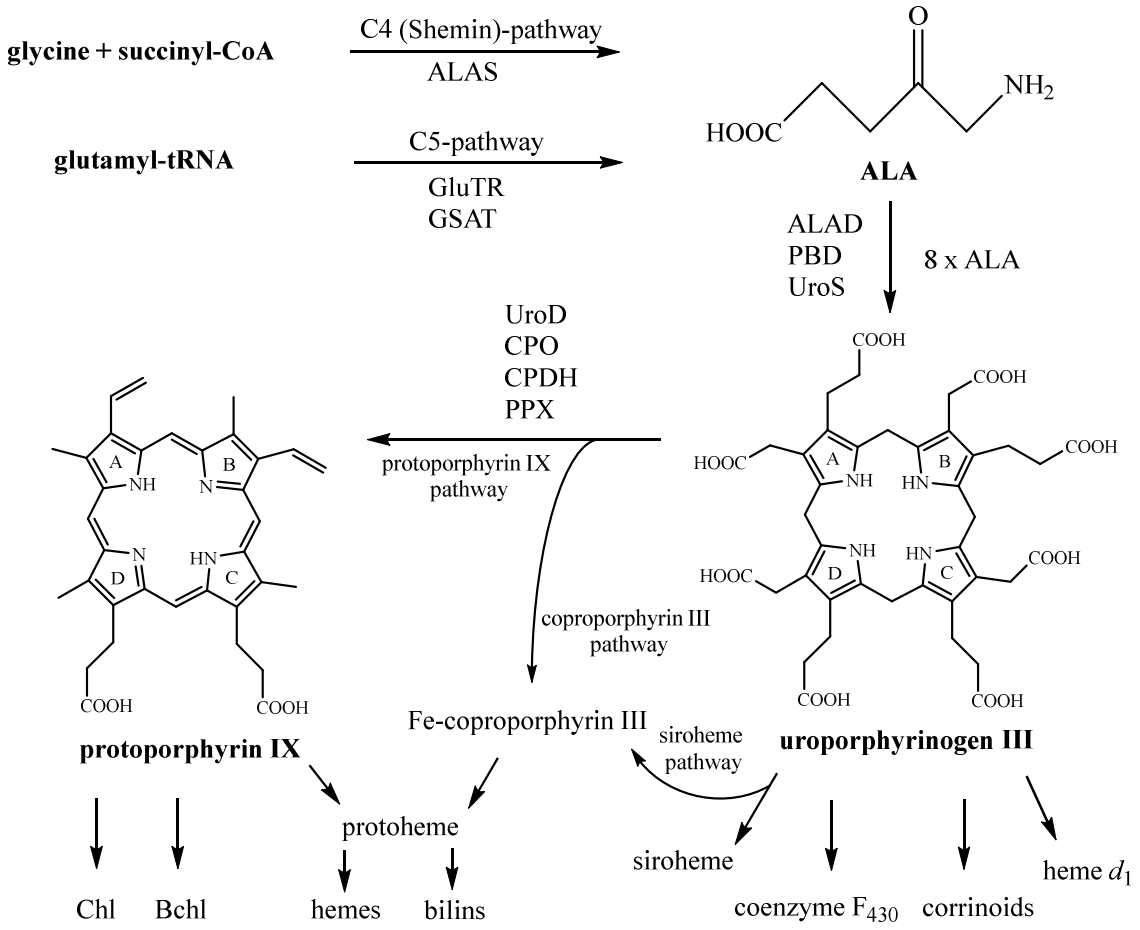

Figure 5: Key intermediates in the biosynthesis of tetrapyrroles.
5-aminolevulinic acid (ALA) is the universal precursor for all tetrapyrroles. Corrinoids, coenzyme F_{430}, siroheme and heme d_1 derive from the intermediate uroporphyrinogen III. Protoporphyrin IX is the last common intermediate of hemes (classic pathway), chlorophylls (Chl), bacteriochlorophylls (Bchl) and bilins. ALAS: ALA-synthase, GluTR: glutamyl-tRNA reductase, GSAT: glutamate-1-semialdehyde aminotransferase, ALAD: 5-aminolevulinate dehydratase, PBD: porphobilinogen deaminase, UroS: uroporphyrinogen III synthase, UroD: uroporphyrinogen III decarboxylase, CPO: coproporphyrinogen III oxidase, CPDH: coproporphyrinogen III dehydrogenase, PPX: protoporphyrinogen oxidase.

The insertion of ferrous iron into the hub metabolite protoporphyrin IX is performed by the Fe-chelatase and leads to protoheme, the precursor for different types of heme and linear tetrapyrroles (Figure 6). The heme pathway requires substantially fewer steps than the Chl pathway, which is initiated by the insertion of Mg^{2+} into protoporphyrin IX (Yin and Bauer, 2013). This step is catalyzed by the ATP-dependent multisubunit enzyme Mg-chelatase.

Mg-protoporphyrin IX is subsequently methylated at the C13 propionate group by the SAM-dependent Mg-protoporphyrin IX methyltransferase BchM (ChlM). A subsequent key step in the biosynthesis pathway of all Chl and Bchl is the formation of the E-ring in 3,8-divinyl-protochlorophyllide *via* oxidative cyclization.

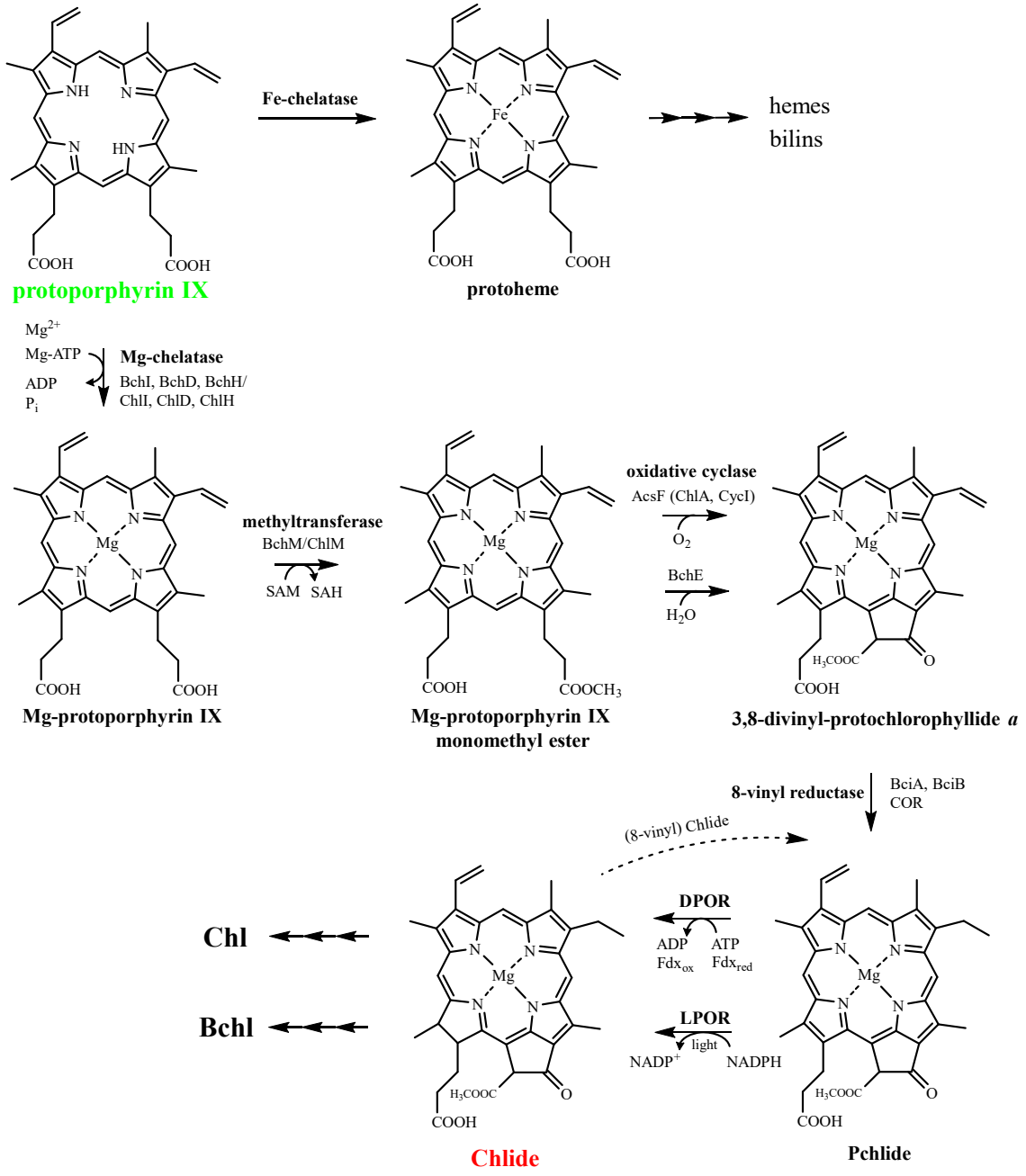

Figure 6: Overview of the biosynthesis of chlorophyllide *a* (Chlide) from protoporphyrin IX. Protoporphyrin IX (green) is a branching point for the biosynthesis pathways of chlorophylls (Chl), bacteriochlorophylls (Bchl) and hemes (classic pathway). Individual enzymes of the biosynthesis pathway of Chlide (red) from Protoporphyrin IX (green) are indicated. Chlide is a hub metabolite for the biosynthesis of Chl and Bchl. The reduction of the vinyl group at the C8 position of Pchlide/Chlide *via* 8-vinyl reductases depends on the organism and can occur at different stages.

This reaction is catalyzed by two evolutionary unrelated systems: In the presence of oxygen, the reaction is performed by the oxygen-dependent monooxygenase AcsF (ChlA, CycI), whereas the oxygen-sensitive radical-SAM enzyme BchE (ChlE) is used in anoxic environments. Some microaerophilic purple bacteria possess both systems (Willows, 2003; Chew and Bryant, 2007; Hallenbeck, 2017). The following steps to Chlide *via* Pchlide are indicated in a linear way in Figure 6. However, it was demonstrated that the order of the subsequent reactions varies between different organisms. 8-vinyl reductase BciA has a substrate preference for 8-vinyl Chlide and BciB can convert 8-vinyl Pchlide or 8-vinyl Chlide. 8-vinyl Chlide is also an alternative substrate of COR (compare Figure 4) (Tsukatani *et al.*, 2013a; Harada *et al.*, 2014; Hallenbeck, 2017). Furthermore, Pchlide and 8-vinyl-Pchlide were identified as substrates of DPOR and light-dependent protochlorophyllide *a* oxidoreductase (LPOR) (Bröcker *et al.*, 2008b).

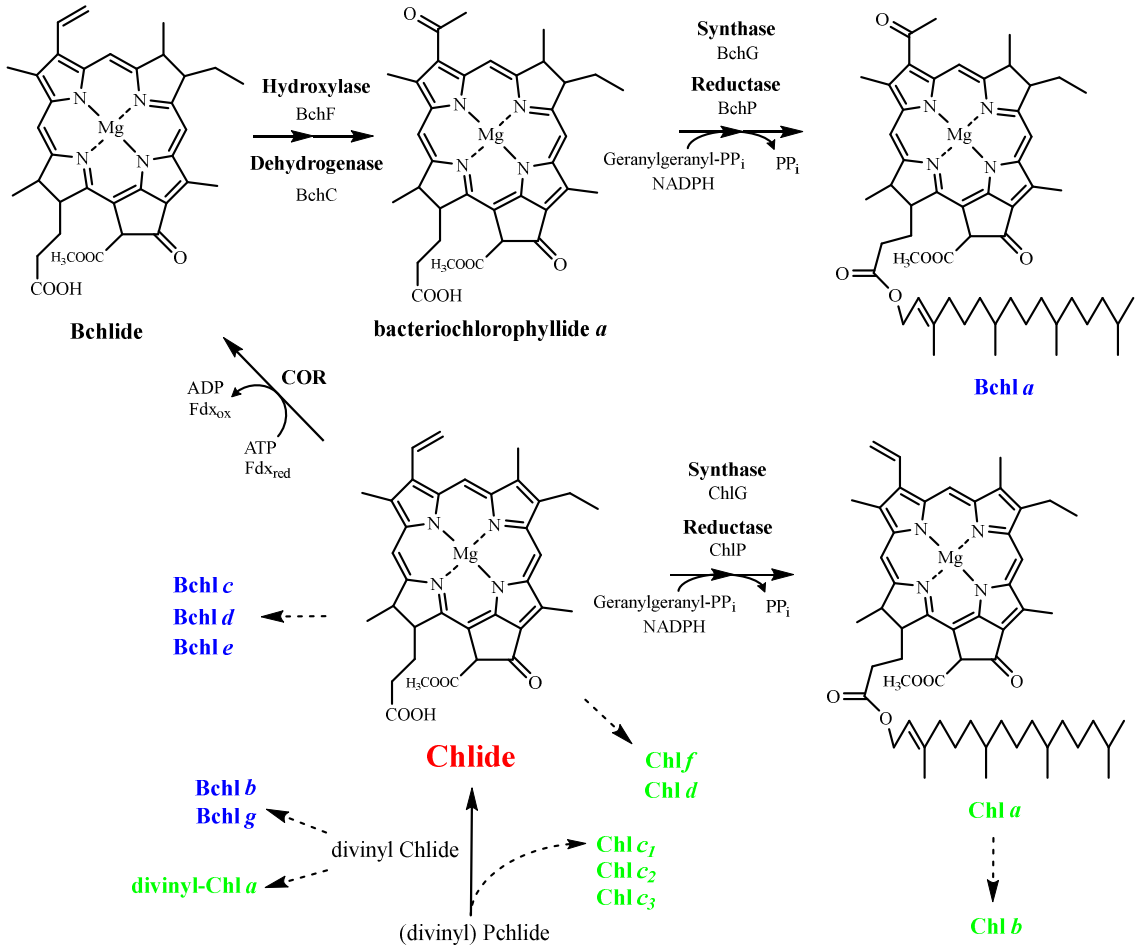

Figure 7: Biosynthesis pathways of chlorophylls (Chl) and bacteriochlorophylls (Bchl).
Chlorophyllide *a* (Chlide, red) is a central hub intermediate for the biosynthesis of Chl (green) and Bchl (blue). Involved enzymes and intermediates for the biosynthesis of Bchl *a* and Chl *a* are shown. The precursors of alternative Chl and Bchl are indicated by dashed arrows.

The reduction of Pchlide to Chlide *via* DPOR or LPOR is the final step of the core pathway for the biosynthesis of Chl and Bchl. The majority of Chls and Bchls are derived from the hub intermediate Chlide (Figure 7). For the biosynthesis of Bchl *a*, the chlorin ring structure of Chlide is converted into a bacteriochlorin ring by the reduction of the C7-C8 double bond of Chlide performed by COR. Subsequently, hydroxylase BchF and dehydrogenase BchC catalyze the formation of an acetyl group at the C3 position of the bacteriochlorin ring. The final step in the biosynthesis of Bchl *a* and Chl *a* is an esterification catalyzed by BchG (ChlG) and a subsequent reduction of the geranylgeranyl group to phytol performed by BchP (ChlP). Various modifications of the tetrapyrrole core lead to other derivatives of Chls and Bchls (Figure 7) (Chew and Bryant, 2007; Hallenbeck, 2017).

1.7 Aim of this study

Nitrogenase and the nitrogenase-like enzymes chlorophyllide *a* oxidoreductase (COR), the dark-operative protochlorophyllide oxidoreductase (DPOR) and the Ni^{2+}-sirohydrochlorin *a*,*c*-diamide reductase (CfbCD) all consist of an ATP-utilizing, electron-donating, homodimeric reductase subcomplex and a heterotetrameric catalytic subcomplex. The reductase subcomplexes are termed $(BchX)_2$ in COR, $(ChlL)_2$ in DPOR, $(NifH)_2$ in nitrogenase and $(CfbC)_2$ in CfbCD. The catalytic subcomplexes are termed $(BchYZ)_2$ in COR, $(ChlNB)_2$ in DPOR, $(NifDK)_2$ in nitrogenase and $(CfbD)_2$ in CfbCD.

The general aim of this study was to construct and functionally characterize various heterologous and chimeric enzymes composed of these nitrogenase-like subcomplexes. For this purpose, COR enzymes from different bacteria had to be recombinantly produced, biochemically characterized and heterologously assembled. Furthermore, crystals of the COR enzyme should be generated for its structural elucidation.

Next, nitrogenase and DPOR subcomplexes (or DPOR variants) should be produced and purified to allow for the formation of chimeric nitrogenase-like enzyme complexes. These chimeric complexes had to be characterized for stability and activity. Several principles for the function of nitrogenase-like enzymes should be deduced.

2. Materials and methods

2.1 Instruments, chemicals and materials

2.1.1 Instruments

The instruments used in the present study are summarized in Table 1.

Table 1: Instruments.

Instrument	Model	Manufacturer
ÄKTA system	ÄKTApurifier	GE Healthcare, Chicago (IL), USA
Agarose gel electrophoresis	Mini-Sub Cell GT	Bio-Rad, Hercules (CA), USA
Agarose gel documentation	DeVision DBOX	Decon Science Tec, Hohengandern, Germany
	UV transilluminator	Wealtec, New Taipei City, Taiwan
Anaerobic chamber	Flexible vinyl anaerobic chamber	Coy Laboratory Products, Grass Lake (MI), USA
	MACS MG-1000 anaerobic workstation	Don Whitley Scientific, Bingley, UK
Autoclave	FVA3/A1	ibs | tecnomara, Fernwald, Germany
Blotting system	Trans-Blot Turbo	Bio-Rad
Blue light transilluminator	Flu-O-blu	Biozym, Hessisch Oldendorf, Germany
Buffer degassing system	self-constructed	self-constructed
Centrifuges	Avanti J-E + rotor JLA 9.100 (500-1'000 mL/tube) Optima L-90K Ultracentrifuge + rotor 45 Ti (up to 70 mL/tube) + rotor 70.1 Ti (up to 10 mL/tube)	Beckman Coulter, Brea (CA), USA
	Megafuge 1.0R (up to 50 mL/tube) MiniSpin + rotor F-45-12-11 (up to 2 mL/tube)	Heraeus Instruments, Hanau, Germany Eppendorf, Hamburg, Germany

Crystal screen documentation	Digital microscope VHX-500F	Keyence, Osaka, Japan
French press	French Pressure Cell Press	Polytec, Waldbronn, Germany
French press cell	French Pressure Cell	Glen Mills, Clifton (NJ), USA
	French Pressure Cell	Thermo Fisher, Waltham (MA), USA
Gel scanner	Bio-5000 Plus	Microtek, Hsinchu, Taiwan
Magnetic stirrer	VS-C7	VWR, Radnor (PA), USA
Microplate reader	Multiskan GO	Thermo Fisher
Microscale thermophoresis (MST) device	Monolith NT.115	NanoTemper, Munich, Germany
NanoDrop	ND-1000	VWR
Peristaltic pump	Peristaltic pump P-3	GE Healthcare
pH determination	CG 842	Xylem Analytics, Weilheim, Germany
Rotary evaporator	Rotavapor R-300	Büchi, Essen, Germany
Scales	Entris 224i-1S Entris 3202-1S	Sartorius, Göttingen, Germany
SDS-PAGE	Mini Protean Tera Cell	Bio-Rad
Shaker	CH-4103 Orbitron Multitron Pro	Infors, Bottmingen, Switzerland
Thermomixer	Thermomixer C Thermomixer compact	Eppendorf Eppendorf
Thermocycler	ProFlex PCR system	Thermo Fisher
UV-Vis spectrophotometer	V-650 Ultrospec 2000	Jasco, Tokyo, Japan GE Healthcare

Vortex	Vortex-Genie 2	Scientific Industries, Bohemia (NY), USA
Purified water	Milli-Q IQ 7000	Merck Millipore, Burlington (MA), USA

2.1.2 Chemicals, enzymes, kits and other materials

Table 2 lists chemicals, enzymes, kits and materials used in the present study. Not specifically listed materials were purchased from Carl Roth (Karlsruhe, Germany), Sigma-Aldrich (St. Louis, MO, USA), GERBU (Heidelberg, Germany), Fisher Chemical (Hampton, NH, USA) and Riedel-de Haën (Seelze, Germany).

Table 2: Chemicals, enzymes, kits and other materials.

Chemicals	Manufacturer
β,γ-Imidoadenosine 5′-triphosphate (AMP-PNP) lithium salt hydrate	Roche, Basel, Switzerland
Agarose (NEEO Ultra-Qualität)	Carl Roth, Karlsruhe, Germany
Ampicillin sodium salt	Carl Roth
Antarctic phosphatase reaction buffer (10x)	New England Biolabs, Ipswich (MA), USA
Adenosine 5′-triphosphate (ATP) disodium salt hydrate (> 99 %)	Sigma-Aldrich, St. Louis (MO), USA
(> 98 %)	Carl Roth
ATP, lyophilized, for ATPase assays	Expedeon, Heidelberg, Germany
Adenosine 5′-diphosphate (ADP) sodium salt (> 95 %)	Sigma-Aldrich
Agarose NEEO ultra-quality	Carl Roth
Bradford reagent	Sigma-Aldrich
Brilliant blue G 250	Carl Roth
Chloramphenicol	Carl Roth
CutSmart buffer (10x)	New England Biolabs
Cyanine 5 succinimidyl (NHS) ester	Lumiprobe
L-cysteine hydrochloride monohydrate	Carl Roth

1,4-Dithio-D,L-threitol (DTT)	GERBU, Heidelberg, Germany
Ethanol absolute	VWR
Ethidium bromide solution (10 mg/mL)	Carl Roth
Fe(III) citrate tribasic monohydrate	Sigma-Aldrich
Gel loading dye purple (6x)	New England Biolabs
GelStar nucleic acid gel stain	Lonza, Basel, Switzerland
GeneRuler DNA ladder mix	Thermo Fisher
4-(2-Hydroxyethyl)-1-piperazine ethanesulfonic acid (HEPES)	GERBU
Instant blue	Sigma-Aldrich
Isopropyl-β-D-galactopyranoside (IPTG)	GERBU
Phosphocreatine disodium salt hydrate (> 97 %)	Sigma-Aldrich
Rotiphorese Gel 30	Carl Roth
Sodium dithionite (DT)	Sigma-Aldrich
Tween 20	Sigma-Aldrich
Enzymes	
DpnI, EcoRI-HF, NotI-HF, SalI-HF, XhoI	New England Biolabs
Antarctic phosphatase	New England Biolabs
Benzonase, turbo nuclease (*Serratia marcescens*, recombinant, produced in *E. coli*, 25 U/µL)	Jena Bioscience, Jena, Germany
Creatine kinase from rabbit muscle	Roche
PreScission protease (2 U/µL)	GE Healthcare
Kits	
Colorimetric ATPase Assay (PiColorLock)	Expedeon
In-Fusion HD Cloning Kit	Clontech, Mountain View (CA), USA
Gel filtration markers kit for protein molecular weights 12’000-200’000 Da	Sigma-Aldrich

PfuUltra II Hotstart PCR Master Mix	Agilent Technologies, Santa Clara (CA), USA
QIAprep Spin Miniprep Kit	Qiagen, Hilden, Germany
QIAquick Gel Extraction Kit	Qiagen
QIAquick PCR Purification Kit	Qiagen
Crystal screens	
NeXtal Tubes Cryos Suite	Qiagen
NeXtal Tubes ProComplex Suite	Qiagen
NeXtal Tubes JCSG+ Suite	Qiagen
NeXtal Tubes JCSG Core Suite I	Qiagen
NeXtal Tubes JCSG Core Suite II	Qiagen
Wizard Cryo	Rigaku, Tokyo, Japan
Morpheus MD1-46	Molecular Dimensions, Sheffield, UK
Intelli-plate 96-3 (Crystal screening plate)	Art Robbins Instruments, Sunnyvale (CA), USA
Other materials	
Amicon ultra 0.5 mL centrifugal filter devices	Merck Millipore
Amicon stirred cell, Model 8010	Merck Millipore
Blot filter paper, 7.5 x 10 cm	Bio-Rad
CM Sepharose CL-6B (Pchlide purification)	GE Healthcare
Cuvettes, QS high precision cell, quartz SUPRASIL	Hellma Analytics, Müllheim, Germany
Cuvettes, polystyrene	Sarstedt, Nümbrecht, Germany
Filtropur S 0.2 sterile filter	Sarstedt
Gel filtration column HiLoad 16/600 and 26/600 Superdex 200	GE Healthcare
NAP-5 columns (desalting columns)	GE Healthcare

Monolith NT.115 Premium Capillaries for MST	NanoTemper
PD SpinTrap G-25	GE Healthcare
Poly-Prep gravity-flow chromatography columns (10 mL)	Bio-Rad
Protino glutathione agarose 4B	Macherey-Nagel, Düren, Germany
Protein molecular weight marker (unstained/prestained)	Thermo Fisher
Polyvinylidene difluoride (PVDF)-membrane (Roti-PVDF 0.45 µm)	Carl Roth
Sep-Pak C18 (Chlide purification)	Waters, Milford (MA), USA
Ultracel 30 kDa ultrafiltration discs (regenerated cellulose)	Merck Millipore

2.2 Bacterial strains, plasmids, primer and synthetic genes

2.2.1 Bacterial strains and plasmids

Bacterial strains and plasmids used in the present study are summarized in Table 3.

Table 3: Bacterial strains and plasmids.

Strain	**Genotype**	**Reference**
E. coli DH10B	*F^- mcrA Δ(mrr-hsdRMS-mcrBC) Φ80lacZΔM15 ΔlacX74 recA1 endA1 araD139 Δ(ara, leu)7697 galU galK λ^- rpsL nupG*	Invitrogen, Carlsbad (CA), USA
E. coli BL21 (λDE3)	*B F^- dcm ompT hsdS(rB^- mB^-) gal λ(DE3)*	Stratagene, La Jolla (CA), USA
R. capsulatus ZY5	Interposon deletion of *F108* (*bchL)*, 54-bp *PstI* restriction fragment in *F108* was replaced with a Kan^R cassette, accumulates Pchlide	(Yang and Bauer, 1990)
R. capsulatus CB1200	*bchF, orf490 :: ΩSp'*, *rif-10*, accumulates Chlide	(Bollivar *et al.*, 1994)
Plasmid	**Description**	**Reference**
pGEX-6P-1	Bacterial vector for recombinant protein production, N-terminal glutathione S-transferase-tag (GST-tag) and PreScission protease site, tac promotor, *lacI*, ori_{pBR322}, Amp^R	GE Healthcare

pGEX-6P-1-*bchX* Hm	pGEX-6P-1 containing synthetic *bchX* from *H. modesticaldum*, *E. coli* codon optimization by Geneart, implemented in *mcs* between EcoRI and XhoI with stop-codon, N-terminal GST-tag	This work
pGEX-6P-1-*bchX* Rp	pGEX-6P-1 containing synthetic *bchX* from *R. palustris*, *E. coli* codon optimization by Geneart, implemented in *mcs* between EcoRI and XhoI with stop-codon, N-terminal GST-tag	This work
pGEX-6P-1-*bchY* Hm	pGEX-6P-1 containing synthetic *bchY* from *H. modesticaldum*, *E. coli* codon optimization by Geneart, implemented in *mcs* between EcoRI and SalI with stop-codon, N-terminal GST-tag	This work
pGEX-6P-1-*bchY* Rp	pGEX-6P-1 containing synthetic *bchY* from *R. palustris*, *E. coli* codon optimization by Geneart, implemented in *mcs* between EcoRI and SalI with stop-codon, N-terminal GST-tag	This work
pGEX-6P-1-*bchYZ* Hm	A derivative of pGEX-6P-1-*bchY* Hm carrying synthetic *bchZ* from *H. modesticaldum*, *E. coli* codon optimization by Geneart, implemented in *mcs* between SalI and NotI with stop-codon, *rbs* was implemented upstream of *bchZ,* N-terminal GST-tag (*bchY*)	This work
pGEX-6P-1-*bchYZ* Rp	A derivative of pGEX-6P-1-*bchY* Rp carrying synthetic *bchZ* from *R. palustris*, *E. coli* codon optimization by Geneart, implemented in *mcs* between SalI and NotI with stop-codon, *rbs* was implemented upstream of *bchZ*, N-terminal GST-tag (*bchY*)	This work
pGEX-6P-1-*bchY* Hm-M1	A derivative of pGEX-6P-1-*bchY* Hm containing amino acid changes E86A, E87A and K88A, N-terminal GST-tag	This work
pGEX-6P-1-*bchY* Hm-M2	A derivative of pGEX-6P-1-*bchY* Hm containing amino acid changes K345A, K346A and K348A, N-terminal GST-tag	This work

pGEX-6P-1-*chlL* Pm	pGEX-6P-1 containing *Prochlorococcus marinus SS120 chlL* cloned into the BamHI/SalI sites, N-terminal GST-tag	(Uliczka, 2007)
pGEX-6P-1-*chlL* Pm Y127D	A derivative of pGEX-6P-1-*chlL* Pm containing amino acid change Y127D, N-terminal GST-tag	(Uliczka, 2007)
pGEX-6P-1-*chlL* Pm Y127S	A derivative of pGEX-6P-1-*chlL* Pm containing amino acid change Y127S, N-terminal GST-tag	(Uliczka, 2007)
pGEX-6P-1-*cLmax*	pGEX-6P-1 containing a modified synthetic *chlL* gene from *P. marinus SS120*. The encoded protein comprises a NifH-like docking interface.	This work
pGEX-6P-1-*cLmin*	pGEX-6P-1 containing a modified synthetic *chlL* gene from *P. marinus SS120*. The encoded protein comprises a NifH-like docking interface.	This work
pGEX-6P-1-*chlNB* Pm	pGEX-6P-1 containing *P. marinus SS120 chlN* and *chlB* genes cloned into the EcoRI/SalI and SalI/NotI sites, *rbs* was implemented upstream of *chlB*, N-terminal GST-tag (*chlN*)	(Uliczka, 2007)
pGEX-6P-1-*bchNBL* Ct	pGEX-6P-1 containing *C. tepidum bchNBL* cloned into the BamHI/NotI sites, *E. coli* optimized *rbs* sequence before *bchL* and *bchB*, N-terminal GST-tag (*chlN*)	(Ganskow, 2006)
pGEX-6P-1-*bchNBnotL* Ct	pGEX-6P-1 containing *C. tepidum bchNBL* cloned into the BamHI/NotI sites, *E. coli* optimized *rbs* sequence upstream of *bchL* and *bchB*, NotI site between *bchB* and *bchL*, N-terminal GST-tag (*chlN*)	(Simone Virus, 2006)
pGEX-6P-1-*bchNB* Ct	pGEX-6P-1-*bchNBnotL* Ct was digested with NotI and re-ligated to remove *bchL*	This work
pGEX-6P-1-*bchL* Ct	pGEX-6P-1 containing *C. tepidum bchL* cloned into the BamHI/NotI sites	(Bröcker, 2005)
pACYCDuet-1	Bacterial vector for the coexpression of two genes. Contains two *mcs* with a T7-promotor each, *lacI*, ori_{P15A}, N-terminal His_6-tag in *mcs-1*, C-terminal S-tag in *mcs-2*, Cm^R	Novagen

pACYCDuet-1-*bchZ* Hm	pACYCDuet-1 containing synthetic *bchZ* from *H. modesticaldum*, *E. coli* codon optimization by Geneart, implemented in *mcs-1* between NcoI and EcoRI with stop-codon, N-terminal His_6-tag in *mcs-1* was removed	This work
pACYCDuet-1-*bchZ* Rp	pACYCDuet-1 containing synthetic *bchZ* from *R. palustris*, *E. coli* codon optimization by Geneart, implemented in *mcs-1* between NcoI and EcoRI with stop-codon, N-terminal His_6-tag in *mcs-1* was removed	This work
pACYCDuet-1-*bchZ* Hm-M1	A derivative of pACYCDuet-1-*bchZ* Hm containing amino acid changes K266A, E267A and K268A	This work
pACYCDuet-1-*bchZ* Hm-M2	A derivative of pACYCDuet-1-*bchZ* Hm containing amino acid changes K154A, K155A and K159A	This work
pET-*bchX* Rd	pET32a vector, N-terminal thioredoxin /His_6/S-tag, T7 promoter, Amp^R, containing *bchX* from *R. denitrificans* between SacI and XhoI	(Wätzlich *et al.*, 2009)
pRKISC	pRK415 vector containing the *E. coli isc* gene cluster ORF1-ORF2-*iscS-iscU-iscA-hscB-hscA-fdx*-ORF3, Tet^R	(Nakamura, Saeki and Takahashi, 1999)

2.2.2 Primer

Table 4 lists all primers used in the present study. Primers were obtained from GATC Biotech (Constance, Germany) and Invitrogen (Carlsbad, CA, USA).

Table 4: Primers used in the present study.
Exchanged nucleotides for site-directed mutagenesis of *bchY* and *bchZ* from *H. modesticaldum* are highlighted in bold font.

Primers used for DNA sequencing	**Sequence 5´-3´**
pGEX-5	CTGGCAAGCCACGTTTGG
pGEX-3	GGAGCTGCATGTGTCAGAG
bchY_Hm_P1	GGTGCAGATATGGGTTTAG
bchZ_Hm_P2	ATTGGGGTGCACTGTATG
bchY_Rp_P3	AATGGCGTGAACTGTATGC
bchZ_Rp_P4	ATGCTGGTTCTGGATCATG
P66	GGATCTCGACGCTCTCCCT
P64	GATTATGCGGCCGTGTACAA

Primers used for mutagenesis	Sequence 5´-3´
YHmM1_P5	GAAATCATCAAA**GCAGCAGCA**CCGGAATTTGTTCC
YHmM1r_P6	GGAACAAATTCCGG**TGCTGCTGC**TTTGATGATTTC
YHmM2_P7	GATCTGGTTGCAGTG**GCAGCA**TAC**GCA**CCGGATATTGCCC
YHmM2r_P8	GGGCAATATCCGG**TGC**GTA**TGCTGC**CACTGCAACCAGATC
ZHmM1_P9	GCATTTATTGCA**GCAGCAGCA**CGTACCACGCTGC
ZHmM1r_P10	GCAGCGTGGTACG**TGCTGCTGC**TGCAATAAATGC
ZHmM2_P11	CCTCGTCTGCCG**GCAGCA**GCAAGCGCA**GCA**CCGCTGG
ZHmM2r_P12	CCAGCGG**TGC**TGCGCTTGC**TGCTGC**CGGCAGACGAGG

2.2.3 Synthetic genes

Synthetic genes used in this work were commercially synthesized as *E. coli* codon usage optimized "GeneArt Strings DNA Fragments" from Invitrogen and are reported in the appendix Table 20.

2.3 Growth media and media additives

2.3.1 Growth media

E. coli was cultivated in LB (lysogeny broth) (Bertani, 1951) as a standard medium. The specific composition is summarized in Table 5. Solid media was obtained by adding 15 g/L agar-agar to the standard medium prior to sterilization.

Table 5: LB medium composition.

Component	Concentration
Peptone/tryptone	10 g/L
Yeast extract	5 g/L
NaCl	5 g/L

R. capsulatus ZY5 (Yang and Bauer, 1990) was cultivated in PY medium in the presence of 5 µg/mL kanamycin, 1 mM $MgCl_2$ and 1 mM $CaCl_2$. *R. capsulatus* CB1200 (Bollivar *et al.*, 1994) was cultivated in RCV 2/3 PY medium supplemented with 10 µg/mL spectinomycin (Weaver *et al.*, 1975; Young *et al.*, 1989). The compositions of PY medium and RCV 2/3 PY medium are listed in Table 6 and Table 7, respectively.

Table 6: PY medium composition.

Component	Concentration
Yeast extract	3 g/L
Peptone/tryptone	3 g/L

Table 7: RCV 2/3 PY medium composition.

RCV 2/3 PY	Concentration
$CaCl_2 \cdot 2\ H_2O$	75 mg/L
D-biotin	15 µg/L
DL-malic acid	4 g/L
EDTA disodium salt	20 mg/L
$FeSO_4$	12 mg/L
KH_2PO_4	0.6 g/L
K_2HPO_4	0.9 g/L
$MgSO_4 \cdot 7\ H_2O$	120 mg/L
$(NH_4)_2SO_4$	1 g/L
Peptone/tryptone	2 g/L
Thiamine hydrochloride	1 mg/L
Trace elements	1 mL/L
Yeast extract	2 g/L
pH 6.8 (NaOH)	

Trace elements	Concentration
$Cu(NO_3)_2 \cdot 3\ H_2O$	40 mg/L
H_3BO_3	2.8 g/L
$MnSO_4 \cdot H_2O$	1.6 g/L
$NaMoO_4 \cdot 2\ H_2O$	0.75 g/L
$ZnSO_4 \cdot 7\ H_2O$	0.24 g/L

2.3.2 Media additives

Antibiotics were prepared as stock solutions, sterilized by filtration and stored at -20 °C. Iron(III) citrate was autoclaved and stored at room temperature. L-cysteine hydrochloride was prepared freshly before use. Table 8 summarizes all used media additives.

Table 8: Media additives.

Antibiotics	Concentration of stock solution	Final concentration
Ampicillin	100 mg/mL	100 µg/mL
Chloramphenicol	34 mg/mL	34 µg/mL
Kanamycin	5 mg/mL	5 µg/mL
Spectomycin	10 mg/mL	10 µg/mL
Tetracycline	10 mg/mL	10 µg/mL
Other media additives		
L-cysteine hydrochloride monohydrate	100 mM	1 mM
Fe(III) citrate tribasic monohydrate	100 mM	1 mM
IPTG	500 mM	50-100 µM

2.4 Microbiological methods

2.4.1 Sterilization

Autoclavable items and solutions were sterilized at 121 °C and 1 bar positive pressure for 20 min. Temperature-sensitive solutions were sterilized by filtration using 0.2 µm pore size filters.

2.4.2 Storage of bacteria

For long-term storage of bacteria, glycerol stocks were prepared from overnight cultures by mixing 1.2 mL culture with 400 µL 80 % (w/v) sterile glycerol. Glycerol stocks were stored at -80 °C.

2.4.3 General cultivation conditions of *E. coli*

Precultures in baffled flasks containing LB medium and the respective antibiotic were inoculated from glycerol stocks or single colonies from plate cultures. For the heterologous production of recombinant proteins, precultures were prepared in 100 mL baffled flasks with 10-30 mL LB medium or 300 mL baffled flasks with 70 mL LB medium. For cloning experiments, a maximum of 10 mL culture was cultivated in glass test tubes. All precultures were incubated aerobically at 37 °C overnight at 200 rpm. LB agar plates were incubated overnight at 37 °C.

Heterologous production of recombinant proteins was generally performed in 1 L baffled flasks with 500 mL LB medium in the presence of the respective media additives. The cultures were inoculated in a ratio of 1:100 (v/v) with overnight precultures. Cultivation was performed aerobically at 37 °C and 180-200 rpm until an OD_{578} of 0.5 was reached. Heterologous production of recombinant proteins was initiated in the presence of 25-50 µM IPTG. The cultivation was continued aerobically overnight for 16-21 h at 17 °C or 25 °C with 160 rpm.

2.4.4 Determination of cell density

The optical density at 578 nm (OD_{578}) was used to monitor cell growth in liquid cultures photometrically. Cultures with high density (OD_{578} > 1) were diluted with LB medium.

2.5 Molecular biological methods

2.5.1 Preparation of RbCl-competent *E. coli* cells (DH10B)

250 mL LB medium in a 1 L baffled flask was inoculated with an overnight preculture (20 mL, 100 mL baffled flask) in a ratio of 1:100 (v/v). Cultures were grown at 37 °C and 180 rpm to an OD_{578} of 0.5-0.6. Cells were harvested by centrifugation (4'000 g, 10 min, 4 °C) in sterile 50 mL centrifuge tubes. Cell pellets were resuspended in a total volume of 100 mL cooled TFB-I-buffer (Table 9). After incubation for 5 min on ice, the cell suspension was centrifuged again (4'000 g, 10 min, 4 °C). The resulting cell pellet was resuspended in TFB-II-buffer (Table 10) using a twofold pellet volume. Cells were incubated for 60 min on ice and stored at -80 °C.

Table 9: TFB-I-buffer.

Component	Concentration
Potassium acetate	30 mM
$CaCl_2$	10 mM
$MnCl_2$	50 mM
RbCl	100 mM
Glycerol	15 % (w/v)
pH 5.8 (acetic acid), sterile filtered	

Table 10: TFB-II-buffer.

Component	Concentration
Piperazine-N,N′-bis (2-ethanesulfonic acid) pH 6.5	10 mM
$CaCl_2$	75 mM
RbCl	10 mM
Glycerol	15 % (w/v)
pH 6.5 (KOH), sterile filtered	

2.5.2 Preparation of $CaCl_2$-competent *E. coli* cells (BL21)

100 mL LB medium in a 500 mL baffled flask was inoculated with an overnight preculture (20 mL, 100 mL baffled flask) in a ratio of 1:100 (v/v). Cultures were grown at 37 °C and 180 rpm to an OD_{578} of 0.6-0.8. Cells were transferred in sterile 50 mL centrifuge tubes, incubated for 10 min on ice and harvested by centrifugation (4'000 g, 10 min, 4 °C). Cell pellets were resuspended in a total volume of 10 mL cooled 0.1 M $CaCl_2$ and 10 % (w/v) glycerol. After incubation for 15 min on ice, the cell suspension was centrifuged again (4'000 g, 10 min, 4 °C) and the resulting cell pellet was resuspended in 10 mL cooled 0.1 M $CaCl_2$ containing 10 % (w/v) glycerol. Aliquots were stored at -80 °C.

2.5.3 Transformation of competent *E. coli* cells

Transformation of chemically competent *E. coli* cells was performed with 50 µL competent cells mixed with 1 µL plasmid DNA (50-200 ng) or 1-7 µL In-Fusion reaction mixture. Cells were incubated on ice for 10 min and exposed to a heat shock for 2 min at 42 °C. 500 µL LB medium was added and the cells were incubated for 45-60 min at 37 °C and 600 rpm. 10-100 µL cell suspension or the pelleted cells after centrifugation were plated on LB agar plates supplemented with the respective antibiotic. LB agar plates were incubated overnight at 37 °C.

2.5.4 Preparation of plasmid DNA

Plasmid DNA for cloning or sequencing purposes was prepared with 4 mL of an *E. coli* DH10B overnight culture using the QIAprep Spin Miniprep Kit (Qiagen) according to the manufacture's instructions. Purified DNA was eluted with 50 µL dH_2O (70 °C) after 5 min incubation at 70 °C.

Alternatively, high amounts of plasmid DNA were prepared (e.g., for analytical plasmid digestion to identify positive clones) according to the following protocol: 4 mL of an *E. coli* DH10B overnight culture were sedimented in a 2 mL reaction tube and the cells were resuspended in 300 µL P1-buffer. After adding 300 µL P2-buffer, the sample was mixed thoroughly by inverting the reaction tube. In the next step, 300 µL P3-buffer was added to the sample and the reaction tube was mixed again. After a centrifugation step (12´100 g, 15 min, RT), the supernatant was transferred to a 1.5 mL reaction tube, supplemented with 600 µL isopropanol and mixed by inverting the reaction tube. Samples were centrifuged (12´100 g, 20 min, RT) and the precipitated DNA was washed carefully using 400 µL 70 % (v/v) EtOH. Subsequently, samples were centrifuged (12´100 g,

5 min, RT) and dried at 37 °C to remove residual EtOH and the DNA was dissolved in 35 µL dH_2O.

Table 11: Composition of buffers P1, P2 and P3.

Component	Concentration
P1	
Tris(hydroxymethyl)aminomethane (Tris) – HCl pH 8.0	50 mM
EDTA	10 mM
RNase A (10 mg/mL stock in 50 % glycerol)	100 µg/mL
P2	
NaOH	200 mM
Sodium dodecyl sulfate (SDS)	1 % (w/v)
P3	
Potassium acetate pH 5.5 (acetic acid)	3 M

2.5.5 Determination of DNA concentration

The concentration of plasmid DNA was analyzed using a ND-1000 spectrophotometer (Peqlab) by measuring the absorbance at 260 nm (A_{260}). This method allows the determination of DNA in a 1-2 µL volume in a range of 2-3´700 ng/µL. The ratio A_{260}/A_{280} was used to estimate the purity of prepared plasmid DNA. A ratio of 1.8-2.0 indicates highly pure DNA (Mülhardt, 2009).

2.5.6 Restriction digest and dephosphorylation of plasmids

In order to prepare plasmids for cloning purposes or to analyze a cloned construct, restriction digests using endonucleases listed in Table 2 were performed. Analytical DNA cleavage was conducted in a volume of 10 µL using 2 µL plasmid DNA (0.2-1 µg/µL), 0.1 µL endonuclease (2 U) and 1 µL 10x CutSmart buffer at 37 °C for 1-2 h. For In-Fusion HD Cloning, plasmid DNA was digested in a total volume of 40 µL using 34 µL plasmid DNA (100-200 ng/µL), 1 µL endonuclease (20 U) and 4 µL 10x CutSmart buffer at 37 °C for 2 h.

Linearized plasmid DNA was dephosphorylated in a total volume of 50 µL using 40 µL digested plasmid DNA, 1 µL antarctic phosphatase (5 U) and 5 µL 10x antarctic phosphatase reaction buffer at 37 °C for 30 min.

2.5.7 Agarose gel electrophoresis and gel extraction

Agarose gel electrophoresis was performed to validate the size of DNA fragments after an analytical restriction digest or to purify DNA fragments for cloning purposes. DNA samples were mixed with 6x purple gel loading dye (New England Biolabs) and loaded onto an agarose gel (1 %, w/v) prepared in 1x TAE-buffer (Table 12). GeneRuler DNA ladder mix (Thermo Fisher) was used as a standard. Gel electrophoresis was conducted for 30-45 min at 115 V in 1x TAE buffer. Analytical gels were stained for 15 min in ethidium bromide solution (10 µg/mL) and visualized using UV light. Preparative gels for DNA purification were stained with GelStar nucleic acid gel stain (Lonza) according to the manufacture's instructions. DNA bands were visualized under blue light and

excised from the gel. Subsequent gel extraction was performed using the QIAquick Gel Extraction Kit (Qiagen) according to the manufacture's instructions. DNA was eluted in 30 µL dH_2O (70 °C).

Table 12: TAE-buffer (1x).

Component	Concentration
Tris	40 mM
Acetic acid	20 mM
EDTA (pH 8.0)	1 mM

2.5.8 Construction of vectors

For the investigation of COR enzymes from *H. modesticaldum* and *R. palustris,* the respective synthetic genes were cloned into vector pGEX-6P-1 to generate the vectors summarized in Table 3. The respective *bchX* genes were cloned individually into vector pGEX-6P-1, while *bchY* and *bchZ* were cloned into this vector for the bicistronic expression of both genes. Therefore, an additional ribosomal binding site was implemented upstream of *bchZ*. Furthermore, *bchZ* genes were cloned separately into vector pACYCDuet-1.

The chimeric *chlL* variants *cLmax* and *cLmin* were cloned into vector pGEX-6P-1 by analogy to *bchX*. These genes encode ChlL protein variants comprising a NifH-like docking interface. Amino acids of the docking interface were substituted based on the alignment shown in (Moser *et al.*, 2013). According to the amount of replaced amino acids, the resulting ChlL variants were termed CLmax and CLmin. For CLmin, only the highly conserved docking residues of NifH were implemented, whereas CLmax contained additional residues of the protein-protein interface. The synthetic genes used for the construction of vectors are listed in the appendix Table 20.

2.5.9 In-Fusion HD Cloning

In this study, the In-Fusion HD Cloning method (Clontech) was utilized to generate plasmid constructs. This system enables for the joining of DNA fragments on the basis of 15 basepair overlaps and does not require specific restriction sites for ligation (Zhu *et al.*, 2007). Genes *bchX*, *bchY*, *bchZ* from *H. modesticaldum* or *R. palustris* and the designed *cLmax* and *cLmin* genes were synthesized as *E. coli* codon-optimized "GeneArt Strings DNA Fragments" (Invitrogen) with 15 bp overlap (compare 2.2.3 Synthetic genes). Vector DNA was linearized by restriction digest (restriction sites in Table 3). In-Fusion reactions were carried out using 50 ng linearized plasmid DNA mixed with 5x molar excess of the insert DNA and 2 µL 5x In-Fusion enzyme premix in a volume of 10 µL. After incubation for 1 h at 50 °C, the mixture was transformed into *E. coli* DH10B. Clones were analyzed by analytical restriction and subsequent DNA sequencing.

2.5.10 DNA sequencing

Generated plasmid constructs were sequenced by GATC Biotech (Constance, Germany) based on the Sanger method. Primers employed for DNA sequencing are listed in Table 4.

2.5.11 Surface entropy reduction using site-directed mutagenesis

Site-directed mutagenesis was used to modify plasmid DNA to obtain amino acid substitutions in the $(BchYZ)_2$ COR subcomplex of *H. modesticaldum*. BchY and BchZ variants with altered protein surfaces were generated, aiming to facilitate protein crystallization. Surface-exposed amino acids with high conformational entropy are less likely to form intermolecular contacts necessary for crystalization. The surface entropy reduction approach (SER) aims to target clusters of exposed amino acids with high conformational entropy by mutagenesis. Since lysines and glutamates are statistically disfavored at interaction interfaces, the SER approach aims to replace these residues with alanines (Goldschmidt *et al.*, 2007). Based on this method, two BchY and BchZ mutants were generated, respectively. The substituted amino acids are listed in Table 3.

Specifically designed primers (Table 4) carrying the mutated DNA sequence were used in a PCR with the PfuUltra II Hotstart PCR Master Mix (Agilent) as summarized in Table 13. Subsequently, PCR samples were treated with 20 Units DpnI (37 °C, 2 h) to digest the template DNA. Amplified plasmid DNA was transformed into *E. coli* DH10B cells.

Table 13: Site-directed mutagenesis PCR.

Component		**Volume**	
PfuUltra II Hotstart PCR Master Mix		25 µL	
Forward primer (10 pmol/µL)		2.5 µL	
Reverse primer (10 pmol/µL)		2.5 µL	
Template DNA (50 ng/µL)		1.0 µL	
dH_2O		19 µL	
PCR step	**Temperature**	**Time**	
Initial denaturation	95 °C	30 s	
Denaturation	95 °C	30 s	x 20
Annealing	55 °C	60 s	
Elongation	72 °C	390 s	

2.6 Protein biochemical methods

2.6.1 Recombinant protein production of COR subcomplexes

In this study, the COR enzymes from *H. modesticaldum* (Hm) *and R. palustris* (Rp) comprising the proteins BchX, BchY and BchZ were recombinantly produced in *E. coli* BL21(DE3). Plasmid pGEX-6P-1-*bchX* Hm (Rp) was used to produce the COR subcomplex $(BchX)_2$. Subcomplex $(BchYZ)_2$ was initially produced with plasmid pGEX-6P-1-*bchYZ* Hm (Rp). Alternatively, subcomplex $(BchYZ)_2$ was obtained by double transformation of plasmids pGEX-6P-1-*bchY* Hm (Rp) and pACYCDuet-1-*bchZ* Hm (Rp). The employed plasmids are described in Table 3.

Cultivation was carried out aerobically in 1 L baffled flasks with 500 mL LB medium containing the respective antibiotic, Fe(III) citrate and L-cysteine (Table 8). Primary cultures were inoculated with an overnight culture of *E. coli* BL21(DE3) in a ratio of 1:100 and grown at 37 °C and 180 rpm to an OD_{578} of 0.5. Recombinant protein production was initiated with 25 µM IPTG. After 17-20 h at 17 °C and 160 rpm, the

cultures were supplemented with 1.7 mM DT, filled in 1 L gas-tight centrifugation bottles and incubated in an anaerobic chamber (Coy Laboratory Products) for 1.5-2 h. Subsequently, cells were harvested in gas-tight centrifugation bottles at 4'000 g, 20 min and 4 °C (Avanti J-E, Beckman Coulter). The resulting pellet from 3 L culture was resuspended under anoxic conditions in 16 mL buffer A (Table 14) containing 10 mM DTT and stored in rubber-sealed glass bottles at -20 °C.

COR subcomplex $(BchX)_2$ from *R. denitrificans* was produced using plasmids pET-*bchX* Rd and pRKISC (Table 3). The IPTG concentration was increased to 300 µM and the cultivation at 17 °C was performed for 21 h. Cells were harvested without addition of DT or DTT.

Table 14: Buffer A.

Component	Concentration
HEPES	100 mM
NaCl	150 mM
$MgCl_2$	10 mM
pH 7.5 (NaOH), N_2-saturated (anoxic)	

2.6.2 Recombinant protein production of DPOR subcomplexes

Further experiments were performed with *P. marinus* DPOR proteins ChlL, ChlN, ChlB or ChlL variants Y127D and Y127S (Uliczka, 2007). DPOR from *C. tepidum* was produced with plasmids generated by Stefanie Ganskow (Ganskow, 2006). The DPOR subcomplexes were produced in analogy to the COR subcomplexes using the plasmids summarized in Table 3. However, protein production was induced with 50 µM IPTG at 25 °C for 17 h and 160 rpm. Cultures for the production of ChlL variants CLmax and CLmin were shifted to 17 °C after IPTG induction.

2.6.3 Cell disruption and ultracentrifugation

Harvested cells were stored at -20 °C and thawed quickly at room temperature before cell disruption under anoxic conditions using a French press (Polytec). The cell suspension was supplemented with 50 U Benzonase (Jena Bioscience) per liter culture volume and filled into the cooled French press cell (Glen Mills/Thermo). For the purification of ChlL variants CLmax and CLmin, 1.6 mL anoxic buffer (100 mM HEPES pH 7.5, 100 mM ATP, 500 mM NaCl and 200 mM $MgCl_2$) was added per 3 L culture volume before cell disruption. Cells were disrupted by a single passage through the cell at 1'000 psi and the lysate was collected in a rubber-sealed glass bottle. Subsequently, the lysate was filled into airtight 10 mL (rotor 70.1 Ti) or 70 mL (rotor 45 Ti) ultracentrifugation tubes and centrifuged for 65 min at 35'000 rpm in an Optima L-90K ultracentrifuge (Beckman Coulter).

2.6.4 Affinity chromatography

Production and purification of GST-tagged DPOR and COR proteins based on plasmids indicated in Table 3 were performed in an anaerobic chamber using N_2-saturated buffers. Therefore, 10 mL gravity-flow columns were filled with 1 mL Protino glutathione agarose 4B (Macherey-Nagel) equilibrated with 2x 5 mL buffer A (Table 14). The resulting supernatant after ultracentrifugation was loaded onto the column and the resulting flowthrough was added to the column a second time. After a washing step with 2x 5 mL buffer A, the protein was proteolytically liberated by addition of 100-200 U PreScission protease in a total volume of 1.5 mL buffer A (incubation overnight at 17 °C). Liberated proteins were collected and residual proteins were eluted using 3x 1 mL buffer A. Alternatively, the column was washed in the presence of 5 mL buffer A, 3x 1 mL buffer A containing 10 mM ATP and 4x 1 mL buffer A before proteolysis. These pre-elution steps were utilized for DPOR proteins and ChlL variants Y127D and Y127S, which were subsequently subjected to ATPase assays and crystalization experiments.

A modified protocol was used for ChlL variants CLmax and CLmin. Prior to the proteolysis step, the column was washed with 5 mL buffer A, 5 mL buffer A containing 10 mM ATP, 5 mL buffer A containing 5 mM ATP and 10 mL buffer A.

2.6.5 Purification of MoFe and CfbCD

CfbCD from *M. barkeri* strain Fusaro DSM804 was kindly provided by José Vazquez Ramos (AG Layer, Albert-Ludwigs-Universität Freiburg). The purification is described elsewhere (Moore *et al.*, 2017). MoFe protein from *A. vinelandii* was kindly provided by Christian Trncik (AG Einsle, Albert-Ludwigs-Universität Freiburg). The purification of MoFe was performed as detailed in previous work (Spatzal *et al.*, 2011).

2.6.6 Concentration of purified proteins

Proteins were concentrated under anoxic conditions if subsequent methods required high protein concentrations. Therefore, Amicon ultra 0.5 mL centrifugal filter devices (Merck Millipore) with a 30 kDa cutoff were used according to the manufacturer's instructions. Alternatively, a 10 mL Amicon stirred cell Model 8010 (Merck Millipore) was operated with Ultracel 30 kDa ultrafiltration discs (Merck Millipore) according to the manufacturer's instructions.

2.6.7 Determination of protein concentration

Bradford assays (Bradford, 1976) were performed to determine the concentration of protein solutions. Commercial Bradford reagent (Sigma) was used according to the manufacturer's instructions with bovine serum albumin as a standard. Protein concentrations (µM) of nitrogenase-like enzyme subcomplexes were calculated based on the dimer (reductase subcomplex) or tetramer (catalytic subcomplex).

2.6.8 Sodium dodecyl sulfate-polyacrylamide gel electrophoresis

Purified proteins were analyzed by sodium dodecyl sulfate-polyacrylamide gel electrophoresis (SDS-PAGE). The presence of SDS unfolds proteins into individual polypeptides, which are separated according to their molecular mass (Laemmli, 1970). Protein samples were mixed with SDS loading buffer and incubated for 10 min at 95 °C.

The denatured samples were stored at -20 °C or directly loaded onto self-casted 12 % acrylamide gels together with 7 µL of an unstained protein molecular weight marker (Thermo Fisher). A prestained marker was used for subsequent blotting purposes. Electrophoresis was carried out at 45 mA (1 gel) until the bromophenol dye band left the gel. Gels were stained with coomassie brilliant blue G 250 (Carl Roth). Alternatively, gels were subjected to blotting.

Table 15: Solutions for SDS-PAGE.

2x SDS loading buffer	**Concentration**
Tris-HCl pH 6.8	100 mM
Glycerol	40 % (w/v)
β-Mercaptoethanol	2 % (v/v)
SDS	3.2 % (w/v)
Bromophenol blue	0.2 % (w/v)
Running gel (12 %)	**Volume (1 gel)**
Rotiphorese Gel 30	2 mL
1.5 M Tris-HCl pH 8.8 + 0.4 % (w/v) SDS	1.25 mL
dH_2O	1.75 mL
10 % (w/v) ammonium persulfate	50 µL
Tetramethylethylendiamine	5 µL
Stacking gel (6 %)	**Volume (1 gel)**
Rotiphorese Gel 30	0.5 mL
0.5 M Tris-HCl pH 6.8 + 0.4 % (w/v) SDS	0.625 mL
dH_2O	1.375 mL
10 % (w/v) ammonium persulfate	25 µL
Tetramethylethylendiamine	2.5 µL
1x Running buffer	**Concentration**
Tris	25 mM
Glycine	192 mM
SDS	0.1 % (w/v)
Coomassie stain	**Concentration**
Ethanol	30 % (v/v)
Acetic acid	10 % (v/v)
Coomassie brilliant blue G 250	0.25 % (w/v)
Destaining solution	**Concentration**
Ethanol	30 % (v/v)
Acetic acid	10 % (v/v)

2.6.9 Western blot and N-terminal sequencing

N-terminal sequencing of proteins was performed to confirm the identity of purified COR proteins. Protein samples were separated by SDS-PAGE and the resulting unstained gel was utilized in a semi-dry western blot. Therefore, gel and two blotting papers were equilibrated in Towbin-buffer for 15 min. The polyvinylidene difluoride (PVDF) membrane was activated in 100 % methanol for 15 min. After blotting (Trans-Blot Turbo, Bio-Rad) for 10 min with 25 V, the PVDF membrane was stained for 30 min with Ponceau S. Subsequently, the membrane was washed thoroughly and the respective bands were subjected to N-terminal sequencing performed by Beate Jaschok-Kentner at the Helmholtz Centre for Infection Research (HZI) Braunschweig.

Table 16: Towbin-buffer and Ponceau S stain.

Towbin-buffer	**Concentration**
Tris-HCl pH 9.5	25 mM
Glycine	192 mM
Methanol	20 % (v/v)
1x Ponceau S stain	**Concentration**
Ponceau S	0.4 % (w/v)
Trichloroacetic acid	6 % (w/v)
Sulfosalicylic acid	6 % (w/v)

2.6.10 Analytical and preparative gel filtration under anoxic conditions

Gel filtration under anoxic conditions was performed to determine the native molecular mass of purified proteins. Alternatively, gel filtration was applied as a second purification step after affinity chromatography to remove protein aggregates. Columns HiLoad 16/600 or 26/600 Superdex 200 (GE Healthcare) were previously equilibrated in the presence of buffer A (Table 14) unless indicated otherwise. A gel filtration marker kit (Sigma-Aldrich) comprising β-amylase (M_r=200'000), albumin (M_r=66'000), carbonic anhydrase (M_r=29'000) and cytochrome c (M_r=12'400) was used to calibrate the respective column. Samples (0.25-3 mL, 2-50 mg/mL) were run with 1-1.5 mL/min and the eluate absorption was monitored at 260, 280 and 420 nm. Preparative chromatography was operated with fraction sizes of 2-5 mL.

2.6.11 UV-Vis spectroscopy

UV-Vis spectra of purified proteins or of COR/DPOR activity assay samples were recorded on a V-650 spectrophotometer (Jasco). Activity assay samples were analyzed in QS high precision cell quartz cuvettes (Hellma Analytics) from 800-500 nm. Protein samples were studied under anoxic conditions with rubber-sealed cuvettes from 600-250 nm. Pchlide and Chlide preparations were quantified in 80 % acetone using extinction coefficients 30.4 $mM^{-1}cm^{-1}$ at 626 nm for Pchlide (Brouers and Michel-Wolwertz, 1983) and 74.9 $mM^{-1}cm^{-1}$ at 667 nm for Chlide (McFeeters *et al.*, 1971). All measurements were performed with a 200 nm/min scanning speed and a UV-Vis bandwidth of 1 nm.

2.6.12 EPR spectroscopy

EPR spectroscopy of COR subcomplexes was kindly performed by Marco Massmig and Dr. Edward J. Reijerse (MPI for Chemical Energy Conversion, Mülheim an der Ruhr) as described elsewhere (Massmig *et al.*, 2020). Samples were prepared under anoxic conditions. Proteins were supplemented with 10 mM DT (15 min incubation), transferred into quartz EPR tubes and frozen in liquid nitrogen.

2.6.13 *In vitro* [Fe-S]-cluster reconstitution

In some cases, [Fe-S]-clusters of purified proteins were chemically reconstituted under anoxic conditions at 17 °C based on previously described methods (Freibert *et al.*, 2017). Ferric ammonium citrate (20 mM) and lithium sulfide (40 mM) stock solutions were prepared freshly in buffer A. Purified proteins (20-100 µM) were reduced with DTT using a 100-fold molar excess of the protein concentration.

After 1 h incubation, ferric ammonium citrate was added stepwise up to a 5-fold molar excess of the protein concentration. The resulting mixture was incubated for 10 min and stepwise supplemented with lithium sulfide up to a 5-fold molar excess of the protein concentration. Subsequently, the mixture was incubated for 5 min and centrifuged at 12´100 g for 5 min. Reconstituted proteins were desalted using NAP-5 columns (GE Healthcare) according to the manufacturer's instructions.

2.6.14 Determination of iron and sulfur contents

The iron content of purified proteins was determined colorimetrically using the bathophenanthroline method (Saywell and Cunningham, 1937; Fortune and Mellon, 1938; Lovenberg *et al.*, 1963). The labile sulfide content of protein samples was determined based on the method reported by (Beinert, 1983).

2.7 Isolation of Chlide and Pchlide

In this study, Chlide was utilized in enzyme activity assays, binding studies and crystallization experiments. The preparation of Chlide was kindly performed by Simone Virus and Sylvia Stroz (Stroz, 2018) based on previously reported methods (Müller *et al.*, 2011). The employed double mutant strain *R. capsulatus* CB1200 (Bollivar *et al.*, 1994) is disrupted in *bchF* and *bchZ*. Therefore, Chlide is accumulated and excreted in the presence of Tween 80 (Müller *et al.*, 2011). *R. capsulatus* CB1200 cells were grown in the presence of 10 µg/mL spectinomycin on two PY plates. After three days at 30 °C, all grown colonies were resuspended in 50 mL RCV 2/3 PY medium. The liquid preculture was incubated in a 100 mL flask at 30 °C and 180 rpm in the dark. Five mL of the red-colored preculture was used to inoculate ten 100 mL flasks containing 45 mL RCV 2/3 PY medium supplemented with 0.2 % Tween 80, respectively. The cultures were cultivated in the dark at 30 °C and 180 rpm for three days. Subsequently, the green-colored cultures were centrifuged (2'000 g, 4 °C, 20 min) and the supernatant was subjected to solid-phase extraction utilizing three subsequent Sep-Pak C18 columns (Waters). The columns were equilibrated with 50 mL methanol and 50 mL RCV 2/3 PY medium (0.2 % Tween 80) using a peristaltic pump. Next, the Chlide containing supernatant was applied to the column and subsequently washed (reversed flow) with 15 mL 20 % (v/v) acetone in 10 mM tricine pH 8. Chlide was eluted in 100 % acetone. The solvent was evaporated at room temperature and the green pigment was dissolved in DMSO.

R. capsulatus ZY5 was used to isolate Pchlide subjected to enzyme activity assays and binding studies. This mutant strain contains a mutation in *F108* (*bchL*). Thus, Pchlide is accumulated and not converted to Chlide. The produced Pchlide is a mixture of 14 % monovinyl Pchlide and 86 % divinyl Pchlide (Yang and Bauer, 1990). Pchlide isolation was kindly performed by Simone Virus based on previously reported methods (Heyes *et al.*, 2002). *R. capsulatus* ZY5 was cultivated under darkness in PY medium in the presence of 5 µg/mL kanamycin, 1 mM $MgCl_2$ and 1 mM $CaCl_2$. Several colonies from a PY plate (3-5 days at 30 °C) were used to inoculate a 50 mL preculture in a 50 mL reaction tube. This culture was incubated on a rotating incubator for 3-4 days at 34 °C. A 600 mL culture in a 1 L flask was inoculated with 20 mL preculture. 12 autoclaved polyurethane foam bungs were added to the culture medium to adsorb the produced pigments. After cultivation for three days at 34 °C and 130 rpm (Multitron Pro, Infors), the foam bungs were dried and pigments were extracted with 2x 100 mL acetone.

The extract was purified using 25 mL CM Sepharose CL-6B (Pharmacia Fine Chemicals) previously equilibrated with 3x 50 mL acetone. The pigment extract was gradually applied onto the column and washed with 125 mL acetone/methanol (95:5, v/v). Pchlide was eluted with 3x 50 mL acetone/methanol (75:25, v/v). A Rotavapor R-300 (Büchi) was used at 400 mbar and 45 °C to evaporate the solvent to a volume of 1-2 mL. The remaining solvent was removed in a stream of nitrogen at room temperature and the pigment was dissolved in DMSO.

Pchlide and Chlide were stored at -20 °C and the respective concentration was determined spectroscopically (2.6.11 UV-Vis spectroscopy).

2.8 Enzyme activity assays

2.8.1 Homologous DPOR and COR activity assays

Purified COR and DPOR enzymes were assayed under anoxic conditions based on methods established in previous studies (Bröcker *et al.*, 2008a; Bröcker *et al.*, 2008b; Wätzlich *et al.*, 2009). Pchlide isolated from *R. capsulatus* ZY5 was used as a substrate in DPOR assays and coupled DPOR/COR assays. Chlide isolated from *R. capsulatus* CB1200 was utilized as COR substrate.

Standard *in vitro* assays were carried out in a total volume of 250 µL in the presence of buffer A (Table 14). A master mix containing 20 mM phosphocreatine, 0.7 mM DT, 5 mM DTT, 2 mM ATP, 21 U creatine phosphokinase and 20 µM substrate was used to initiate the assay. Standard assays were conducted with 300-444 pmol catalytic subcomplex and 800-1450 pmol reductase subcomplex. Alternatively, the reductase subcomplex was supplemented as cell-free extract. The required amount was determined in preliminary assays. Reactions were incubated at 25 or 37 °C and 500 rpm for 60 min in the dark.

Coupled DPOR/COR activity was examined as follows: Cell-free extracts containing the DPOR subcomplexes or purified proteins were used to produce Chlide *via* the DPOR enzyme. The ratio of reductase or catalytic subcomplex-containing cell-free extract was determined in preliminary assays. After 30 min at 25 °C and 500 rpm, DPOR assays were supplemented with 2.5 µL 200 mM ATP and COR subcomplexes $(BchX)_2$ and $(BchYZ)_2$ using 800-1450 pmol reductase subcomplex and 300-444 pmol catalytic subcomplex. Subsequently, assays were incubated at 37 °C and 500 rpm for 30 min. Reactions were stopped with 500 µL acetone and subjected to UV-Vis analysis after two centrifugation steps (12´100 g, 15 min, 4 °C). Control experiments were performed in the absence of proteins.

2.8.2 Heterologous and chimeric activity assays

The interaction of nitrogenase-like DPOR, COR and CfbCD proteins was characterized in heterologous and chimeric activity assays employing DPOR and COR enzymes from different organisms. Assays were performed by combining catalytic and reductase subcomplexes of different sources in the described standard assay. Chimeric activity between CfbD and different COR and DPOR reductases was investigated by José Vazquez Ramos (AG Layer, Albert-Ludwigs-Universität Freiburg) as described previously (Moore *et al.*, 2017). The following modifications were made: Assays were

carried out in buffer A supplemented with 2 mM DT, 4 mM DTT and 5-8 µM Ni^{2+}-sirohydrochlorin *a*,*c*-diamide for 1, 2 and 20 h at 37 °C. Reductase and catalytic subcomplexes were employed in a molar ratio of 1:1 or 2:1. Additionally, assays were performed in the presence of an ATP-regenerating system in analogy to the DPOR/COR standard assays. Table 17 lists all assayed proteins.

Table 17: Proteins employed in heterologous and chimeric activity assays.
All combinations of the specified reductase (*) and catalytic components (#) of nitrogenase-like enzymes were employed in heterologous and chimeric activity assays.

COR	Organism	Reference
$(BchX)_2$*	*H. modesticaldum*	This work
	R. palustris	This work
	R. denitrificans	(Wätzlich *et al.*, 2009)
$(BchYZ)_2$#	*H. modesticaldum*	This work
	R. palustris	This work
DPOR		
$(ChlL)_2$*	*P. marinus*	(Uliczka, 2007)
$(BchL)_2$*	*C. tepidum*	(Ganskow, 2006)
$(ChlNB)_2$#	*P. marinus*	(Uliczka, 2007)
$(BchNB)_2$#	*C. tepidum*	(Ganskow, 2006)
CfbCD		
CfbC*	*M. barkeri*	(Moore *et al.*, 2017)
CfbD#	*M. barkeri*	(Moore *et al.*, 2017)

2.8.3 Preparation of the methyl viologen cation radical as an alternative reductant

In some homologous DPOR assays, the reductant DT was substituted with the methyl viologen cation radical ($MV^{+\cdot}$). $MV^{+\cdot}$ was produced in 1 mL anoxic 0.1 M Na_2CO_3 supplemented with 10 mg glucose and 5 mg methyl viologen dichloride. The mixture was incubated for 1 h at 50 °C under anoxic conditions and the resulting concentration of the violet-blue $MV^{+\cdot}$ was determined spectroscopically using the extinction coefficient ε_{600} = 8.25 mM^{-1} cm^{-1} (Yu and Wolin, 1969).

2.9 Reductant-independent ATPase activity assays

The reductant-independent ATPase activity of *P. marinus* $(ChlL)_2$ and variants Y127D and Y127S was investigated using a colorimetric phosphate quantification assay (PiColorLock, Expedeon). Reactions were performed in a total volume of 200 µL buffer A (Table 14) with 1 µM $(ChlL)_2$ or variants Y127D and Y127S. Furthermore, reductant-independent ATPase activity of $(ChlL)_2$ or variants Y127D and Y127S was monitored in the presence of 0.5 µM MoFe or $(ChlNB)_2$.

A standard assay was initiated by the addition of 10 µL (10 mM) ATP and incubated at 25 °C for 10, 30 and 60 min. Subsequently, samples were mixed with freshly prepared phosphate detection reagent according to the manufacturer's instructions. The absorption of the resulting malachite green complex was measured at a wavelength of 600 nm in a microplate reader (Multiskan GO, Thermo Scientific). The background phosphate amounts were monitored in control experiments in the absence of ATP or individual proteins. All results were reproduced in three independent experiments.

2.10 Nucleotide-dependent interaction of $(ChlL)_2$ with the MoFe protein

The nucleotide-dependent interaction of *P. marinus* $(ChlL)_2$ or variants Y127D, Y127S, CLmax and CLmin with the MoFe protein was investigated (Figure 8). Therefore, 2 nmol of the respective GST-tagged reductase (bait protein) was immobilized on 0.3 mL Protino glutathione agarose 4B (Macherey-Nagel) previously equilibrated with buffer A (Table 14). The reductase subcomplex was supplemented with 450 µL (2.5 nmol) MoFe protein (prey protein) in buffer A in the presence of 10 mM ATP, 10 mM ADP, 10 mM ADP·AlF_4^- or 1.5 mM AMP-PNP, respectively. ADP·AlF_4^- was prepared as detailed elsewhere (Moser *et al.*, 2019). After 15 min incubation, unbound proteins were removed with 3x 0.5 mL and 1x 1 mL buffer A containing the respective nucleotide. Bound proteins were proteolytically liberated using 40 U PreScission protease for 17 h at 17 °C and analyzed by SDS-PAGE. Band intensities of bait and prey proteins were determined by means of densitometry using GelQuant.NET (BiochemLabSolutions). Bait to prey protein ratios were calculated, taking into account the molecular mass of the respective subcomplexes. All experiments were performed in triplicates.

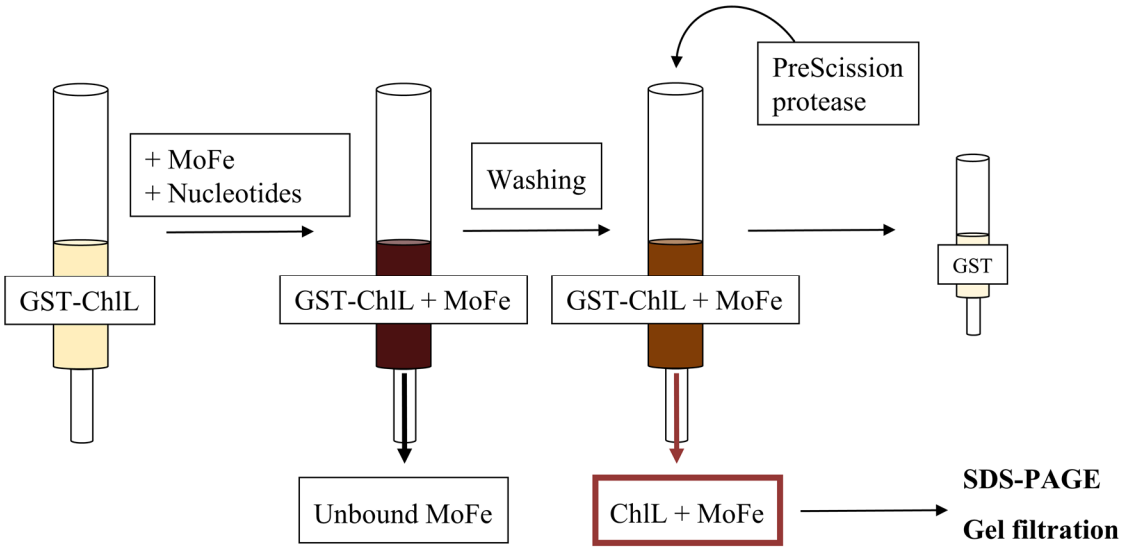

Figure 8: Schematic representation of the interaction-assay used to detect complex formation between MoFe and DPOR reductase $(ChlL)_2$.
Column bound GST-ChlL (2 nmol) was supplemented with 2.5 nmol MoFe and nucleotides ATP (10 mM), ADP (10 mM), AMP-PNP (1.5 mM) or MgADP·AlF_4^- (10 mM), respectively. After incubation, excess MoFe was washed from the column and the protein complex was liberated by PreScission protease treatment. Eluted proteins were analyzed by SDS-PAGE or gel filtration.

2.11 Protein crystallization

In this study, sitting drop vapor diffusion was used for crystallization screenings. A protein/precipitant mixture is equilibrated against a reservoir containing a higher precipitant concentration. Water diffuses from the protein/precipitant mixture to the reservoir, driving the target protein towards a supersaturated state (Gavira, 2016).

Crystallization screenings were performed under anoxic conditions in a MACS MG-1000 anaerobic workstation (Don Whitley Scientific) using 96-well plates and commercially available screens listed in Table 2. The employed Intelli-plate 96-3 (Art Robbins

Instruments) offers 96 reservoirs per plate with three wells (1-2 µL) per reservoir. Each reservoir was filled with 60 µL screening buffer and the plate was incubated for two days in the anaerobic workstation (including 2x 30 min with open lid) to ensure anoxic conditions before adding the protein solution. Plates were sealed with plastic film and stored at 17 °C. Chlide containing plates were incubated in the dark (plates sealed with aluminum foil). Proteins and protein complexes subjected to crystallization screening experiments and the respective conditions are summarized in Table 18. Diffraction analysis with potential protein crystals was performed at the HZI Braunschweig. Alternatively, experiments were kindly performed by Dr. Peer Lucat (HZI Braunschweig) at the Deutsches Elektronen-Synchrotron (DESI) Hamburg.

Table 18: List of performed crystallization screenings.
Protein or protein complexes were purified as described in the Materials and Methods section. Chlide was added to the protein solution if not indicated otherwise. Proteins subjected to gel filtration prior to crystallization screening are labeled with "GPC". For each prepared plate, the used screening kit, proteins and additives, drop compositions and concentrations of purified proteins are listed. Hm: *H. modesticaldum*, Rp: *R. palustris*.

No.	Screen	Proteins and additives	Drop composition (µL protein + µL reservoir)	Protein concen-tration (mg/mL)
P1	JCSG I	$(BchYZ)_2$ Hm + 5x molar excess Chlide (added during affinity chromatography)	1+1	18.4
P2	JCSG II		1+1	18.4
P3	Cryos Suite		1+1	18.4
P4	Refinement of JCSG II 56,82 and Cryos Suite 75		1.1+0.9	18.4
P5	JCSG I	$(BchYZ)_2$ Hm + 3x molar excess $(BchX)_2$ Hm + 4x molar excess AMP-PNP + 3x molar excess Chlide	1+1	26.0
		$(BchYZ)_2$ Hm + 3x molar excess Chlide	1+1	26.0
P6	JCSG II	$(BchYZ)_2$ Hm + 3x molar excess $(BchX)_2$ Hm + 4x molar excess AMP-PNP + 3x molar excess Chlide	1+1	26.0
		$(BchYZ)_2$ Hm + 3x molar excess Chlide	1+1	26.0
P7	Cryos Suite	$(BchYZ)_2$ Hm + 3x molar excess $(BchX)_2$ Hm + 4x molar excess AMP-PNP + 3x molar excess Chlide	1+1	26.0
		$(BchYZ)_2$ Hm + 3x molar excess Chlide	1+1	26.0
P8	JCSG I	$(BchYZ)_2$ Hm	1+1	18.3
P9	JCSG II		1+1	18.3
P10	Cryos Suite		1+1	18.3
P11	Cryos Suite		0.8+1.2	18.3
			1+1	18.3
			1.2+0.8	18.3

P12	ProComplex	$(BchYZ)_2$ Hm	1+1	16.5
		$(BchYZ)_2$ Hm + 5x molar excess Chlide (added during affinity chromatography)	1+1	17.1
P13	JCSG+	$(BchYZ)_2$ Hm	1+1	16.5
		$(BchYZ)_2$ Hm + 5x molar excess Chlide (added during affinity chromatography)	1+1	17.1
P14	JCSG+	$(BchYZ)_2$ Hm	1+1	16.5
		$(BchYZ)_2$ Hm + 5x molar excess Chlide (added during affinity chromatography)	1+1	17.1
P15	Cryos Suite	$(BchYZ)_2$ Rp	1+1	24.3
		$(BchYZ)_2$ Rp + 5x molar excess Chlide (added during affinity chromatography)	1+1	18.1
P16	JCSG+	$(BchYZ)_2$ Rp	1+1	24.3
		$(BchYZ)_2$ Rp + 5x molar excess Chlide (added during affinity chromatography)	1+1	18.1
P17	Cryos Suite	$(BchYZ)_2$ Hm (GPC)	1+1	14.0
		$(BchYZ)_2$ Hm (GPC) + 3x molar excess Chlide	1+1	14.0
P18	ProComplex	$(BchYZ)_2$ Hm (GPC)	1+1	14.0
		$(BchYZ)_2$ Hm (GPC) + 3x molar excess Chlide	1+1	14.0
P19	Cryos Suite	$(BchYZ)_2$ Hm (GPC) + 3x molar excess Chlide	1+1	14.0
P20		$(BchYZ)_2$ Hm (GPC) + 3x molar excess Chlide before GPC	1+1	8.5
P21	JCSG+	$(BchYZ)_2$ Hm (GPC) + 3x molar excess Chlide before GPC	1+1	8.5
P22	Refinement of P18F5	$(BchYZ)_2$ Hm (GPC) + 3x molar excess Chlide	1+1	5.0
		$(BchYZ)_2$ Hm (GPC) + 3x molar excess Chlide	1.2+0.8	5.0
P23	Cryos Suite	$(BchYZ)_2$ M1 + 3x molar excess Chlide	1+1	5.0
		$(BchYZ)_2$ M2 + 3x molar excess Chlide	1+1	9.0
P24	ProComplex	$(BchYZ)_2$ M1 + 3x molar excess Chlide	1+1	5.0
		$(BchYZ)_2$ M2 + 3x molar excess Chlide	1+1	9.0
P25	JCSG+	$(BchYZ)_2$ M1 + 3x molar excess Chlide	1+1	5.0
		$(BchYZ)_2$ M2 + 3x molar excess Chlide	1+1	9.0
P26	Refinement of P18F5	$(BchYZ)_2$ Hm (GPC) + 3x molar excess Chlide	1+1	14.0
P27	Cryos Suite	$(BchYZ)_2$ M2 + 3x molar excess Chlide, [FeS] cluster were chemically reconstituted	1+1	17.8
P28	ProComplex		1+1	17.8
P29	JSCG+		1+1	9.2
P30	JCSG II		1+1	9.2
P31	Refinement of P30A11, P28A3 and P27F7		0.8+1.2	
			1+1	
			1.2+0.8	
P32	JB Penta-erythritol	$(BchYZ)_2$ Hm (GPC) + 3x molar excess Chlide	1+1	5.2
		$(BchYZ)_2$ Hm (GPC)	1+1	5.2

P33	Morpheus	$(BchYZ)_2$ Hm (GPC) + 3x molar excess Chlide	1+1	11.6
		$(BchYZ)_2$ Hm (GPC)	1+1	11.6
P34	Morpheus	$(BchYZ)_2$ Hm (GPC) + 3x molar excess Chlide	1+1	9.4
		$(BchYZ)_2$ Hm (GPC)	1+1	9.4
P35	Wizard Cryo	$(BchYZ)_2$ Hm (GPC) + 3x molar excess Chlide	1+1	5.7
		$(BchYZ)_2$ Hm (GPC)	1+1	5.7
P36	Wizard Cryo	$(BchYZ)_2$ M2 (GPC) + 3x molar excess Chlide	1+1	8.3
		$(BchYZ)_2$ M2 (GPC)	1+1	8.3
P37	Cryos Suite	$(BchYZ)_2$ Rp (GPC) + 3x molar excess Chlide	1+1	16.5
		$(BchYZ)_2$ Rp (GPC)	1+1	16.5
P38	JCSG I	$(BchYZ)_2$ M2 (GPC) + 3x molar excess Chlide	1+1	10.7
		$(BchYZ)_2$ M2 (GPC)	1+1	10.7
P39	Morpheus	$(ChlL)_2MoFe(ChlL)_2$, complex formation on glutathione agarose resin, 1.5 mM AMP-PNP	1+1	18.4
			1+1	9.2
			1+1	5.0
P40	Cryos Suite		1+1	18.4
			1+1	9.2
			1+1	5.0
P41	Morpheus	MoFe + 4x molar excess $(ChlL)_2$ + 2 mM AMP-PNP	1+1	13.9
			1+1	7.0
		MoFe + 3x molar excess $(ChlL)_2$ Y127S + 2 mM AMP-PNP	1+1	6.6
P42	Cryos Suite	MoFe + 4x molar excess $(ChlL)_2$ + 2 mM AMP-PNP	1+1	13.9
			1+1	7.0
		MoFe + 3x molar excess $(ChlL)_2$ Y127S + 2 mM AMP-PNP	1+1	6.6
P43	ProComplex	MoFe + 4x molar excess $(ChlL)_2$ + 2 mM AMP-PNP	1+1	13.9
			1+1	7.0
P44	JCSG+		1+1	13.9
			1+1	7.0
P45	Wizard Cryo		1+1	13.9
			1+1	7.0
P46	Refinement of P42: 68, 70 and P45: 78	MoFe + 4x molar excess $(ChlL)_2$ (GPC) + 2 mM AMP-PNP, MoFe + 3x molar excess $(ChlL)_2$ Y127S + 2 mM AMP-PNP	1+1	
			1.1+0.9	
			1.2+0.8	
P47	Cryos Suite	MoFe + 3x molar excess $(ChlL)_2$ (GPC) + 5 mM AMP-PNP + 5 mM DTT	1+1	13.0
P48	Morpheus		1+1	13.0
P49	Wizard Cryo		1+1	13.0

2.12 Microscale thermophoresis

Microscale thermophoresis (MST) allows for the detection and quantification of biomolecular interactions based on the directed movement of molecules in a temperature gradient (thermophoresis). This movement of molecules is affected by changes in size, charge, hydration shell and conformation of the analyzed molecules. MST utilizes attached or intrinsic fluorophores to monitor the mobility of molecules in close-to-native conditions (Jerabek-Willemsen *et al.*, 2014). The basic principle of MST is depicted in Figure 9.

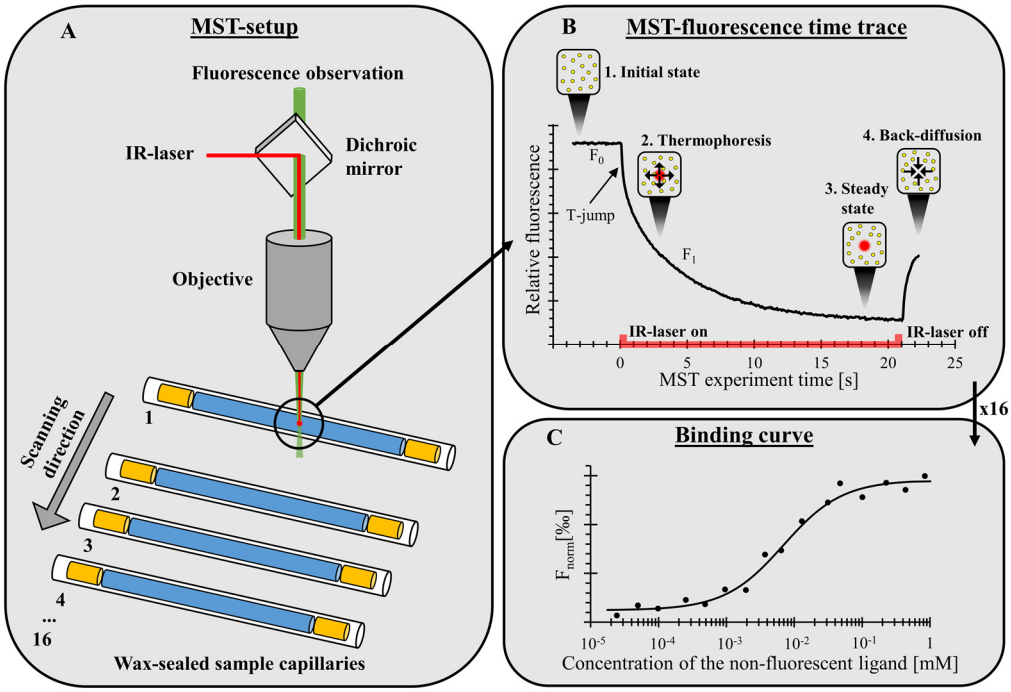

Figure 9: Schematic representation of the basic principles of MST.
A: Schematic representation of the MST-setup. Fluorescent molecules and non-fluorescent molecules (ligands) are loaded into a glass capillary. In this study, all capillaries were sealed with wax to ensure anoxic conditions. A microscopic temperature gradient is generated by an infrared (IR) laser and the fluorescence of labeled molecules in the heated region is monitored. **B**: Typical fluorescence time trace of a MST experiment. Upon IR-laser activation, a fast fluorescence change (<1 s) termed temperature jump (T-jump) is observed. Subsequently, thermophoresis occurs in a much slower time scale from seconds to minutes. The initial fluorophore distribution changes as molecules from the locally heated region move towards the outer colder region. Accordingly, fluorescence intensities within the monitored region are decreasing until a steady-state is reached. Finally, the IR-laser is switched off and the initial state is slowly restored, driven by mass diffusion. **C**: Binding curve yielded by a series of MST experiments using increasing amounts of non-fluorescent ligands mixed with constant amounts of fluorescent molecules. The normalized fluorescence (F_{norm}, linear y-axis) is plotted against the concentration of the titrated non-fluorescent ligand (log10 x-axis). F_{norm} in per mil (‰) is defined as the quotient of the fluorescence after thermodiffusion (F_1) and the initial fluorescence (F_0).

A sample solution of fluorescent molecules and non-fluorescent molecules (ligands) is loaded into a glass capillary. Infrared (IR)-laser light (1480 nm) is focused on the solution, generating a microscopic temperature gradient of 1-6 °C in a 2 nL volume. Concurrently, fluorescent molecules are excited and emitted light from the heated region is monitored. Upon IR-laser activation, the constant initial fluorescence intensity changes due to two

occurring effects: The first effect is termed temperature jump (T-jump) and describes a fast (<1 s) temperature-dependent fluorescence change. The T-jump is an inherent property of the fluorophore and is affected by the fluorophore's local surroundings like conformational changes and binding events. Subsequently, thermophoresis occurs in a much slower time scale from seconds to minutes. The fluorophore distribution changes as molecules from the locally heated region move towards the outer colder region. Thereby, fluorescence intensities within the monitored region are decreasing until a steady-state is reached. The movement is affected by molecular properties such as size, charge, hydration shell and conformation. Accordingly, the monitored changes in fluorescence over time can be used to detect ligand binding. Finally, the IR-laser is switched off and the initial state is slowly restored, driven by mass diffusion (Seidel *et al.*, 2013; Jerabek-Willemsen *et al.*, 2014).

The determination of binding constants requires a series of MST experiments using increasing amounts of non-fluorescent ligands mixed with constant amounts of fluorescent molecules. The normalized fluorescence (F_{norm}, linear y-axis) is plotted against the concentration of the titrated non-fluorescent ligand (log10 x-axis) to calculate binding constants. F_{norm} in per mil (‰) is defined as the quotient of the fluorescence after thermodiffusion (F_1) and the initial fluorescence (F_0) or fluorescence after T-jump (Seidel *et al.*, 2013; Jerabek-Willemsen *et al.*, 2014). The Monolith NT.115 (NanoTemper) allows to determine F_1 after different time points during the thermophoresis phase. In this study, F_1 was determined after 4-5 s.

MST under anoxic conditions was applied to examine the homologous interaction between the DPOR subcomplexes $(ChlNB)_2$ and $(ChlL)_2$ in the presence of ADP or the ATP analog AMP-PNP. Alternatively, chimeric interactions between $(ChlL)_2$ and MoFe were analyzed. Labeling reactions were performed in a total volume of 200 µL buffer E (Table 19) containing 10 µM protein and 60 µM cyanine 5 succinimidyl (NHS) ester (Lumiprobe). After 30 min incubation in the dark at 17 °C, the unreacted dye was removed according to the manufacturer's instructions with PD SpinTrap G-25 columns (GE Healthcare) equilibrated with buffer E.

Labeled proteins were adjusted to 40-200 nM with buffer E supplemented with 0.05 % (w/v) Tween 20. In order to verify sufficient labeling and exclude protein adsorption to capillary surfaces, assay pretests were carried out according to the manufacturer's instructions (NanoTemper). The respective unlabeled protein subcomplex was prepared in a series of 16 dilutions (1:2) in buffer E in a total volume of 10 µL (e.g. 200 µM, 100 µM, …, 6.1 nM). Each dilution was supplemented with 10 µL of labeled protein and filled into three Monolith NT.115 premium capillaries (NanoTemper) in an anaerobic chamber (Coy Laboratory Products). The capillaries were sealed with wax (pressed into solid tealight wax) and measured in a Monolith NT.115 (NanoTemper) at room temperature. Instrument parameters were adjusted to 20-100 % LED power and medium MST power.

Table 19: Buffer E.

Component	Concentration
HEPES	20 mM
NaCl	150 mM
$MgCl_2$	5 mM
pH 7.5 (NaOH), N_2-saturated (anoxic)	

3. Results and discussion

In the first part of the present study, COR enzymes from *H. modesticaldum* and *R. palustris* were investigated. The production and purification of individual COR subcomplexes was established and resulting proteins were characterized biochemically. Moreover, COR subcomplexes were subjected to crystallization experiments and heterologous or chimeric activity assays. In the second part, *P. marinus* $(ChlL)_2$ reductase and variants were tested in combination with MoFe as a potential substitute for the nitrogenase reductase $(NifH)_2$.

3.1 Chlorophyllide *a* oxidoreductase (COR)

Protein crystal structures are of central importance to elucidate the detailed reaction mechanism of enzymes. However, the crystalization process remains a bottleneck due to the challenging prediction of protein crystallizability (Gavira, 2016). To date, no crystal structure is available for the COR enzyme, which catalyzes the stereospecific two-electron reduction of Chlide to Bchlide. Crystal structures of the related enzymes nitrogenase and DPOR provided important insights into the family of nitrogenase and nitrogenase-like enzymes (Schindelin *et al.*, 1997; Moser *et al.*, 2013). Nitrogenase, DPOR and COR share a high degree of sequence identity. Similarly, the cofactor ligands are highly conserved for DPOR and COR. The [4Fe-4S] cluster of the COR enzyme was characterized *via* EPR spectroscopy by analogy to the DPOR enzyme (Wätzlich *et al.*, 2009; Kiesel *et al.*, 2015). Moreover, previous studies concluded that the initial electron transfer steps leading to the formation of Bchlide are closely related to the DPOR reaction mechanism (Kiesel *et al.*, 2015). In the first part of this study, COR enzymes from *H. modesticaldum* (termed COR Hm) and *R. palustris* (termed COR Rp) were investigated and crystalization screenings were performed.

3.1.1 Cloning, production and purification of COR subcomplexes $(BchX)_2$ and $(BchYZ)_2$

To study the COR enzyme, the corresponding genes *bchX*, *bchY* and *bchZ* from the thermophilic anoxygenic phototroph *H. modesticaldum* and from the metabolically versatile phototrophic purple nonsulfur bacterium *R. palustris* were cloned into the *E. coli* expression vector pGEX-6P-1. The resulting plasmids (Table 3) were used to produce the proteins in *E. coli* BL21(DE3). In a first approach, COR subcomplex $(BchYZ)_2$ was

bicistronically overproduced using plasmid pGEX-6P-1-*bchYZ* Hm (or pGEX-6P-1-*bchYZ* Rp). Alternatively, $(BchYZ)_2$ was produced using a dual-plasmid strategy employing plasmid pGEX-6P-1-*bchY* Hm (or pGEX-6P-1-*bchY* Rp) in combination with pACYCDuet-1-*bchZ* Hm (or pACYCDuet-1-*bchZ* Rp). Both strategies make use of the strong interaction between GST-tagged BchY and untagged BchZ to co-purify the $(BchYZ)_2$ subcomplex as demonstrated for related DPOR and COR enzymes (Fujita and Bauer, 2000; Wätzlich *et al.*, 2009). COR subcomplex $(BchX)_2$ was overproduced using plasmid pGEX-6P-1-*bchX* Hm (or pGEX-6P-1-*bchX* Rp). Proteins were purified *via* the N-terminal GST-tag under anoxic conditions employing PreScission protease for the liberation of the untagged target protein. The SDS-PAGE analysis for the purified proteins is depicted in Figure 10.

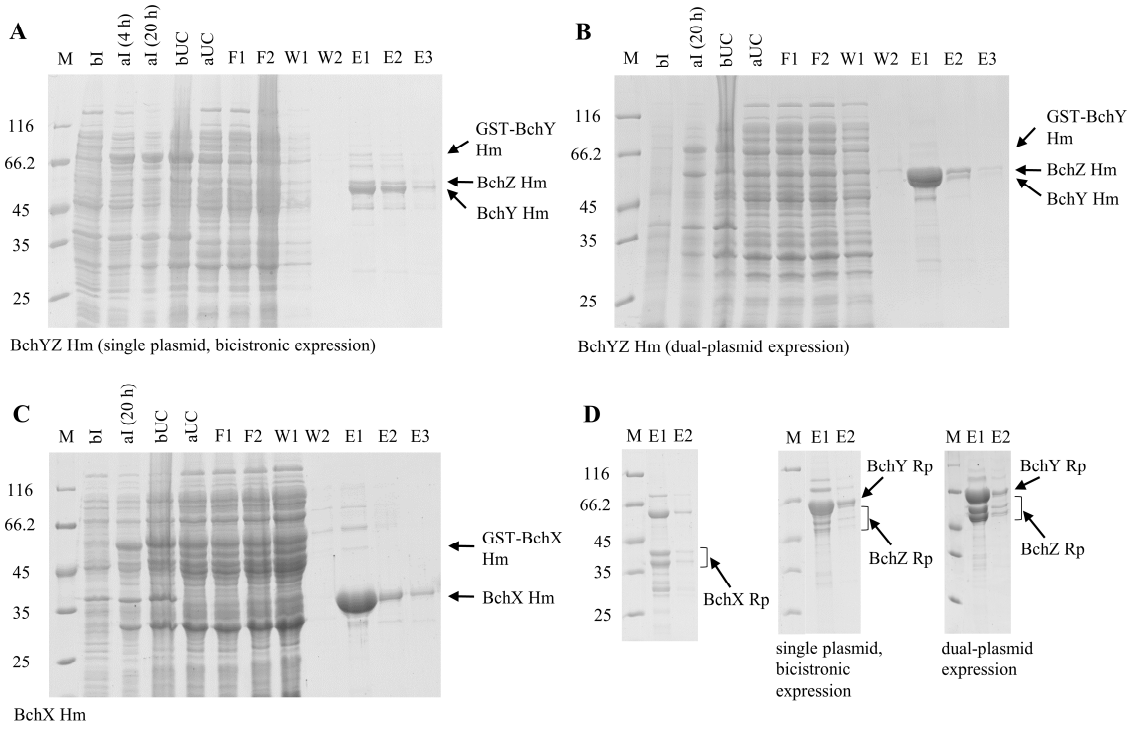

Figure 10: SDS-PAGE analysis of BchY, BchZ and BchX from *H. modesticaldum* and *R. palustris*.
Proteins were produced in *E. coli* BL21(DE3) and purified *via* the N-terminal GST-tag under anoxic conditions. Samples were separated through 12 % SDS-PAGE. The detailed methodology is described in the materials and methods section. **A**: SDS-PAGE of the production and purification of BchY Hm and BchZ Hm using pGEX-6P-1-*bchYZ* Hm. **B**: SDS-PAGE of the production and purification of BchY Hm and BchZ Hm using pGEX-6P-1-*bchY* Hm in combination with pACYCDuet-1-*bchZ* Hm. **C**: SDS-PAGE of the production and purification of BchX Hm using pGEX-6P-1-*bchX* Hm. **D**: SDS-PAGE of proteins obtained by employing plasmids pGEX-6P-1-*bchX* Rp, pGEX-6P-1-*bchYZ* Rp and the combination of pGEX-6P-1-*bchY* Rp and pACYCDuet-1-*bchZ* Rp.
Lanes M: Molecular mass marker, relative molecular masses (x 1'000) are indicated. *Lanes bI*: Whole-cell sample taken before induction. *Lane aI 4 h*: Whole-cell sample taken 4 h after induction. *Lanes aI 20 h*: Whole-cell sample taken 20 h after induction. *Lanes bUC*: Sample of the cell lysate taken before ultracentrifugation. *Lanes aUC*: Sample of the supernatant after ultracentrifugation. *Lanes F1-F2*: Samples of the column flowthrough taken after the first and second column pass, respectively (1 mL column volume). *Lanes W1-W2*: Samples of the washing fractions 1-2. *Lanes E1-E3*: Samples of elution fractions after PreScission protease cleavage. Hm: *H. modesticaldum,* Rp: *R. palustris*.

For both applied strategies to co-purify $(BchYZ)_2$ Hm, SDS-PAGE revealed BchY Hm and BchZ Hm bands in good agreement with the calculated molecular masses of the respective proteins (Figure 10 A and B, GST-BchY Hm: 79'800, BchY Hm: 53'800, BchZ Hm: 57'100). However, the bicistronic expression of BchY Hm and BchZ Hm resulted in a substoichiometric production of BchZ Hm compared to BchY Hm (Figure 10 A, lanes E1-E3). The dual-plasmid expression strategy using pGEX-6P-1-*bchY* Hm and pACYCDuet-1-*bchZ* Hm resulted in an improved BchY/BchZ ratio. This is illustrated by the increased intensity of the BchZ Hm band in the whole-cell SDS-samples taken 20 h after induction (compare Figure 10 A and B, lane aI 20 h) and by the elution samples (compare Figure 10 A and B, lanes E1-E3).

Figure 10 C indicates the successful purification of BchX Hm (calculated molecular mass of 31'500). The identity of BchY Hm, BchZ Hm and BchX Hm was confirmed by N-terminal sequencing (data not shown). Thereby, the weak band below BchY Hm revealed the N-terminal sequence of BchZ Hm, indicating that both purification strategies lead to substoichiometric amounts of C-terminally degraded BchZ Hm.

Identical strategies were used to purify the COR Rp proteins BchY Rp, BchZ Rp and BchX Rp. However, considerable amounts of potential BchZ Rp and BchX Rp protein degradation were observed (Figure 10 D). The identity of BchY Rp, BchZ Rp and BchX Rp was confirmed by N-terminal sequencing (data not shown). Dominant degradation products were identified as BchX Rp (two bands) and BchZ Rp (two bands) degradation (Figure 10 D). Alternative cultivation conditions and purification protocols did not result in lower amounts of degradation products. These findings suggest COR Hm as the most suitable protein complex for subsequent crystallization experiments. It was also concluded to use the dual-plasmid expression strategy for the production of COR subcomplex $(BchYZ)_2$ Hm.

3.1.2 Spectroscopic analysis of COR subcomplexes $(BchX)_2$ and $(BchYZ)_2$

Purified COR subcomplexes $(BchX)_2$ and $(BchYZ)_2$ always revealed a brown color indicative for the presence of a [4Fe-4S] cofactor. Previous studies reported [4Fe-4S] centers as cofactors of subcomplexes $(ChlL)_2$ and $(ChlNB)_2$ of DPOR from *P. marinus* and $(BchX)_2$ and $(BchYZ)_2$ of COR from *R. denitrificans* (Bröcker *et al.*, 2010; Moser *et al.*, 2013; Kiesel *et al.*, 2015).

Accordingly, cofactors of COR Hm and COR Rp subcomplexes $(BchX)_2$ and $(BchYZ)_2$ were explored using UV-Vis spectroscopy (Figure 11).

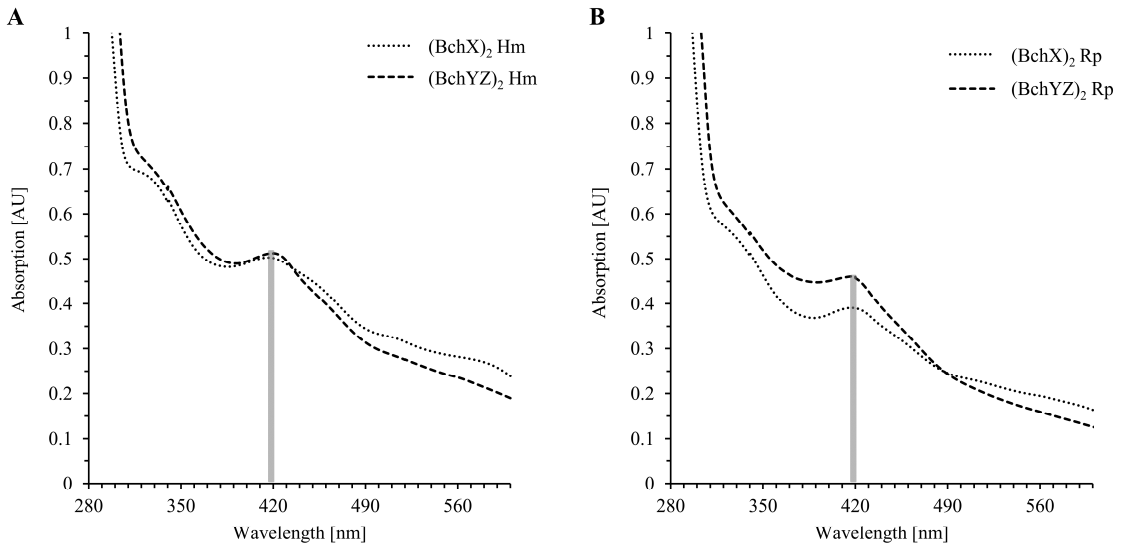

Figure 11: UV-Vis absorption spectra of COR subcomplexes $(BchX)_2$ and $(BchYZ)_2$ from *H. modesticaldum* and *R. palustris*.
A: UV-Vis absorption spectra of COR subcomplexes $(BchX)_2$ (dotted line) and $(BchYZ)_2$ (dashed line) from *H. modesticaldum* (Hm). **B**: UV-Vis absorption spectra of COR subcomplexes $(BchX)_2$ (dotted line) and $(BchYZ)_2$ (dashed line) from *R. palustris* (Rp). Measurements were performed under anoxic conditions with protein concentrations of 100 µM $(BchX)_2$ Hm, 83 µM $(BchYZ)_2$ Hm, 89 µM $(BchX)_2$ Rp and 110 µM $(BchYZ)_2$ Rp. Absorption maxima at 418 ± 2 nm are indicated by grey shading.

Subcomplexes $(BchX)_2$ and $(BchYZ)_2$ of the two analyzed COR enzymes showed closely related absorption spectra. Interestingly, the abovementioned protein degradation of BchZ Rp and BchX Rp did not lead to detectable spectroscopic differences between COR Hm and Rp subcomplexes. In all cases, a maximum at 418 ± 2 nm was detected. This is in agreement with spectroscopic results for COR subcomplexes $(BchX)_2$ and $(BchYZ)_2$ from *R. denitrificans* (Kiesel *et al.*, 2015). A maximum at 428 nm was reported for related DPOR subcomplexes $(BchL)_2$ and $(BchNB)_2$ from *C. tepidum* or $(ChlL)_2$ and $(ChlNB)_2$ from *P. marinus* (Bröcker *et al.*, 2008a; Bröcker *et al.*, 2008b). Furthermore, the recorded spectra for COR subcomplexes $(BchX)_2$ and $(BchYZ)_2$ are comparable to spectra reported for the [4Fe-4S] containing iron protein from *A. vinelandii* (Bulen and LeComte, 1966). A slightly differing cluster environment might explain subtle differences in the absorption maxima between these enzymes.

Nitrogenase and nitrogenase-like enzymes COR and DPOR share an overall octameric protein architecture and most of the cofactor ligands (Figure 12). Cys98/Cys103 and Cys133/Cys138 (*A. vinelandii*/Hm numbering) in nitrogenase-like reductases are highly conserved (Figure 12 A).

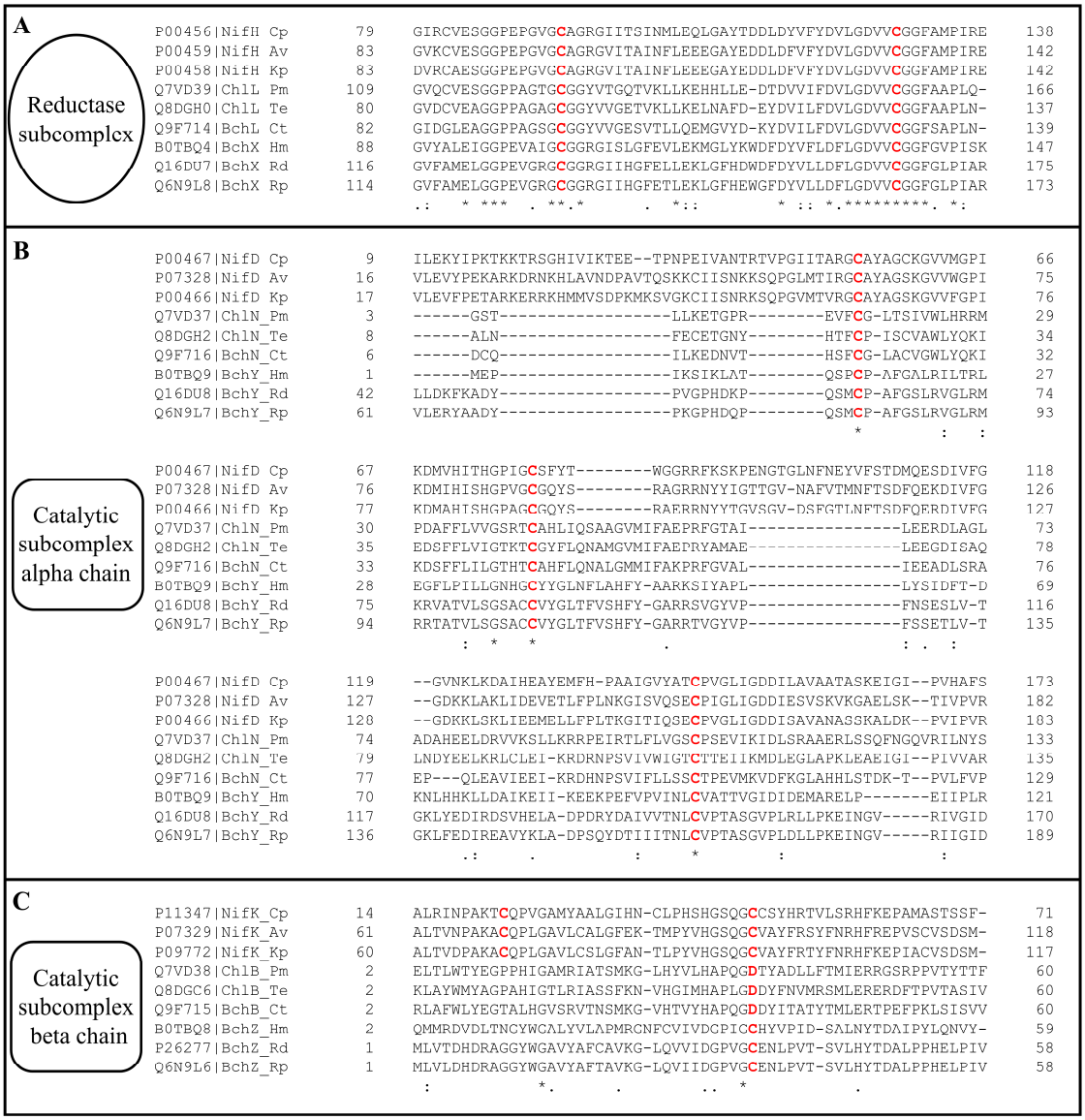

Figure 12: Sequence alignment of COR, DPOR and nitrogenase proteins indicating highly conserved cofactor ligands.
The alignment was generated with Clustal Omega (Sievers *et al.*, 2011). UniProt accession numbers are given for each protein sequence. Alignment sections without conserved cofactor ligands were omitted for clarity. **A**: Sequence alignment of nitrogenase, DPOR and COR reductase proteins. Cofactor ligands Cys98/Cys103 and Cys133/Cys138 (*A. vinelandii*/Hm numbering) and the respective conserved residues of homologous enzymes are highlighted red. **B**: Sequence alignment of the catalytic subcomplex (alpha chain) of nitrogenase, DPOR and COR. Cofactor ligands Cys62/Cys15, Cys88/Cys40 and Cys154/Cys98 (*A. vinelandii*/Hm numbering) and the respective conserved residues of homologous enzymes are highlighted red. Nitrogenase M-cluster ligands (positions 275 and 442, *A. vinelandii* numbering) were omitted. **C**: Sequence alignment of the catalytic subcomplex (beta chain) of nitrogenase, DPOR and COR. Cofactor ligands Cys95/Cys37 (*A. vinelandii*/Hm numbering) and the respective residues of homologous enzymes are highlighted red. Cys70 (P-cluster ligand, *A. vinelandii* numbering) is not conserved in COR and DPOR enzymes. Remaining nitrogenase P-cluster ligands (positions 153 and 188, *A. vinelandii* numbering) were omitted. Fully conserved residues are indicated by asterisk (*), residues with similar properties by colon (:) and residues with weakly similar properties by period (.). Cp: *Clostridium pasteurianum*, Av: *A. vinelandii*, Kp: *Klebsiella pneumoniae*, Pm: *P. marinus*, Te: *Thermosynechococcus elongatus*, Ct: *C. tepidum*, Hm: *H. modesticaldum*, Rd: *R. denitrificans*, Rp: *R. palustris*.

Obviously, the complex cofactor architecture of the nitrogenase catalytic subcomplex requires additional ligands to ligate the more complicated P-cluster and M-cluster, which are not observed in COR and DPOR enzymes. However, residues Cys62/Cys15, Cys88/Cys40 and Cys154/Cys98 of NifD/BchY (*A. vinelandii*/Hm numbering) are conserved in the corresponding COR and DPOR proteins (Figure 12 B). Position Cys95/Cys37 in NifK/BchZ (*A. vinelandii*/Hm numbering) are conserved between nitrogenase and COR. In contrast, DPOR enzymes make use of an unusual asperate ligand (Figure 12 C) in ChlB (Asp36, *P. marinus* numbering).

Initial EPR measurements using reduced samples (DT, 10 mM) were not successful for COR subcomplexes $(BchYZ)_2$ Hm, $(BchX)_2$ Hm and $(BchX)_2$ Rp. Only subcomplex $(BchYZ)_2$ Rp revealed a signal indicative for a [4Fe-4S] cluster. The EPR spectrum (Figure 13) indicates the presence of one [4Fe-4S] cluster species in subcomplex $(BchYZ)_2$ Rp with two proposed [4Fe-4S] clusters. In contrast, different protein environments of the two [4Fe-4S] clusters of subcomplex $(BchYZ)_2$ from *R. denitrificans* were reported (Kiesel *et al.*, 2015). Overall, these results and the highly conserved cofactor ligands of COR, DPOR and nitrogenase strongly suggested a [4Fe-4S] cluster as metal cofactors for COR Hm and COR Rp subcomplexes $(BchYZ)_2$ and $(BchX)_2$, respectively.

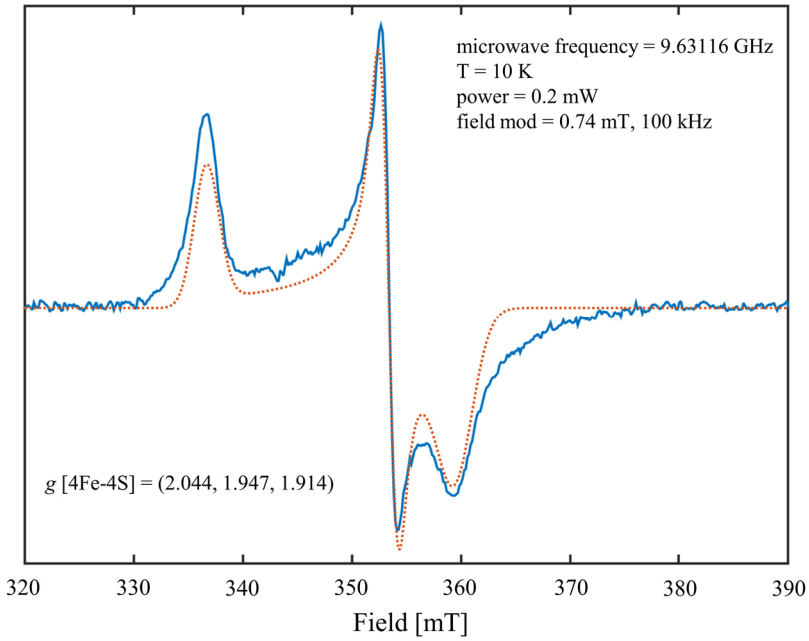

Figure 13: EPR spectrum of COR subcomplex $(BchYZ)_2$ from *R. palustris*.
COR subcomplex $(BchYZ)_2$ from *R. palustris* (180 µM) was reduced in the presence of dithionite (10 mM) and EPR spectra were recorded as described in the materials and methods section. The experimental (blue) and simulated (orange) EPR spectrum of subcomplex $(BchYZ)_2$ is indicative for a [4Fe-4S] cluster.

3.1.3 Homologous COR activity assays

In vitro activity assays under anoxic conditions were used to reconstitute COR enzymes by combining subcomplexes $(BchX)_2$ and $(BchYZ)_2$ in the presence of an ATP-regenerating system, electron donor and substrate. COR enzymes were investigated by two different strategies: Either COR substrate Chlide was used directly or Chlide was generated from Pchlide *via* catalysis of DPOR from *P. marinus*. UV-Vis spectra of extracted assays are shown in Figure 14.

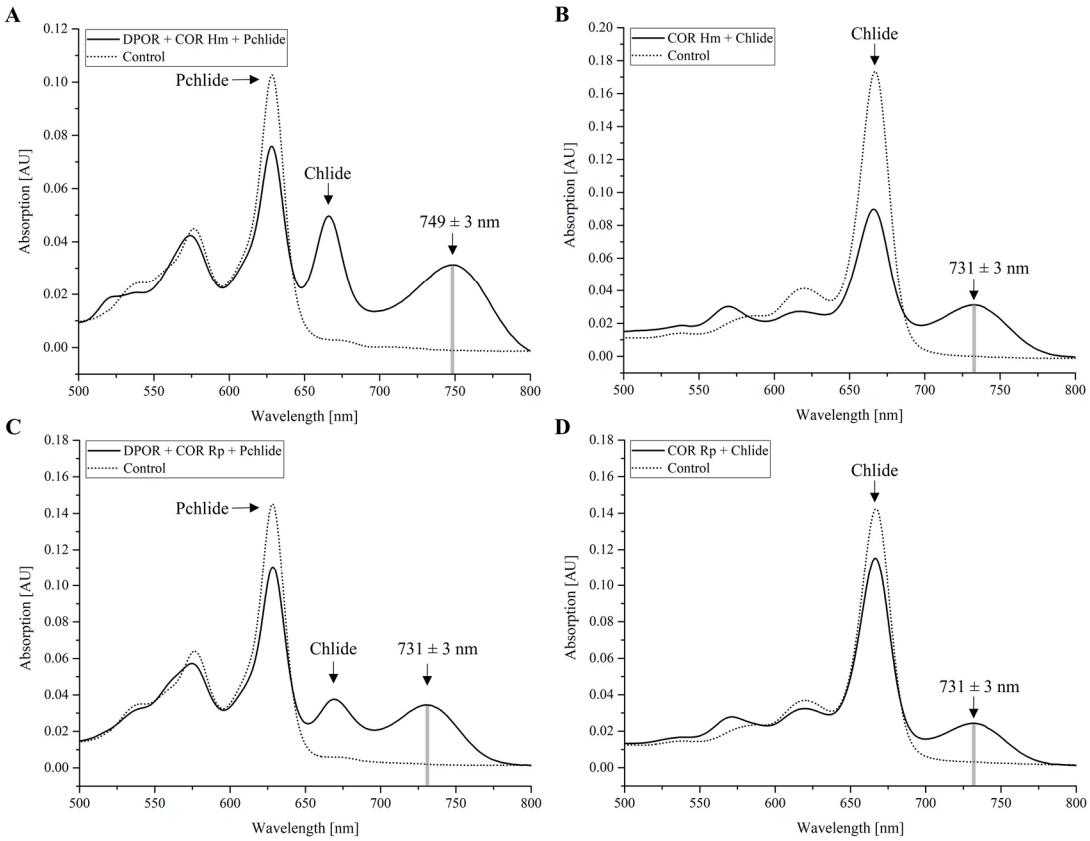

Figure 14: UV-Vis absorption spectra of COR activity assays.
COR activity was confirmed by coupled DPOR/COR activity assays using Pchlide, which is further converted *via* catalysis of DPOR to Chlide. Alternatively, assays were supplemented with Chlide in the absence of DPOR proteins. Pchlide, Chlide and COR reaction products are indicated by arrow. Control experiments were performed in the absence of proteins (dotted lines). Assays were performed in the presence of an ATP-regenerating system, 0.7 mM DT, 5 mM DTT and 20 µM substrate. Each 250 µL assay was supplemented with 500 µL acetone and centrifuged before measurement. Hm: *H. modesticaldum*, Rp: *R. palustris* **A**: UV-Vis absorption spectra of a coupled DPOR/COR Hm activity assay. Chlide was supplied *via* DPOR from *P. marinus* using cell-free extracts containing DPOR subcomplexes $(ChlL)_2$ (100 µL) and $(ChlNB)_2$ (15 µL). Cell-free extract ratios were determined in preliminary assays. Assays were incubated for 30 min at 25 °C. Then, 2.5 µL ATP (200 mM), 444 pmol $(BchYZ)_2$ Hm and 1.45 nmol $(BchX)_2$ Hm were added and assays were incubated for additional 30 min at 37 °C. **B**: UV-Vis absorption spectra of a COR Hm activity assay. The assay contained 400 pmol $(BchYZ)_2$ Hm and 800 pmol $(BchX)_2$ Hm. Assays were incubated for 60 min at 37 °C. **C**: UV-Vis absorption spectra of a coupled DPOR/COR Rp activity assay performed as described for A. **D**: UV-Vis absorption spectra of a COR Rp activity assay performed as described for B. The assay contained 400 pmol $(BchYZ)_2$ Rp and 1.2 nmol $(BchX)_2$ Rp.

COR activity was detected for both investigated homologous enzyme systems. Control experiments lacking COR subcomplexes $(BchX)_2$ and $(BchYZ)_2$ only showed absorption maxima of the respective substrate (Figure 14, dotted lines, Pchlide at 626 nm in A/C and Chlide at 665 nm in B/D). Similar results were obtained for control reactions in the presence of the catalytic subcomplex $(BchYZ)_2$ but in the absence of the reductase subcomplex $(BchX)_2$ (data not shown). Obviously, the employed reducing agent DT does not facilitate for the catalytic reduction of $(BchYZ)_2$ Hm and Rp. The enzymatic conversion in the presence of subcomplexes $(BchX)_2$ and $(BchYZ)_2$ resulted in new absorption maxima in the spectra of the extracted assays: Coupled DPOR/COR Rp assays revealed an absorption maximum at 731 ± 3 nm (Figure 14 C). Similar absorption maxima were observed in non-coupled COR Rp assays supplemented with Chlide (Figure 14 D). This also correlates with results obtained from a non-coupled COR Hm assay (Figure 14 B). The absorption maxima obtained in this study are in agreement with previously reported absorption maxima of Pchlide (626 nm), Chlide (665 nm) and the COR product Bchlide (734 nm) (Fujita and Bauer, 2000; Nomata *et al.*, 2005, 2006; Wätzlich *et al.*, 2009; Kiesel *et al.*, 2015). However, an altered absorption maximum at 749 ± 3 nm was detected for coupled DPOR/COR Hm assays (Figure 14 A).

The light-harvesting apparatus of *R. palustris* contains Bchl *a*, whereas *H. modesticaldum* uses Bchl *g* (Heinnickel and Golbeck, 2007; Brotosudarmo *et al.*, 2009). Bchl *g* has an ethylidene group at the C8 position, while Bchl *a* has a C8-ethyl group. It was demonstrated that COR enzymes of different origin are able to perform both reactions: The reduction of the C7-C8 double bond in Chlide resulting in a bacteriochlorin ring with a C8-ethyl group (COR Rp) and the reduction of 8-vinyl-Chlide to yield the C8-ethylidene group of Bchlide *g* in *B. viridis* and *H. modesticaldum* (compare Figure 4). Moreover, COR from *H. modesticaldum* is not accepting Chlide as a substrate. However, the conversion of 8-vinyl-Chlide results in a pigment with an absorption maximum at 756 nm. It has been demonstrated that the red-shifted absorption maximum is caused by the C8-ethylidene group (Tsukatani *et al.*, 2013a; Tsukatani *et al.*, 2013b).

According to these reported results, the observed red-shifted absorption maximum in the coupled DPOR/COR Hm assay (Figure 14 A) might be the result of the C8-ethylidene group in Bchlide *g*. The red-shift was not observed for the COR Rp since *R. palustris* is a Bchl *a* producing organism and the C8-ethylidene group is only present in Bchl *b* and Bchl *g* (Tsukatani *et al.*, 2013b). This is also supported by the used DPOR substrate

Pchlide, which contains 86 % divinyl Pchlide (Yang and Bauer, 1990) and the ability of DPOR to convert divinyl Pchlide (Bröcker *et al.*, 2008b).

3.1.4 Analytical and preparative gel filtration under anoxic conditions

COR subcomplexes were further explored using gel filtration. Oligomeric state and native molecular masses were analyzed under anoxic conditions. Preparative gel filtration was performed for several crystalization experiments. Representative gel filtrations of COR subcomplexes $(BchYZ)_2$ Hm and $(BchX)_2$ Hm are shown in Figure 15.

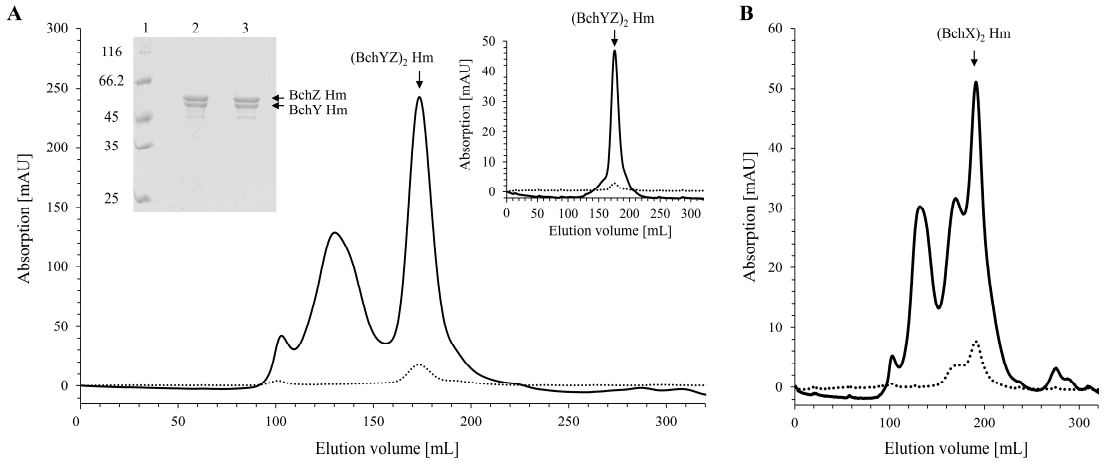

Figure 15: Gel filtration chromatography of COR subcomplexes $(BchYZ)_2$ and $(BchX)_2$ from *H. modesticaldum*.
A: Gel filtration chromatography of $(BchYZ)_2$ from *H. modesticaldum* (Hm). After affinity chromatography, a 500 µL sample (18 mg/mL) was loaded onto a HiLoad 26/600 Superdex 200 column previously equilibrated with buffer A (100 mM HEPES pH 7.5, 150 mM NaCl, 10 mM $MgCl_2$). Gel filtration was performed at a flow rate of 1.5 mL/min and the eluate absorption was monitored at 280 nm (black line) and 420 nm (dotted line). The elution volume of the $(BchYZ)_2$ tetramer is indicated by arrow. A relative molecular mass of 218'000 was determined (calculated molecular mass: 221'900). Left inset: SDS-PAGE of $(BchYZ)_2$ tetramer elution fractions after gel filtration. *Lane 1*: Molecular mass marker, relative molecular masses (x 1'000) are indicated. *Lane 2*: Concentrated $(BchYZ)_2$ tetramer elution fraction. *Lane 3*: Concentrated $(BchYZ)_2$ tetramer elution fraction after storage at 17 °C for two weeks. BchZ and BchY are highlighted by arrows. Right inset: Gel filtration chromatography of concentrated $(BchYZ)_2$ tetramer elution fractions after storage at 17 °C for one week. **B**: Gel filtration chromatography of $(BchX)_2$ Hm. After affinity chromatography, a 500 µL sample (9 mg/mL) was loaded onto a HiLoad 26/600 Superdex 200 column previously equilibrated with buffer A. Gel filtration was performed as described for A. The potential $(BchX)_2$ dimer is indicated by arrow. A relative molecular mass of 109'000 was determined (calculated molecular mass: 63'000).

A native molecular mass of 218'000 was concluded for the COR subcomplex $(BchYZ)_2$ Hm (Figure 15 A, elution volume: 174 mL). This is in agreement with a proposed tetrameric structure of $(BchYZ)_2$ Hm (calculated molecular mass: 221'900) in analogy to

homologous catalytic subcomplexes of nitrogenase and DPOR (Tezcan *et al.*, 2005; Bröcker *et al.*, 2008a; Bröcker *et al.*, 2008b) or COR from *R. denitrificans* (Kiesel *et al.*, 2015). However, the employed sample revealed additional broad elution signals with maxima at ~102 and ~130 mL (280 nm). The respective protein fractions contained BchY and BchZ but did not indicate the presence of [FeS] as judged from the monitored absorption at 420 nm (elution volume: ~130 mL). It was concluded that substantial amounts of non-matured BchY and BchZ aggregates were obtained after affinity chromatography. These aggregates were efficiently removed using gel filtration.

SDS-PAGE analysis of $(BchYZ)_2$ tetramer elution fractions (elution volume: ~174 mL) revealed two intense bands corresponding to BchY (lower band) and BchZ (upper band). The fractionated $(BchYZ)_2$ tetramer was stable over two weeks as judged by SDS-PAGE and subsequent gel filtration (Figure 15 A). However, the $(BchYZ)_2$ tetramer elution fractions still contained minor amounts of the previously described C-terminally degraded BchZ Hm.

Gel filtration of COR subcomplex $(BchX)_2$ Hm indicated a highly heterogeneous protein sample (Figure 15 B). The elution profile revealed signals with a maximum at ~103 and ~132 mL (280 nm), which is indicative for protein aggregates. The absence of [FeS] cofactors is suggested by the weak 420 nm signal. Additional absorption maxima were observed at ~170 and ~191 mL. In contrast to the first two maxima, these fractions showed an increased 420 nm signal. Accordingly, the presence of a [FeS] cofactor was concluded. For the strongest elution maximum (elution volume: ~191 mL, 280 and 420 nm), a native molecular mass of 109'000 was determined. This is larger than a proposed dimeric structure of $(BchX)_2$ Hm (calculated molecular mass: 63'000). A non-globular shape of the $(BchX)_2$ dimer might be responsible for the increased elution volume (Walls and Loughran, 2017). Thus, the identified protein complex with a relative molecular mass of 109'000 might indicate a $(BchX)_2$ dimer as also reported for the related nitrogenase and DPOR reductases (Tezcan *et al.*, 2005; Bröcker *et al.*, 2008a).

In summary, COR subcomplex $(BchYZ)_2$ Hm proved to be a stable tetramer after preparative gel filtration. It remained to be investigated if the octameric COR complex, consisting of subcomplexes $(BchYZ)_2$ and $(BchX)_2$, could be stabilized for further crystalization attempts. A series of experiments to assemble the octameric COR complex in the presence of ATP analogs was performed as described for nitrogenase and DPOR

enzymes (Schindelin *et al.*, 1997; Moser *et al.*, 2013). Therefore, the previously reported column-based purification strategy of the octameric DPOR complex was used (Moser and Bröcker, 2011). All attempts to obtain a stable octameric COR complex from *H. modesticaldum* or from *R. palustris* did not result in sufficient amounts of the protein complex for subsequent crystalization experiments (data not shown). This might indicate a weaker interaction between reductase and catalytic subcomplex when compared to the described DPOR system from *P. marinus* (Moser *et al.*, 2013). Consequently, the majority of crystalization experiments were directed towards the catalytic COR subcomplex $(BchYZ)_2$ Hm.

3.1.5 Towards the three-dimensional structure of COR

To elucidate the mechanism of the C7-C8 double bond reduction and the reported alternative reductions at the C8 ligand of Chlide, structural investigation of the COR enzyme was intended. To date, no crystal structure of COR is available. In the present study, a series of crystalization experiments with COR proteins and protein variants were performed (Table 18).

In an attempt to facilitate the crystalization of COR subcomplex $(BchYZ)_2$ Hm, variants of the COR proteins BchY Hm and BchZ Hm were generated using the surface entropy reduction approach to replace amino acids of high conformational entropy with alanine (Goldschmidt *et al.*, 2007). Two BchY and two BchZ variants were generated *via* mutagenesis. The modified proteins were produced as described for the wild-type $(BchYZ)_2$ Hm to form the mutagenized subcomplexes termed $(BchYZ)_2$ M1 and $(BchYZ)_2$ M2. Mutagenized subcomplex $(BchYZ)_2$ M1 contains the proposed cluster 1 mutations in BchY and BchZ, whereas mutagenized subcomplex $(BchYZ)_2$ M2 contains the proposed cluster 2 mutations in BchY and BchZ (Figure 16 A and B).

SDS-PAGE analysis revealed a substoichiometric production of BchZ M1 compared to BchY M1 (Figure 16 C, lane 2). A substantially decreased COR activity of $(BchYZ)_2$ M1 (25 %) compared to wild-type $(BchYZ)_2$ (100 %) was determined (data not shown). Obviously, the modified surface residues of BchY M1 and BchZ M1 lower the affinity of these proteins to form the tetrameric protein subcomplex. As a result, the co-purification of BchZ M1 *via* the GST-tagged BchY M1 was hampered. Efficient interaction between BchY and BchZ was observed for variant $(BchYZ)_2$ M2 (Figure 16 C, lane 4). Furthermore, gel filtration of $(BchYZ)_2$ M2 indicated a tetrameric protein complex in

good agreement with the wild-type $(BchYZ)_2$ protein complex (data not shown). In consequence, $(BchYZ)_2$ M2 was considered as an alternative catalytic COR complex for subsequent crystalization experiments.

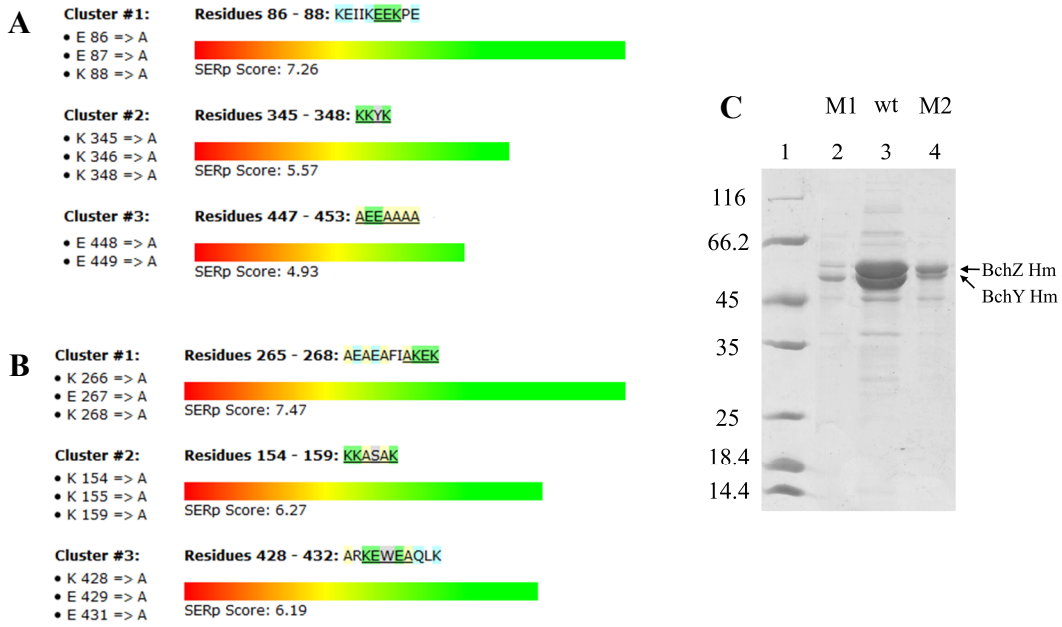

Figure 16: Surface entropy reduction prediction (SERp) of subunits BchY Hm and BchZ Hm and SDS-PAGE analysis of wild-type and variant $(BchYZ)_2$ Hm complexes.
The SERp server was used to predict clusters of high conformational entropy (Goldschmidt *et al.*, 2007). Mutagenized residues are highlighted green. **A**: SERp server results for BchY Hm. The proposed clusters 1 and 2 were used to generate BchY variants M1 and M2. **B**: SERp server results for BchZ. The proposed clusters 1 and 2 were used to generate BchZ variants M1 and M2. Protein variants BchY M1 and BchZ M1 were combined to obtain $(BchYZ)_2$ M1. Protein variants BchY M2 and BchZ M2 were combined to obtain $(BchYZ)_2$ M2. **C**: SDS-PAGE of wild-type and variant $(BchYZ)_2$ Hm complexes. The production and purification of BchY and BchZ protein variants was performed as described for the wild-type proteins. *Lane 1*: Molecular mass marker, relative molecular masses (x 1'000) are indicated. *Lane 2*: BchY M1 and BchZ M1. *Lane 3*: Wild-type (wt) BchY and BchZ. *Lane 4*: BchY M2 and BchZ M2.

The performed crystallization experiments employing commercial screening kits, diverse concentrations of COR subcomplexes and additives (Chlide, ATP analogs) are summarized in Table 18. Potential crystals subjected to initial X-ray diffraction analysis are shown in Figure 17. All attempts to crystallize the $(BchYZ)_2$ COR subcomplex or the octameric COR enzyme by combining individual COR subcomplexes in the presence of ATP analogs and Chlide did not result in single crystals sufficient for X-ray data collection. Insufficient maturation or purification might be hampering successful crystallization of the oxygen-sensitive [4Fe-4S] proteins.

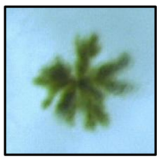

P7-C3
$(BchYZ)_2$ Hm + Chlide
0.08 M TRIS-HCl pH 8.5
1.6 M Ammonium phosphate
20 % (v/v) Glycerol

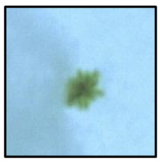

P18-D4
$(BchYZ)_2$ Hm (GPC) + Chlide
0.2 M Ammonium sulfate
0.1 M TRIS pH 7.5
20 % (w/v) PEG 5000 MME

P10-F1
$(BchYZ)_2$ Hm
0.17 M Magnesium formate
15 % (v/v) Glycerol

P18-F5
$(BchYZ)_2$ Hm (GPC) + Chlide
0.1 M Sodium chloride
0.1 M TRIS pH 8
8 % (w/v) PEG 20000

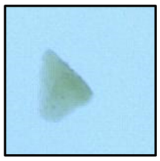

P17-A6
$(BchYZ)_2$ Hm (GPC) + Chlide
0.14 M Calcium chloride
0.07 M Sodium acetate pH 4.6
14 % (v/v) Isopropanol
30 % (v/v) Glycerol

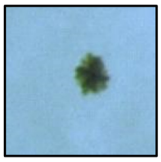

P30-A11
$(BchYZ)_2$ M2 (GPC) + Chlide
0.1 M Tris-HCl pH 8.5
2.0 M Ammonium dihydrogen phosphate

Figure 17: Pictures of potential protein crystals subjected to initial X-ray diffraction experiments. Potential crystals of COR subcomplex $(BchYZ)_2$ from *H. modesticaldum* (Hm) or variant $(BchYZ)_2$ M2 subjected to X-ray diffraction experiments are shown. Proteins were produced as detailed in the materials and methods section. "GPC" labeled proteins were subjected to gel filtration prior to crystalization. Screen number, well number and buffer conditions of individual experiments are indicated (compare Table 18). In all cases, no X-ray diffraction pattern was observed.

3.1.6 Heterologous and chimeric enzyme systems

The protein docking surface facilitating the interaction and electron transfer between reductase and catalytic subcomplex of nitrogenase-like enzymes was investigated in heterologous and chimeric enzyme activity assays. Therefore, CfbCD subcomplexes from *M. barkeri* (Mb), COR subcomplexes from *H. modesticaldum* (Hm), *R. palustris* (Rp) and *R. denitrificans* (Rd) and DPOR subcomplexes from *P. marinus* (Pm) and *C. tepidum* (Ct) were combined in standard activity assays. The relative activities of the reconstituted homologous enzymes were set to 100 % and detected activities of reconstituted heterologous or chimeric enzymes were related to that value. Experiments with CfbCD were performed in collaboration with José Vazquez Ramos (AG Layer, Albert-Ludwigs-Universität Freiburg).

Figure 18 A summarizes the enzymatic activities of all investigated heterologous or chimeric enzyme systems. An overall of 24 combinations are shown: Heterologous COR enzymes consisting of COR Hm, COR Rp and COR Rd subcomplexes and heterologous DPOR enzymes consisting of DPOR Pm and DPOR Ct subcomplexes. Moreover, chimeric enzyme systems were investigated by combining individual reductase and catalytic subcomplexes from COR, DPOR and CfbCD. Previously investigated combinations are indicated in parentheses (Wätzlich *et al.*, 2009).

A	$(BchX)_2$ Hm	$(BchX)_2$ Rp	$(BchX)_2$ Rd	$(ChlL)_2$ Pm	$(BchL)_2$ Ct	$(CfbC)_2$ Mb
$(BchYZ)_2$ Hm	100 %	ND	ND	ND	ND	ND
$(BchYZ)_2$ Rp	ND	100 %	25 %	ND	ND	ND
$(ChlNB)_2$ Pm	ND	ND	(ND)	100 %	(3 %)	ND
$(BchNB)_2$ Ct	ND	ND	(50 %)	(100 %)	100 %	-
$(CfbD)_2$ Mb	ND	ND	ND	ND	ND	100 %

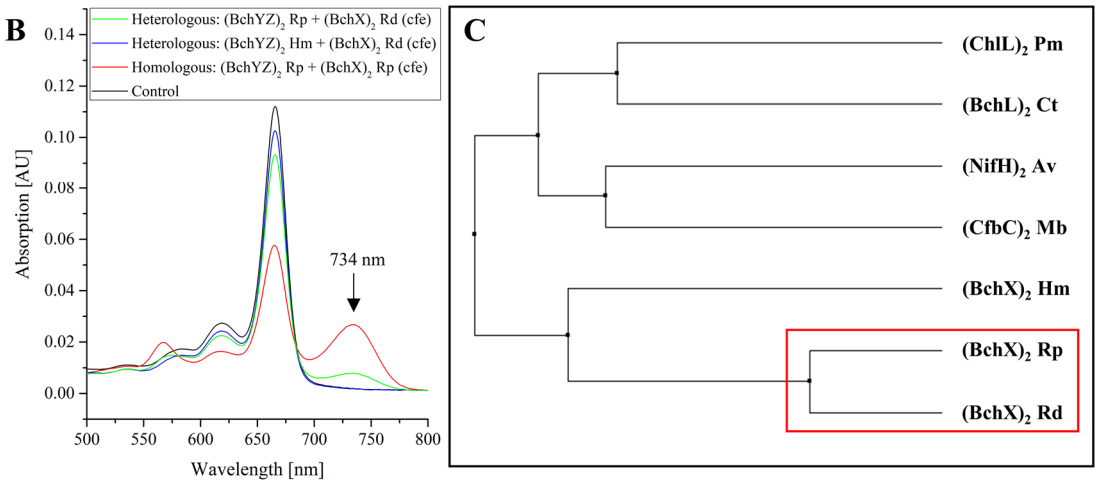

Figure 18: Enzymatic activities of nitrogenase-like heterologous and chimeric enzyme systems. Standard assays were performed as described in the materials and methods section (1 h incubation at 37 °C). **A**: Summary of all investigated heterologous enzyme assays. The indicated reductase subcomplexes (columns) were combined with the indicated catalytic subcomplexes (rows). The activities of homologous enzymes were set to 100 %. Previously reported results are shown in parentheses (Wätzlich *et al.*, 2009). ND: No heterologous enzyme activity detected. -: Combination not analyzed. **B**: Representative UV-Vis absorption spectra indicating an active heterologous COR enzyme consisting of $(BchYZ)_2$ Rp and $(BchX)_2$ Rd (green line). The homologous COR Rp control is shown in red. The heterologous combination $(BchYZ)_2$ Hm and $(BchX)_2$ Rd is not active (blue line). In all depicted assays, the reductase component was supplied as cell-free extract (cfe). Control experiments were performed in the absence of proteins (black line). **C**: Phylogenetic tree (average distance) of several nitrogenase-like reductases. Clustal Omega (Sievers et al., 2011) was used to generate a multiple sequence alignment and the phylogenetic tree was assembled with Jalview 2.1 (Waterhouse *et al.*, 2009) utilizing the BLOSUM62 substitution matrix. $(BchX)_2$ Rp and $(BchX)_2$ Rd are closely related (red box). Hm: *H. modesticaldum*, Rp: *R. palustris*, Rd: *R. denitrificans*, Pm: *P. marinus*, Ct: *C. tepidum*, Mb: *M. barkeri*, Av: *A. vinelandii*.

The majority of the reconstituted heterologous or chimeric enzyme systems assayed in the present study did not result in detectable activity under the employed conditions. However, one of the 20 newly investigated combinations resulted in an active heterologous COR enzyme composed of subcomplexes $(BchYZ)_2$ Rp and $(BchX)_2$ Rd. Representative UV-Vis spectra of the corresponding assays are shown in Figure 18 B. In control experiments lacking both subcomplexes, no product formation was observed (Figure 18 B, black line). Heterologous COR activity was not obtained using

subcomplexes $(BchX)_2$ Rd and $(BchYZ)_2$ Hm (Figure 18 B, blue line). Likewise, all other investigated heterologous or chimeric combinations did not result in detectable enzyme activity. However, in the presence of 300 pmol $(BchYZ)_2$ Rp and 100 µL of a $(BchX)_2$ Rd containing cell-free extract, a heterologous activity of 25 % compared to the homologous COR Rp system was detected (compare Figure 18 B, green and red line). Related heterologous activities of nitrogenase-like enzymes have also been reported for heterologous DPOR (Wätzlich *et al.*, 2009) and nitrogenase enzymes (Emerich and Burris, 1978).

These observations are consistent with the phylogenetic tree of nitrogenase-like reductases depicted in Figure 18 C. $(BchX)_2$ Rp and $(BchX)_2$ Rd are shown on the same branch in a close average distance, whereas $(BchX)_2$ Hm is branching of earlier. Other studies also highlighted the low primary sequence similarities of Bchl *g*-producing heliobacterial COR enzymes when compared to COR enzymes from Bchl *a*- and *b*-producing bacteria (Tsukatani *et al.*, 2013b).

CfbCD was proposed as a potential ancestor of nitrogenase-like protein complexes (Boyd and Peters, 2013). The inactive chimeric enzymes composed of CfbCD and COR/DPOR subcomplexes might suggest that COR and DPOR have evolved substantially from the evolutionary ancestor. This is in agreement with interaction-assays, which revealed only a weak interaction between CfbD and $(BchX)_2$ Hm, $(ChlL)_2$ Pm or $(ChlL)_2$ variants (Appendix Figure 28).

It might be concluded that the docking surface involved in the protein-protein interaction and subsequent inter-subcomplex electron transfer are partially conserved in COR enzymes from *R. palustris* and *R. denitrificans.* The inactive chimeric enzymes formed between COR, DPOR and CfbCD subcomplexes indicate that docking surface and electron transfer of these enzymes have evolved significantly. However, given the limited number of investigated combinations, caution must be exercised. Previous studies described two chimeric enzymes consisting of COR reductase $(BchX)_2$ Ct and $(BchX)_2$ Rd and the catalytic DPOR subcomplex $(BchNB)_2$ Ct, which underscores that all nitrogenase-like systems have evolved from a common ancestor (Wätzlich *et al.*, 2009).

3.1.7 The methyl viologen cation radical as an alternative reductant for DPOR from *P. marinus*

DT is widely used as an *in vitro* electron donor for nitrogenase and nitrogenase-like enzymes (Wätzlich *et al.*, 2009; Badalyan *et al.*, 2019). However, this strong reductant performs irreversible electrochemical reactions and has limited use in spectroscopic investigations due to its low extinction coefficient. In contrast, methyl viologen (MV) allows for reversible electrochemical reactions and changes its spectroscopic properties substantially in the reduced and oxidized form, making it an attractive alternative reductant or electrochemical mediator. Moreover, viologen derivatives or MV in low concentrations (μM) have been reported to support full nitrogenase activity (Badalyan *et al.*, 2019).

In this study, initial experiments were performed using the methyl viologen cation radical ($MV^{+\cdot}$) as a reductant for DPOR from *P. marinus*. The three reversible redox states of MV are as follows: The colorless di-cation MV^{2+} is reduced to the violet-blue radical cation $MV^{+\cdot}$ (1), which can be further reduced to the yellow-brown molecular form MV^0 (2) (Heyrovský, 1987; Ding *et al.*, 2019).

$$MV^{2+} + e^- \rightleftharpoons MV^{+\cdot} \quad (1)$$

$$MV^{+\cdot} + e^- \rightleftharpoons MV^0 \quad (2)$$

$MV^{+\cdot}$ was prepared by oxidation of glucose as detailed in the material and methods section and the concentration of the violet-blue $MV^{+\cdot}$ was determined spectroscopically using the extinction coefficient ε_{600}= 8.25 mM^{-1} cm^{-1} (Yu and Wolin, 1969). Representative UV-Vis spectra of pigment extracts from DPOR assays are shown in Figure 19. The assays were performed under anoxic conditions, but the subsequent UV-Vis analysis was conducted in the presence of oxygen. Thus, residual $MV^{+\cdot}$ is oxidized and the strong absorption signal of $MV^{+\cdot}$ is not overlapping with the expected signals of the investigated pigments (compare UV-Vis spectra of reduced and oxidized MV in Appendix Figure 29). As depicted in Figure 19 A, the employed concentrations of $MV^{+\cdot}$ (0.3-1.2 mM) resulted in the formation of Chlide (665 nm) at 25 °C (Figure 19 A, blue spectra) and 37 °C (Figure 19 A, red spectra).

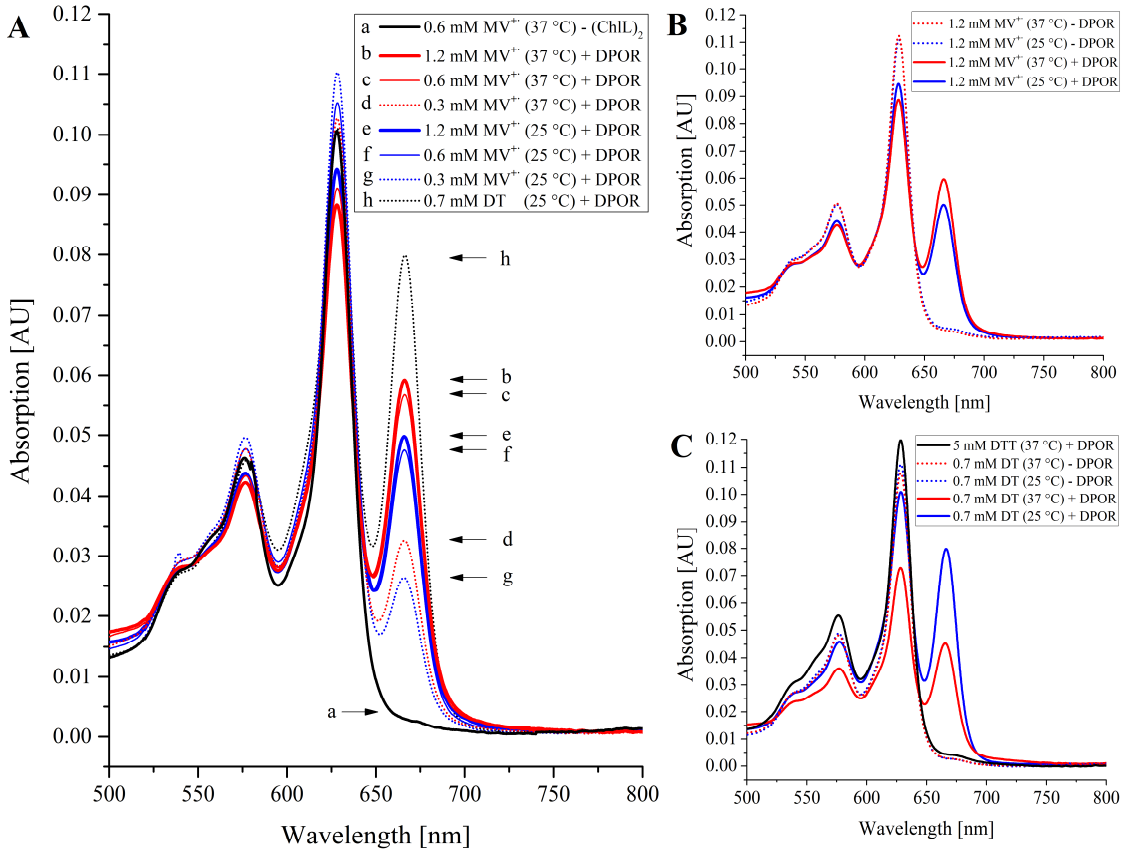

Figure 19: UV-Vis absorption spectra of DPOR activity assays using the methyl viologen cation radical ($MV^{+\cdot}$) as electron donor.
Assays (250 µL) were performed in the presence of 400 pmol $(ChlNB)_2$ and 1.2 nmol $(ChlL)_2$ from *P. marinus*, an ATP-regenerating system, 20 µM Pchlide and the indicated amounts of dithionite (DT), $MV^{+\cdot}$ or dithiothreitol (DTT), respectively. Each assay was supplemented with 500 µL acetone and centrifuged before measurement. **A**: UV-Vis absorption spectra of DPOR activity assays using 0.3-1.2 mM $MV^{+\cdot}$. The assays were performed at 25 °C (blue, e-g) and 37 °C (red, b-d). Control experiments were performed in the absence of $(ChlL)_2$ (black line, a) and with reductant DT (black dotted line, h). **B**: UV-Vis absorption spectra of DPOR activity assays using 1.2 mM $MV^{+\cdot}$ in the presence and absence of DPOR subcomplexes $(ChlNB)_2$ and $(ChlL)_2$ (25 and 37 °C). **C**: UV-Vis absorption spectra of DPOR activity assays using reductants DT and DTT in the presence and absence of DPOR subcomplexes $(ChlNB)_2$ and $(ChlL)_2$ (25 and 37 °C).

Clearly, DPOR from *P. marinus* is able to use $MV^{+\cdot}$ as electron donor. The highest DPOR activity was observed for assays with 1.2 mM $MV^{+\cdot}$ at 37 °C (Figure 19 A, spectrum b). However, assays employing electron donor DT (0.7 mM, 25 °C) still resulted in a 35 % higher DPOR activity when compared to assays using 1.2 mM $MV^{+\cdot}$ (Figure 19 A, compare spectrum b and h). DPOR activity decreased significantly in the presence of 2.4 and 4.8 mM $MV^{+\cdot}$ (data not shown). The inhibitory effect of $MV^{+\cdot}$ at mM concentrations was also described for the nitrogenase system (Badalyan *et al.*, 2019).

Interestingly, DT and $MV^{+\cdot}$ efficiently functioned as an electron donor for DPOR catalysis at 25 and 37 °C. While both reductants revealed no significant effect on Pchlide (626 nm)

in the absence of DPOR at 25 and 37 °C (Figure 19 B and C, dotted spectra), assays at 37 °C using reductant $MV^{+\cdot}$ resulted in higher amounts of Chlide when compared to assays at 25 °C (Figure 19 B, compare red and blue spectrum). In contrast, lower amounts of Chlide were produced in the presence of DT at 37 °C when compared to assays at 25 °C (Figure 19 C, compare red and blue spectrum). Although assays in the presence of DT (37 °C) resulted in a lower amount of Chlide (665 nm), the Pchide signal (626 nm) was remarkably reduced (Figure 19 C, red spectrum). This observation was reproduced in multiple independent experiments and might indicate the artificial over-reduction of Pchlide by DPOR in the presence of DT at 37 °C. This type of DT reduction at 37 °C might result in a complete loss of the conjugated system of Pchlide.

Electron donors with different potentials were employed to determine a preliminary midpoint potential range of DPOR subcomplex $(ChlL)_2$ from *P. marinus*. DTT (-330 mV, pH 7) was not able to facilitate DPOR activity (Figure 19 C, black spectrum), whereas DT (-660 mV, pH 7) and $MV^{+\cdot}$ (-443 mV, pH 6.8) efficiently function as electron donors of DPOR (Cleland, 1964; Mayhew, 1978; Bird and Kuhn, 1981).

It was concluded that the midpoint potential of $(ChlL)_2$ is lower than -330 mV and likely between -330 and -443 mV. These results are in agreement with initial spectroelectrochemical titration experiments of subcomplex $(ChlL)_2$ performed by Dr. Patricia Rodríguez Macía and Yu Sun (collaboration with Prof. Kylie Vincent, University of Oxford), which indicated a midpoint potential of approximately -418 mV for subcomplex $(ChlL)_2$.

3.2 Towards an alternative nitrogenase reductase

The design of an alternative nitrogenase reductase represents an important goal for subsequent synthetic biology approaches and for the further investigations of nitrogenase cofactor maturation. A previous structure-based investigation of DPOR and nitrogenase revealed that the position of amino acids facilitating the contact between reductase and catalytic subcomplex are conserved with respect to their spatial position. However, the individual amino acids are not conserved between DPOR and nitrogenase (Moser *et al.*, 2013). These findings are in agreement with the results of chimeric nitrogenase/DPOR experiments. The combination of nitrogenase subcomplex $(NifH)_2$ from *A. vinelandii* and DPOR subcomplexes $(BchNB)_2$ from *C. tepidum* or $(ChlNB)_2$ from *Thermosynechococcus elongatus* and *P. marinus* did not reveal detectable enzyme activity (Wätzlich *et al.*, 2009). Further experiments showed that subcomplex $(BchL)_2$ from *R. sphaeroides* is not able to support nitrogenase activity or association with the MoFe protein of *A. vinelandii* (Sarma *et al.*, 2008). DPOR reductase $(ChlL)_2$ from *P. marinus* is a promising candidate for the engineering of an alternative nitrogenase reductase. *P. marinus* is performing oxygenic photosynthesis. Therefore, $(ChlL)_2$ is potentially more stable in the presence of oxygen when compared to nitrogenase reductase $(NifH)_2$. Furthermore, $(ChlL)_2$ contains key structural elements of the docking face of $(NifH)_2$ (Figure 20). In the second part of this study, the *P. marinus* $(ChlL)_2$ reductase and related variants were examined for their ability to substitute nitrogenase reductase $(NifH)_2$.

3.2.1 Design, cloning, production and purification of $(ChlL)_2$ variants CLmax and CLmin

P. marinus $(ChlL)_2$ variants CLmax and CLmin were designed based on a structural analysis of DPOR (pdb code: 2YNM) and nitrogenase (pdb code: 1M34). This comparative investigation revealed 35 ChlL or 34 NifH residues located at the inter-subcomplex docking face of DPOR or nitrogenase, respectively (Moser *et al.*, 2013). Accordingly, these 27 (CLmax) or 8 (CLmin) residues were mutagenized, aiming to facilitate the interaction of $(ChlL)_2$ with MoFe (Figure 20). Variant CLmin only contains mutations in the highly conserved docking loop region, whereas variant CLmax also covers interface located residues which are not conserved among sequences of $(NifH)_2$. Mutations in close distance to [4Fe-4S] cluster ligands (for example Gly125, Pm

numbering) or mutations that might influence the backbone secondary structure (for example Tyr132, Pm numbering) were omitted. The synthetic genes *cLmax* and *cLmin* were cloned into vector pGEX-6P-1 and the respective proteins were produced in *E. coli* BL21(DE3). CLmax and CLmin were purified *via* the N-terminal GST-tag under anoxic conditions employing on-column PreScission protease treatment for the specific elution of the target proteins.

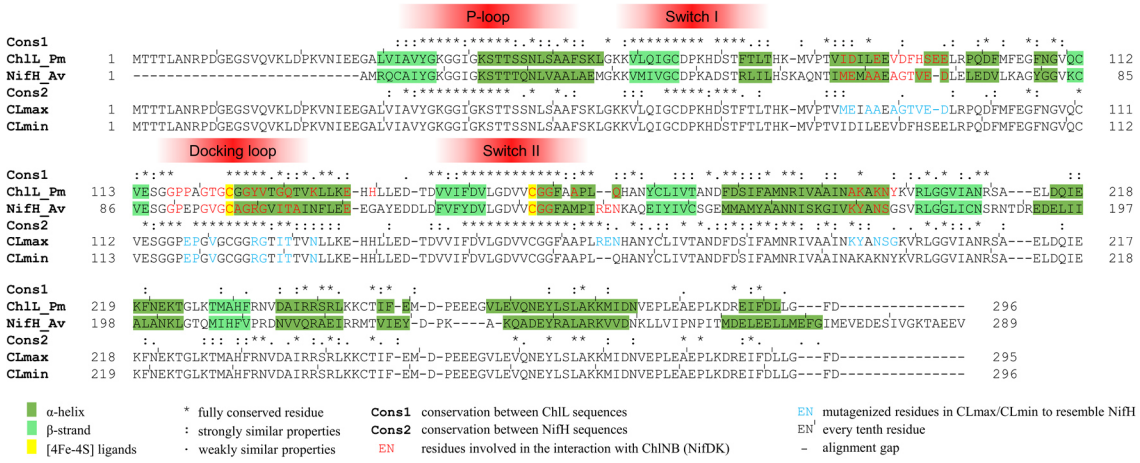

Figure 20: Sequence alignment of ChlL, NifH and ChlL variants CLmax and CLmin.
The alignment represents a structure-based alignment of ChlL and NifH depicted in (Moser *et al.*, 2013). Sequence conservation of ChlL (Cons1) and NifH (Cons2) are indicated: Fully conserved residues by asterisk (*), residues with similar properties by colon (:) and residues with weakly similar properties by period (.). Docking faces between ChlL and ChlNB (pdb code: 2YNM) or NifH and NifDK (pdb code: 1M34) are highlighted by red-colored residues. ChlL variants CLmax and CLmin were engineered to resemble the docking face of NifH. Mutagenized residues of CLmax and CLmin are highlighted in blue. α-helices (dark green) and β-strands (bright green) of ChlL and NifH are indicated by shading. Conserved [4Fe-4S] cluster ligands of NifH and ChlL are marked by yellow shading. Pm: *P. marinus*, Av: *A. vinelandii*.

The SDS-PAGE analysis of purified CLmax and CLmin is depicted in Figure 21 A and B. Variants CLmax and CLmin revealed bands (~35'000) in agreement with the calculated molecular masses of the respective target proteins (32'400, respectively). This is consistent with earlier purifications of the wild-type $(ChlL)_2$ Pm reductase (Bröcker *et al.*, 2008b). However, variants CLmax and CLmin showed increased amounts of potential chaperone contaminations (Figure 21 A and B, band at ~66'000). Therefore, the removal of contaminant proteins using an ATP incubation step was performed: The addition of ATP to the lysis buffer and the implementation of a pre-elution in the presence of ATP effectuated the release of substantial amounts of potential chaperones associated with CLmin (Figure 21 B, lanes 9-14). The same approach only revealed a smaller effect for the purification of CLmax. The SDS-PAGE for the purification of CLmax indicated the co-elution of an additional protein with a relative molecular mass of 66'000 (Figure 21 A, lanes 11-14).

CLmax and CLmin were further explored using UV-Vis spectroscopy after chemical reconstitution of [FeS] clusters (Figure 21 C). Both variants showed an absorption signal at 424 ± 4 nm as also observed for the wild-type $(ChlL)_2$ protein from *P. marinus* (Bröcker *et al.*, 2008b). Moreover, the signals clearly decreased in the presence of DT (Figure 21 C, left and middle panel) or molecular oxygen (Figure 21 C, right panel), indicating the presence of the redox-active and oxygen-sensitive cofactors. For unreconstituted CLmax and CLmin proteins, low iron contents (CLmax: 0.2 mol/mol dimer, CLmin: 0.8 mol/mol dimer) and sulfur contents (CLmax: 0.1 mol/mol dimer, CLmin: 0.9 mol/mol dimer) were determined. The chemical reconstitution of [FeS] clusters resulted in an overall increased iron content (CLmax: 2.2 mol/mol dimer, CLmin: 2.9 mol/mol dimer) and sulfur content (CLmax: 3.0 mol/mol dimer, CLmin: 4.4 mol/mol dimer), respectively.

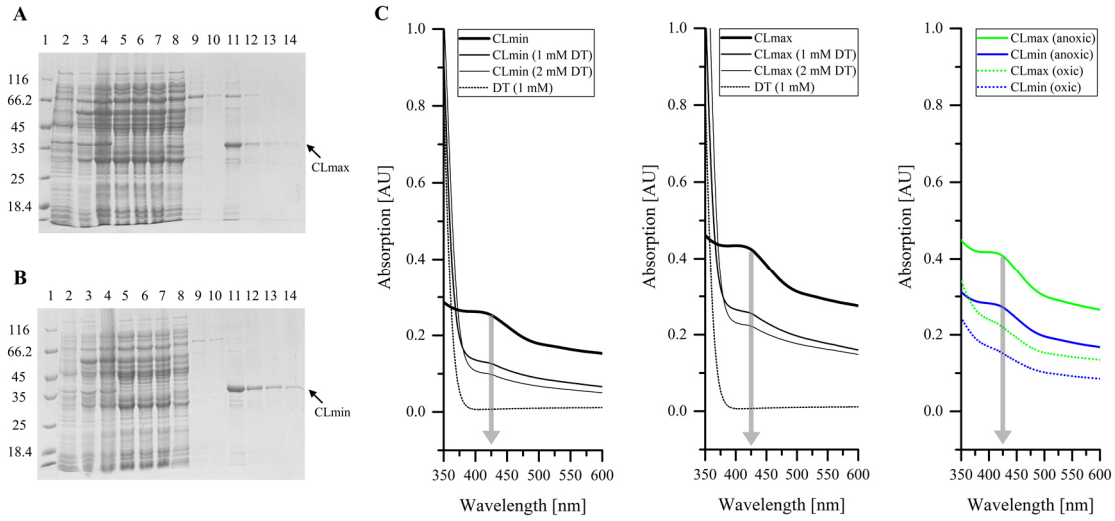

Figure 21: SDS-PAGE and UV-Vis analysis of $(ChlL)_2$ variants CLmax and CLmin.
Proteins were produced in *E. coli* BL21(DE3) and purified *via* the N-terminal GST-tag under anoxic conditions. Samples were separated on a 12 % SDS-PAGE. The detailed methodology is described in the materials and methods section. **A**: SDS-PAGE analysis of the production and purification of $(ChlL)_2$ variant CLmax. **B**: SDS-PAGE of the production and purification of $(ChlL)_2$ variant CLmin. *Lanes 1*: Molecular mass marker, relative molecular masses (x 1'000) are indicated. *Lanes 2*: Whole-cell sample before induction. *Lanes 3*: Whole-cell sample 17 h after induction. *Lanes 4*: Sample of the cell lysate before ultracentrifugation. *Lanes 5*: Sample of the supernatant after ultracentrifugation. *Lanes 6-7*: Samples of the column flowthrough after the first and second column pass, respectively (1 mL column volume). *Lanes 8*: Wash fraction 1 (buffer A). *Lanes 9*: Wash fraction 2 (5-10 mM ATP in buffer A). *Lanes 10*: Wash fraction 3 (buffer A). *Lanes 11-14*: Samples of elution fractions after PreScission protease cleavage. **C**: UV-Vis analysis of $(ChlL)_2$ variants CLmax (34 µM) and CLmin (19 µM). Proteins were purified and [FeS] clusters were reconstituted as described in the materials and methods section. CLmax and CLmin showed an absorption signal at 424 ± 4 nm as also observed for the wild-type $(ChlL)_2$ (grey shading). Variant CLmin (left panel) and CLmax (middle panel) were analyzed in the absence and presence of dithionite (DT, 1 mM and 2 mM). Furthermore, spectra were recorded before and after exposing the proteins to air (17 h, 4 °C, right panel).

These findings suggested that the mutations at the docking face of CLmax and CLmin hamper the *in vivo* assembly of the respective [FeS] clusters. However, as judged from the iron/sulfur determination and UV-Vis analysis, the chemical reconstitution of CLmax and CLmin allowed for the *in vitro* maturation of the redox-active [FeS] clusters.

3.2.2 Interaction of $(ChlL)_2$ and variants CLmax and CLmin with the MoFe protein of nitrogenase

To investigate the potential interaction of $(ChlL)_2$ from *P. marinus* and variants CLmax and CLmin with the MoFe protein of nitrogenase, the GST-tagged reductase subcomplex (bait protein) was immobilized on Protino glutathione agarose. Subsequently, purified MoFe protein from *A. vinelandii* (prey protein, provided by Christian Trncik, AG Einsle, Albert-Ludwigs-Universität Freiburg) was added and the subcomplexes were incubated in the presence of 2 mM $AlCl_3$, 10 mM MgADP and 50 mM NaF as recently described for trapping of the homologous DPOR complex (Moser *et al.*, 2013). After a washing step to remove unbound MoFe, the bait protein was proteolytically liberated from the affinity matrix. The SDS-PAGE analysis of the resulting elution fractions is shown in Figure 22.

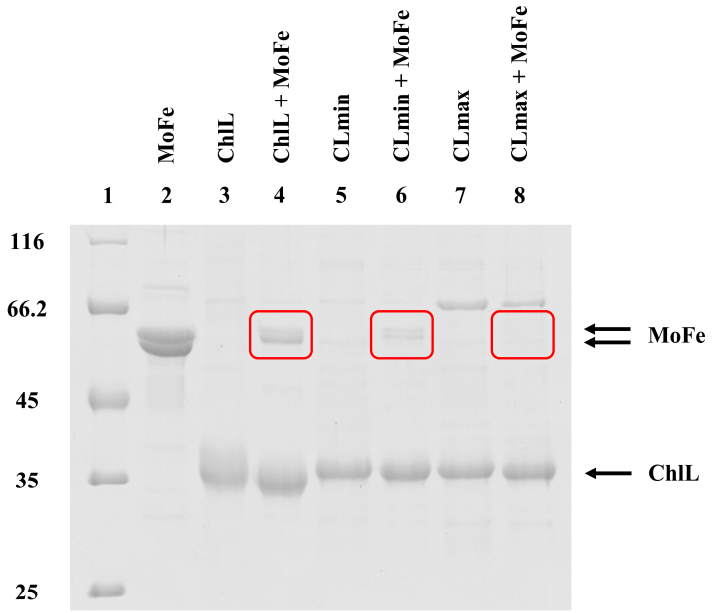

Figure 22: SDS-PAGE analysis of elution fractions from the interaction-assay indicating complex formation between MoFe from *A. vinelandii* and $(ChlL)_2$ from *P. marinus*.
GST-tagged reductase subcomplexes $(ChlL)_2$ or variants CLmax/CLmin were immobilized and trapping of MoFe was performed in the presence of $AlCl_3$, MgADP and NaF. Resulting protein complexes were liberated by PreScission protease treatment. *Lane 1*: Molecular mass marker, relative molecular masses (x 1'000) are indicated. *Lane 2*: Purified MoFe protein. *Lane 3*: Purified ChlL. *Lane 4*: Elution fraction of the interaction-assay ChlL + MoFe. *Lane 5*: Purified CLmin. *Lane 6*: Elution fraction of the interaction-assay CLmin + MoFe. *Lane 7*: Purified CLmax. *Lane 8*: Elution fraction of the interaction-assay CLmax + MoFe. Trapped MoFe protein is highlighted red.

As indicated in Figure 22 (lane 4), wild-type $(ChlL)_2$, with a calculated molecular mass of 32'400, co-eluted with high amounts of MoFe (subunits NifD and NifK, 55'300 and 59'500, respectively). Variant CLmin revealed a reduced affinity to MoFe compared to the wild-type $(ChlL)_2$, while no interaction was detected between MoFe and variant CLmax (compare Figure 22, lanes 4, 6, 8). Further investigations performed by Christian Trncik (AG Einsle, Albert-Ludwigs-Universität Freiburg) showed that wild-type $(ChlL)_2$ and both variants were not able to support nitrogenase activity (data not shown). These findings were further analyzed by gel filtration analyses of CLmin and CLmax. Both variants revealed strong aggregate formation with only minimal amounts of the target protein eluting as a dimer (data not shown). These results clearly indicated that the employed mutagenesis strategy not only effectuated the docking region of CLmin and CLmax. Furthermore, an overall effect on the ternary and quarternary structure was to be expected.

Instead, wild-type $(ChlL)_2$ was identified as a potential binding partner of MoFe (Figure 22, lane 4). Obviously, this chimeric protein complex does not facilitate enzymatic nitrogenase activity as also described in a previous study (Moser *et al.*, 2013). Taking into account the complex protein dynamics during the sequence of association and dissociation between reductase and catalytic complex in the nitrogenase system, the abovementioned structural comparison of nitrogenase and DPOR might not represent the only docking geometry in the time course of nitrogenase catalysis (Tezcan *et al.*, 2005; Einsle and Rees, 2020; Rutledge and Tezcan, 2020). Despite the fact that electron transfer between $(ChlL)_2$ and MoFe was not detected, the presented data clearly indicated the static complex formation between MoFe and $(ChlL)_2$.

3.2.3 Reductase $(ChlL)_2$ and MoFe are forming a nitrogenase-like ternary complex

The chimeric complex formed between $(ChlL)_2$ and MoFe was further explored using gel filtration under anoxic conditions in the presence of MgADP, $AlCl_3$ and NaF (Figure 23). Control experiments of individual subcomplexes $(ChlL)_2$ and MoFe revealed the expected chromatograms for the $(ChlL)_2$ dimer (elution volume: 73.8 mL) and MoFe tetramer (elution volume: 63.7 mL). A relative molecular mass of 355'000 (elution volume: 55.6 mL) was determined for the resulting chimeric protein complex of $(ChlL)_2$ and MoFe (Figure 23, red). In agreement with the relative molecular mass, SDS-PAGE and subsequent densitometric analysis of the fractionated complex (Figure 23, lane 5)

revealed a ratio of approximately 2.1 mol $(ChlL)_2$ dimer per mol MoFe tetramer. A chimeric octamer with a stoichiometry of $(ChlL)_2MoFe(ChlL)_2$ was concluded (calculated molecular mass of 359'078). Accordingly, the described complex resembles the octameric protein architecture observed for nitrogenase or DPOR complexes (Schindelin *et al.*, 1997; Moser *et al.*, 2013).

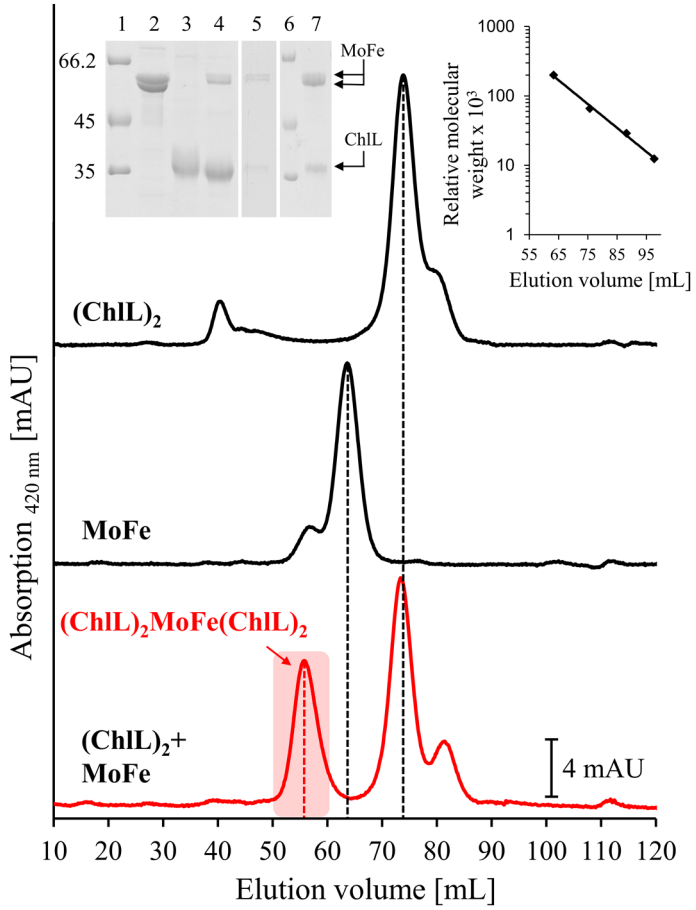

Figure 23: Assembly and native molecular-mass determination of the chimeric $(ChlL)_2MoFe(ChlL)_2$ complex.
Immobilized GST-tagged $(ChlL)_2$ was supplemented with MoFe in the presence of MgADP, $AlCl_3$ and NaF. The resulting chimeric complex was liberated by PreScission protease cleavage. The native molecular masses of the eluted complex (red) and individual subcomplexes MoFe and $(ChlL)_2$ (black) were analyzed on a HiLoad Superdex 200 16/60 column previously calibrated (right inset) by using protein standards β-amylase (M_r=200'000), albumin (M_r=66'000), carbonic anhydrase (M_r=29'000) and cytochrome c (M_r=12'400). SDS-PAGE (left inset): *Lanes 1 and 6*: Molecular mass marker, relative molecular masses (x 1'000) are indicated. *Lane 2*: Purified MoFe protein. *Lane 3*: Purified $(ChlL)_2$. *Lane 4*: Elution of the chimeric complex after protease cleavage. *Lane 5*: Fractions of the chimeric complex, as obtained by means of gel filtration (elution volume 55–60 mL). *Lane 7*: Identical sample concentrated by ultrafiltration.

3.2.4 Nucleotide-dependent interaction of $(ChlL)_2$ and MoFe

Nucleotide-induced conformational alterations and affinity changes are of central importance for the dynamic switch mechanism of nitrogenase (Howard and Rees, 1994; Seefeldt and Dean, 1997; Einsle and Rees, 2020). Therefore, the formation of the chimeric $(ChlL)_2MoFe(ChlL)_2$ complex was investigated in the presence of 10 mM ATP, 10 mM ADP and 1.5 mM AMP-PNP, respectively. Further experiments were performed with $(ChlL)_2$ variants to analyze the influence of single amino acid exchanges in the docking face of $(ChlL)_2$. The central importance of residue Tyr127 was reported previously: A complete loss of DPOR activity was observed for $(ChlL)_2$ variants Y127D and Y127S (Wätzlich *et al.*, 2009). The present study provided further insights by using the described interaction-assay (Figure 8) to analyze the interaction of the $(ChlL)_2$ variants Y127D and Y127S with DPOR subcomplex $(ChlNB)_2$. In agreement with the reported loss of DPOR activity, no interaction of subcomplex $(ChlNB)_2$ with $(ChlL)_2$ variants Y127D or Y127S was determined (Appendix Figure 30 A).

In order to compare the DPOR and nitrogenase system, the formation of the chimeric $(ChlL)_2MoFe(ChlL)_2$ complex was explored employing $(ChlL)_2$ variants Y127D and Y127S in the presence of different nucleotides. The investigation revealed that the complex formation between MoFe and wild-type $(ChlL)_2$ is not significantly modulated by ATP, ADP and AMP-PNP, respectively (Figure 24, lanes 6-8). Thus, the nucleotide-controlled affinity changes are not indicated for the chimeric $(ChlL)_2MoFe(ChlL)_2$ complex. It was concluded that the $(ChlL)_2MoFe(ChlL)_2$ complex represents a trapped state of the usually transient interaction between catalytic and reductase subcomplex in a nitrogenase-like system. Interestingly, variant $(ChlL)_2$ Y127D revealed a complete loss of MoFe interaction (Figure 24, lanes 9-11). Obviously, the negatively charged aspartate at the docking face of $(ChlL)_2$ abolishes the interaction with MoFe. Similar results were obtained for the interaction with the DPOR $(ChlNB)_2$ subcomplex (Appendix Figure 30). As expected, nitrogenase catalysis was not supported by $(ChlL)_2$ variant Y127D (data not shown).

Interestingly, variant $(ChlL)_2$ Y127S revealed a completely different type of interaction with MoFe when compared to the interaction with DPOR subcomplex $(ChlNB)_2$. A low binding affinity was detected in the presence of ADP as indicated by the binding of 0.02 mol MoFe per mol $(ChlL)_2$ (Figure 24, lane 13). This value was substantially

increased to 0.12 in the presence of ATP (Figure 24, lane 12). A maximum of 0.71 mol MoFe per mol $(ChlL)_2$ was observed in the presence of the ATP analog AMP-PNP (Figure 24, lane 14). These findings highlight the central importance of residue Tyr127 in the docking face of $(ChlL)_2$: Variant $(ChlL)_2$ Y127S restores the nucleotide-modulated interaction in the chimeric complex with MoFe as described for the homologous nitrogenase and DPOR systems (Seefeldt and Dean, 1997; Tezcan *et al.*, 2005; Moser *et al.*, 2013; Seefeldt, Hoffman, *et al.*, 2018). Despite the dynamic protein-protein interaction, variant Y127S was not able to support dinitrogen or azide reduction or the oxidation of Ti(III) citrate in a chimeric nitrogenase assay (performed by Christian Trncik, AG Einsle, Albert-Ludwigs-Universität Freiburg, data not shown).

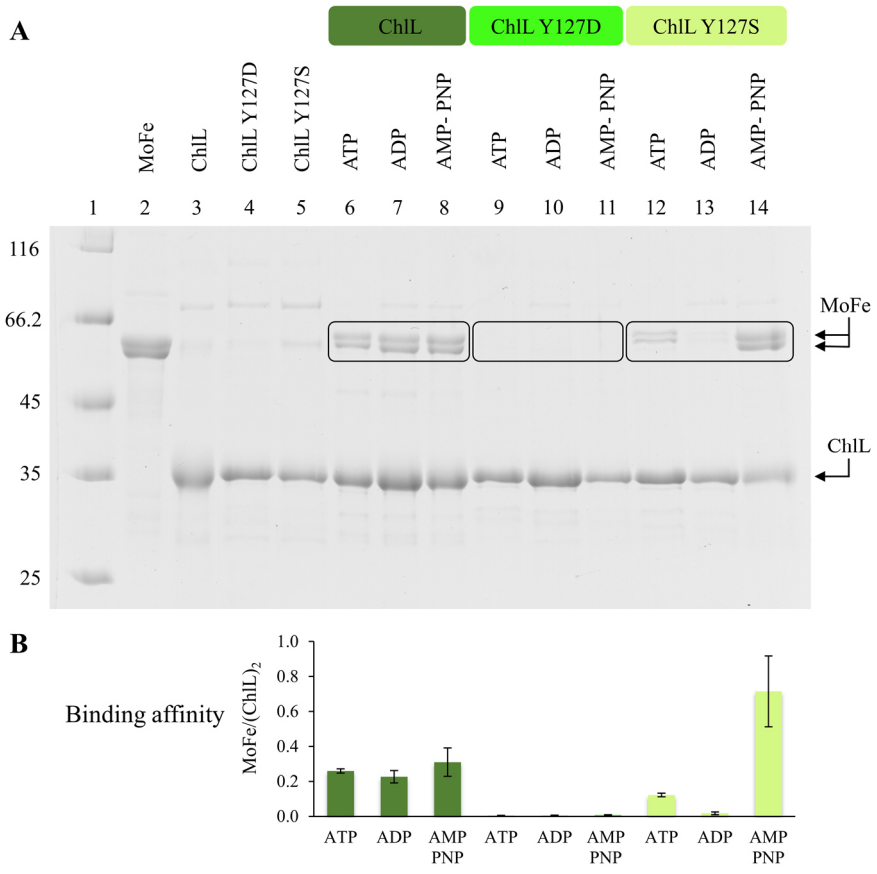

Figure 24: Nucleotide-dependent interaction of $(ChlL)_2$ and $(ChlL)_2$ variants Y127D/Y127S with MoFe.
A: SDS-PAGE analysis indicating the protein-protein interactions of the immobilized reductase $(ChlL)_2$ or variants Y127D and Y127S with MoFe in the presence of ATP, ADP and AMP-PNP. *Lanes 1*: Molecular mass marker, relative molecular masses (x 1'000) are indicated. *Lanes 2-5*: Purified MoFe, $(ChlL)_2$, $(ChlL)_2$ Y127D and $(ChlL)_2$ Y127S. *Lanes 6-8*, *9-11 and 12-14*: Interaction of $(ChlL)_2$, $(ChlL)_2$ Y127D and $(ChlL)_2$ Y127S with MoFe in the presence of ATP, ADP or AMP-PNP, respectively. **B**: Protein quantification by densitometry using GelQuant.NET software. Binding affinities are shown as MoFe/$(ChlL)_2$ ratios. Mean values of three independent experiments with standard deviation are shown.

3.2.5 Reductant-independent ATPase activity of $(ChlL)_2$ and variants Y127D/Y127S

In an attempt to follow alternative catalytic activities of the chimeric $(ChlL)_2MoFe(ChlL)_2$ complex, the reductant-independent ATPase activity of $(ChlL)_2$ was investigated. ATP binding to the reductase subcomplex triggers the association with MoFe in the nitrogenase system. Subsequent ATP hydrolysis is required for the dissociation of the transient complex after electron transfer (Seefeldt, Peters, *et al.*, 2018; Rutledge and Tezcan, 2020). The ATPase activity of nitrogenase in the absence of reducing agents (reductant-independent) was reported previously (Ljones and Burris, 1972; Imam and Eady, 1980; Cordewener *et al.*, 1987, 1988; Larsen, Christensen and Watt, 1995). Thereby, the presence of MoFe stimulates the ATPase activity of the reductase subcomplex. A related stimulation of the ATPase activity of $(ChlL)_2$ in the presence of $(ChlNB)_2$ was also demonstrated for the DPOR system (Bröcker *et al.*, 2010). Accordingly, further experimental evidence of the interplay of $(ChlL)_2$ and MoFe was obtained by analyzing the ATPase activity of $(ChlL)_2$ and related variants in the absence and presence of MoFe or $(ChlNB)_2$. For this purpose, the release of free phosphate by the reductase subcomplex was followed by a commercial malachite green assay.

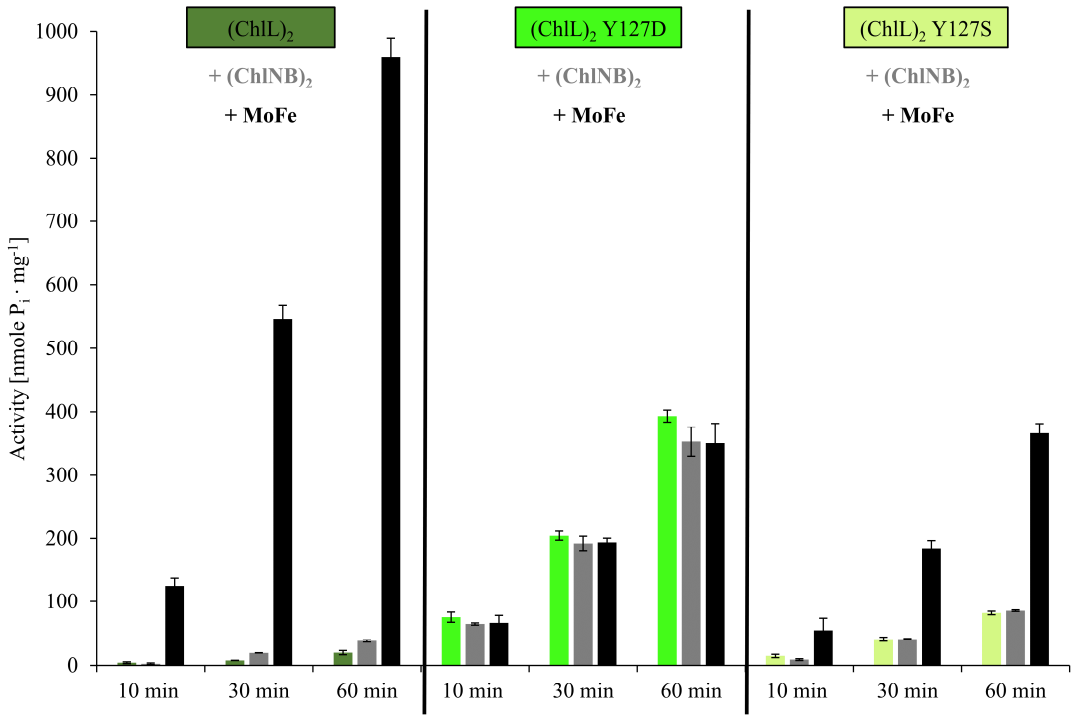

Figure 25: Reductant-independent ATPase activity of $(ChlL)_2$ or variants Y127D and Y127S.
The basal ATPase activity of $(ChlL)_2$ (dark green) and variants Y127D (bright green) and Y127S (yellow-green) are shown. The modulated ATPase activity in the presence of MoFe from *A. vinelandii* and DPOR subcomplex $(ChlNB)_2$ from *P. marinus* is depicted in black and grey, respectively. Mean values of three independent experiments with standard deviation are shown.

The wild-type $(ChlL)_2$ revealed a basal ATPase activity of 0.3 nmol mg^{-1} min^{-1} under the employed *in vitro* conditions (Figure 25). In contrast, an increased ATPase activity of 6.5 and 1.4 nmol mg^{-1} min^{-1} was determined for $(ChlL)_2$ variant Y127D and Y127S, respectively. Clearly, the substitution of Tyr127 by aspartate or serine altered the conformation of the reductase into a more ATPase active state in the absence of a catalytic subcomplex. The basal ATPase activity of wild-type $(ChlL)_2$ was increased to 0.6 nmol mg^{-1} min^{-1} in the presence of DPOR subcomplex $(ChlNB)_2$. Interestingly, the basal ATPase activities of both $(ChlL)_2$ variants were not significantly altered in the presence of DPOR subcomplex $(ChlNB)_2$. These findings support the observations that both $(ChlL)_2$ variants are not able to facilitate DPOR activity (Wätzlich *et al.*, 2009) and that protein-protein interactions of both $(ChlL)_2$ variants with $(ChlNB)_2$ were not detected (Appendix Figure 30 A).

The low basal ATPase activity of the wild-type $(ChlL)_2$ reductase was substantially increased to a value of 16.0 nmol mg^{-1} min^{-1} in the presence of MoFe. It was concluded that the formation of the chimeric $(ChlL)_2$MoFe$(ChlL)_2$ complex induces core structural rearrangements in $(ChlL)_2$, ultimately resulting in an increased ATPase activity of $(ChlL)_2$. In agreement with the abovementioned abolished protein-protein interaction between MoFe and $(ChlL)_2$ variant Y127D (Figure 24), the ATPase activity of $(ChlL)_2$ variant Y127D was not significantly altered in the presence of MoFe. However, experiments with $(ChlL)_2$ variant Y127S in the presence of MoFe resulted in an increased ATPase activity. This might indicate that the serine at position 127 enables the inter-subcomplex crosstalk with MoFe.

Overall, the ATPase activity of $(ChlL)_2$ variant Y127S is triggered in response to the chimeric interaction with the catalytic MoFe subcomplex of nitrogenase (Figure 25). Furthermore, the single mutation Y127S at the docking face of $(ChlL)_2$ allows for the nucleotide-dependent interaction of $(ChlL)_2$ with MoFe (Figure 24) as reported for the DPOR and nitrogenase system. Although the investigated reductases were unable to support nitrogenase activity, variant $(ChlL)_2$ Y127S might be regarded as an initial step towards an alternative nitrogenase reductase. Apart from a fine-tuned dynamic complex formation and ATPase activity, the further design of an alternative nitrogenase reductase requires a more subtle adaptation of electron transfer steps. Nevertheless, the investigated reductase $(ChlL)_2$ Y127S might be an interesting platform for the future development of a more oxygen-tolerant nitrogenase reductase. Finally, an alternative nitrogenase

reductase might reveal yet uncharacterized interactions of NifH with proteins of the M- and P-cluster maturation machinery.

3.3 Microscale thermophoresis

Microscale thermophoresis (MST) is a sensitive biophysical method to analyze and quantify biomolecular interactions using the physical principle of thermophoresis. Among a broad range of biomolecular interactions, this technique is used for the investigation of protein-protein interactions or the interactions of proteins with small molecules (Wienken *et al.*, 2010; Seidel *et al.*, 2013; Jerabek-Willemsen *et al.*, 2014; Webert *et al.*, 2014). Recently, the binding of nucleotides to the $(NifH)_2$ reductase of nitrogenase was investigated by means of MST (Pence, 2020). However, MST has not been utilized for the investigation of inter-subcomplex interactions of nitrogenase or nitrogenase-like enzymes in the current literature.

In the present study, preliminary MST experiments with nitrogenase subcomplexes MoFe and $(NifH)_2$ from *A. vinelandii* and DPOR subcomplexes $(ChlL)_2$ and $(ChlNB)_2$ from *P. marinus* were performed under anoxic conditions. Applicability of MST for the analysis of inter-subcomplex interactions of nitrogenase-like enzymes was investigated for the homologous DPOR and nitrogenase systems and for the chimeric interaction between MoFe and $(ChlL)_2$. Initial experiments indicated that labeling of the catalytic components MoFe and $(ChlNB)_2$ resulted in the most consistent data when compared to experiments with labeled reductase subcomplexes (data not shown). Therefore, MST experiments were performed with labeled $(ChlNB)_2$ (or MoFe) protein supplemented with 16 dilutions of the unlabeled reductase subcomplex. This strategy also avoids additional fluorescence changes that might occur due to interactions between nucleotides and a labeled reductase subcomplex.

Experiments with labeled MoFe and "ligand" $(NifH)_2$ indicated a strong ligand-dependent initial fluorescence change (data not shown). Upon binding of the nitrogenase subcomplexes, the fluorescence probe might be affected by fluorescence quenching. As an alternative to the temperature-related fluorescence intensity changes recorded during MST, the initial fluorescence intensities can be used to calculate binding constants (López-Méndez *et al.*, 2021). However, it was not possible to process the resulting data using MO.Affinity Analysis v2.3 (NanoTemper) due to a limited concentration range of the unlabeled ligand. The initial fluorescence was more consistent in MST experiments

employing subcomplexes MoFe or $(ChlNB)_2$ in combination with $(ChlL)_2$. Accordingly, the temperature-related fluorescence intensity changes were analyzed with MO.Affinity Analysis v2.3 (NanoTemper) using the built-in K_d binding model. Representative MST-fluorescence time traces and preliminary binding curves of the inter-subcomplex interaction of MoFe and $(ChlL)_2$ are shown in Figure 26.

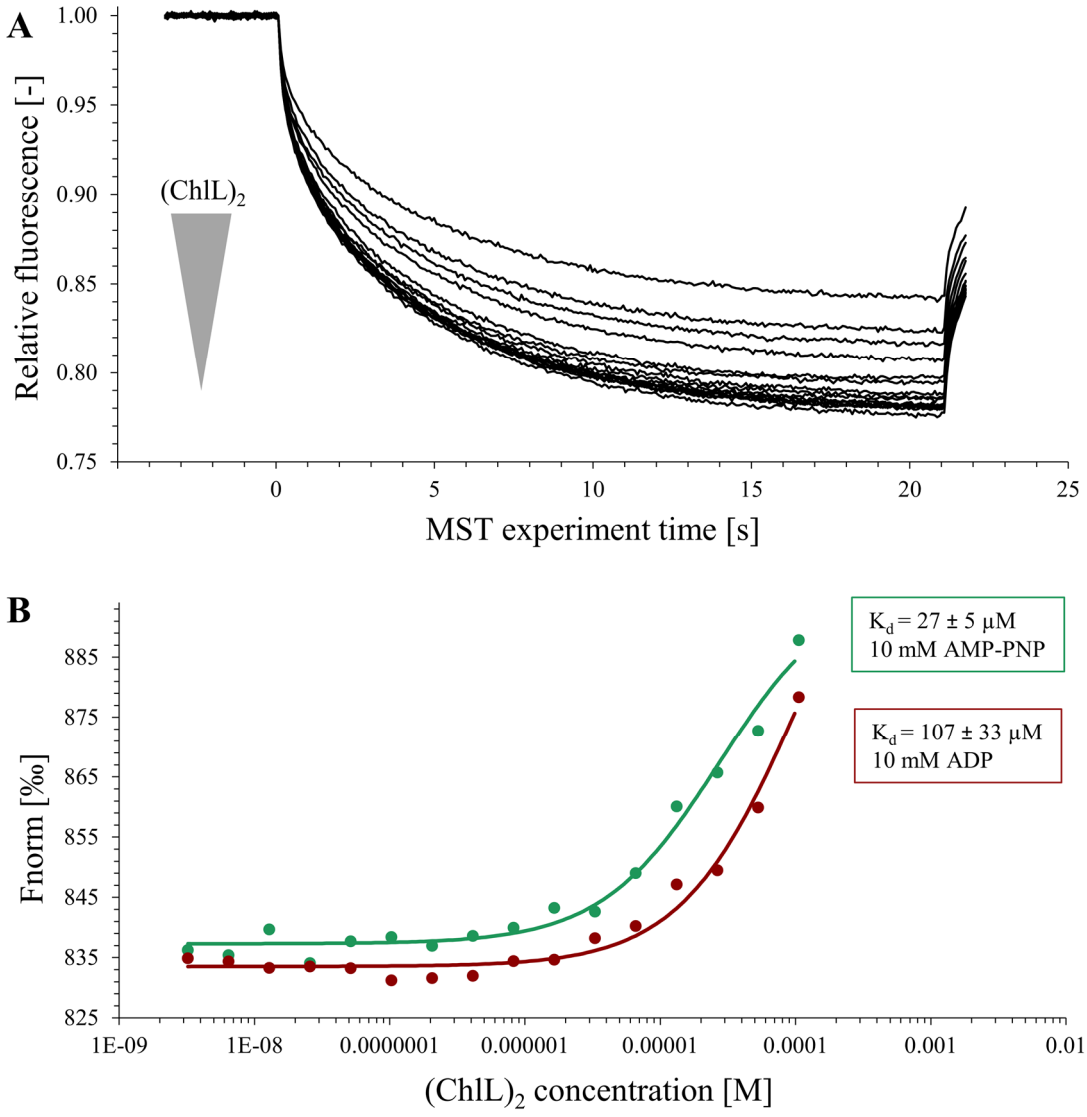

Figure 26: Preliminary MST results of the interaction between MoFe and $(ChlL)_2$.
Experiments were performed under anoxic conditions using wax-sealed MST capillaries. MoFe was labeled with cyanine 5 succinimidyl ester (Lumiprobe). **A**: Representative MST-fluorescence time traces. Labeled MoFe protein (40 nM final concentration) was supplemented with ligand $(ChlL)_2$ (0.1 mM-3.2 nM final concentration) in the presence of 10 mM AMP-PNP. The decreasing $(ChlL)_2$ concentration is indicated by grey shading. **B**: Preliminary binding curves of the chimeric interaction between MoFe and $(ChlL)_2$. Labeled MoFe (40 nM final concentration) was supplemented with the indicated concentrations of ligand $(ChlL)_2$. Experiments were performed at room temperature on a Monolith NT.115 (NanoTemper) in the presence of 10 mM AMP-PNP (green) and 10 mM ADP (red), respectively.

Using the initial fluorescence (0 s) and the fluorescence after thermodiffusion (4 s) depicted in the exemplary MST-fluorescence time trace chart (Figure 26 A), a K_d value of 27 ± 5 µM was determined in the presence of 10 mM AMP-PNP (Figure 26 B). A weaker interaction between MoFe and $(ChlL)_2$ was observed in the presence of 10 mM ADP (K_d = 107 ± 33 µM). Further preliminary K_d values calculated from MST experiments with nitrogenase-like subcomplexes are summarized in Figure 27.

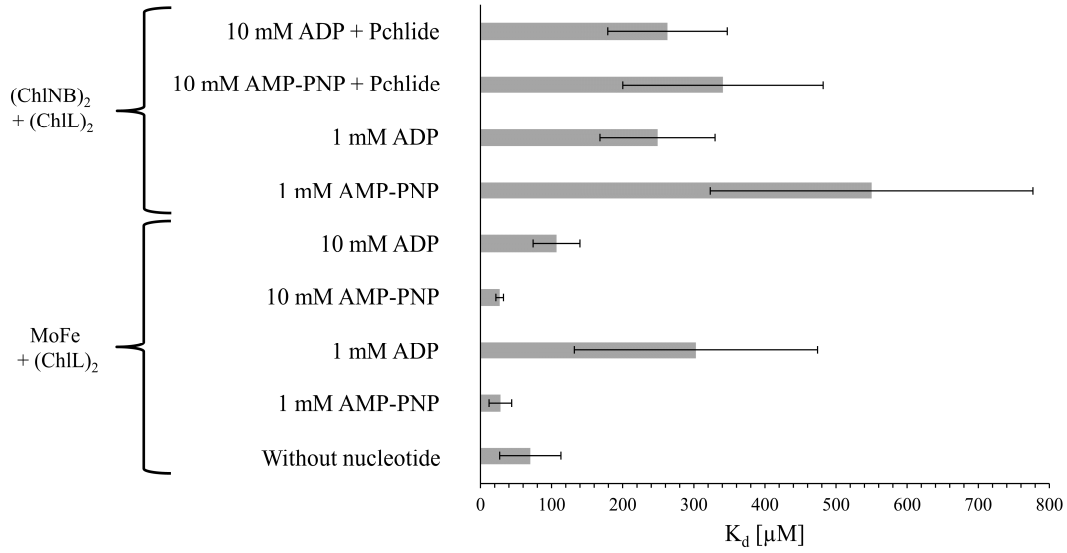

Figure 27: Preliminary MST results of the inter-subcomplex interactions of nitrogenase-like enzymes.
The homologous interaction between DPOR subcomplexes $(ChlL)_2$ and $(ChlNB)_2$ and the chimeric interaction between subcomplexes MoFe and $(ChlL)_2$ were analyzed using MST. Sixteen dilutions of the ligand $(ChlL)_2$ were supplemented with labeled MoFe or $(ChlNB)_2$, respectively. The K_d values were calculated from three technical replicates using MO.Affinity Analysis v2.3 (NanoTemper).

The results indicate that the chimeric interaction between MoFe and $(ChlL)_2$ is stronger than the homologous interaction between $(ChlL)_2$ and $(ChlNB)_2$. This is in agreement with results from the described on-column interaction assay: Substantial amounts of MoFe co-eluted with $(ChlL)_2$ in the interaction assay (Figure 24), whereas $(ChlNB)_2$ revealed a weaker affinity to $(ChlL)_2$ (Appendix Figure 30 B). No significant changes in the K_d values were observed for the interaction of $(ChlL)_2$ and $(ChlNB)_2$ in the presence of Pchlide, ADP and AMP-PNP. In contrast, the affinity of $(ChlL)_2$ to MoFe was increased in the presence of AMP-PNP. However, the presented preliminary results have a number of limitations: None of the investigated interactions resulted in a complete binding curve which clearly affects the precision of the K_d fit model (Figure 26 B).

It seems that the binding constants of the investigated interactions are in a µM range. Accordingly, the titrated unlabeled ligand $(ChlL)_2$ is likely needed in mM concentrations to saturate the binding partner. The solubility of ligands in high concentrations has been described as a common limitation of MST (Seidel *et al.*, 2013).

Previous MST studies of FeS proteins highlighted that the redox state of the protein cofactor strongly effectuates bindings affinities (Webert *et al.*, 2014; Freibert *et al.*, 2015). Attempts to oxidize the MoFe protein with 1 mM indigo carmine after labeling did not result in a stronger interaction with reduced NifH (data not shown). Overall, MST might be used to investigate the interaction of nucleotides with nitrogenase-like reductases (Pence, 2020). However, this method might not be suitable for the investigation of the inter-subcomplex interactions of nitrogenase-like enzymes due to the required high mM concentrations of the unlabeled subcomplex.

4. Summary

The class of nitrogenase-like enzymes consists of a homodimeric, electron-donating, ATP-utilizing reductase subcomplex and a heterotetrameric catalytic subcomplex. Here, the formation of heterologous and chimeric enzymes, combining subcomplexes of nitrogenase, chlorophyllide *a* oxidoreductase (COR), dark-operative protochlorophyllide oxidoreductase (DPOR) (both from bacteriochlorophyll biosynthesis) and Ni^{2+}-sirohydrochlorin *a*,*c*-diamide reductase (CfbCD, from cofactor F_{430} biosynthesis) was functionally analyzed.

First, the COR enzymes from *Heliobacterium modesticaldum* and *Rhodopseudomonas palustris* were recombinantly produced and biochemically characterized. Spectroscopic and bioinformatic analyses indicated the presence of two [4Fe-4S] clusters. The pigments produced by COR from *H. modesticaldum* and from *R. palustris* revealed a distinct UV-Vis spectrum in activity assays, supporting the proposed alternative 8-vinyl reductase activity (1,4-dihydrogenation) of COR from *H. modesticaldum*. An octameric COR enzyme was assembled in analogy to nitrogenase or DPOR and revealed a significantly weaker interaction of the COR subcomplexes. A heterologous COR enzyme consisting of subcomplexes $(BchX)_2$ from *Roseobacter denitrificans* and $(BchYZ)_2$ from *R. palustris* was enzymatically active. Various experimental strategies for the crystallization of COR did not result in suitable diffracting protein crystals.

The second part of this study investigated the formation of chimeric complexes of various reductases with the nitrogenase MoFe protein from *Azotobacter vinelandii*. Gel filtration experiments indicated the formation of a chimeric, nitrogenase-like $(ChlL)_2MoFe(ChlL)_2$ complex between MoFe and DPOR reductase $(ChlL)_2$ from *Prochlorococcus marinus*. On-column interaction-assays and initial microscale thermophoresis experiments suggested that the chimeric interaction between MoFe and $(ChlL)_2$ is stronger than the inter-subcomplex interaction in the homologous DPOR system. An investigation of the nucleotide-dependent association and dissociation of the chimeric complex revealed no significant modulation of the binding affinity in the presence of the $(ChlL)_2$ wild-type protein and various nucleotides. However, $(ChlL)_2$ variant Y127S showed a dynamic nucleotide-dependent complex formation with MoFe as described for the nitrogenase system. Although no nitrogenase activity was observed, the ATPase activity of $(ChlL)_2$ and $(ChlL)_2$ variant Y127S was triggered upon association with MoFe, indicating an

inter-subcomplex crosstalk. The described $(ChlL)_2$ variant Y127S might be an attractive platform for the characterization of the diverse functions of NifH and the future design of a more robust nitrogenase reductase.

5. Outlook

In order to further elucidate the detailed reaction mechanism of COR, the three-dimensional structure of COR is required. The following points might be addressed in future studies:

- An alternative purification strategy of the $(BchYZ)_2$ subcomplex using an N-terminal GST-tag and a C-terminal Strep-tag (BchZ) to increase protein purity and homogeneity. This approach might prevent the C-terminal degradation of BchZ.
- The identification of effective conditions to assemble the octameric COR complex. Alternatively, $(BchX)_2$ variants might be used for the trapping of the octameric COR complex as reported for the nitrogenase and DPOR system (Ryle and Seefeldt, 1996; Bröcker *et al.*, 2010).
- The development of new powerful methods like single-particle electron cryo-microscopy (cryo-EM) and X-ray free electron laser (XFEL) protein crystallography might allow for the structural investigation using proteins in solution or microcrystals, respectively (Liu and Lee, 2019; Yip *et al.*, 2020).

The engineering of organisms with the ability to fix nitrogen is an attractive possibility and a continuous stimulus for nitrogenase research. The following points might be considered in future studies towards an alternative nitrogenase reductase:

- A comparative analysis of midpoint potentials of the [4Fe-4S] clusters of $(ChlL)_2$, $(ChlL)_2$ variants and $(NifH)_2$ in the presence of different nucleotides.
- The three-dimensional structure of the chimeric complex of MoFe and $(ChlL)_2$ or variant $(ChlL)_2$ Y127S might support the development of chimeric nitrogenase activity using an alternative reductase.
- $(ChlL)_2$ or variant $(ChlL)_2$ Y127S might be used in interaction studies with P- or M-cluster maturation proteins (e.g. NifEN)

6. References

Badalyan, A. *et al.* (2019) "An Efficient Viologen-Based Electron Donor to Nitrogenase", *Biochemistry*, 58, p. 4590−4595.

Battersby, A. R. (2000) "Tetrapyrroles: The pigments of life", *Natural Product Reports*, 17(6), pp. 507–526.

Beinert, H. (1983) "Semi-micro methods for analysis of labile sulfide and of labile sulfide plus sulfane sulfur in unusually stable iron-sulfur proteins", *Analytical Biochemistry*, 131(2), pp. 373–378.

Bertani, G. (1951) "Studies on Lysogenesis. I. The Mode of Phage Liberation by Lysogenic *Escherichia coli*", *Journal of Bacteriology*, 62(3), pp. 293–300.

Bird, C. L. and Kuhn, A. T. (1981) "Electrochemistry of the viologens", *Chemical Society Reviews*, 10(1), pp. 49–82.

Bollivar, D. W. *et al.* (1994) "Directed mutational analysis of bacteriochlorophyll *a* biosynthesis in *Rhodobacter capsulatus*", *Journal of Molecular Biology*, pp. 622–640.

Boyd, E. S. and Peters, J. W. (2013) "New insights into the evolutionary history of biological nitrogen fixation", *Frontiers in Microbiology*, 4, pp. 1–12.

Bradford, M. M. (1976) "A Rapid and Sensitive Method for the Quantitation of Microgram Quantities of Protein Utilizing the Principle of Protein-Dye Binding", *Analytical Biochemistry*, 72, pp. 248–254.

Bröcker, M. J. (2006) *Diplomarbeit: Charakterisierung der lichtunabhängigen Protochlorophyllid Oxidoreduktase aus Chlorobium tepidum*. TU Braunschweig.

Bröcker, M. J., Virus, S., *et al.* (2008a) "ATP-driven reduction by dark-operative protochlorophyllide oxidoreductase from *Chlorobium tepidum* mechanistically resembles nitrogenase catalysis", *Journal of Biological Chemistry*, 283(16), pp. 10559–10567.

Bröcker, M. J., Wätzlich, D., *et al.* (2008b) "Substrate recognition of nitrogenase-like dark operative protochlorophyllide oxidoreductase from *Prochlorococcus marinus*", *Journal of Biological Chemistry*, 283(44), pp. 29873–29881.

Bröcker, M. J. *et al.* (2010) “Biosynthesis of (bacterio)chlorophylls: ATP-dependent transient subunit interaction and electron transfer of dark operative protochlorophyllide oxidoreductase”, *Journal of Biological Chemistry*, 285(11), pp. 8268–8277.

Brotosudarmo, T. H. P. *et al.* (2009) “Single-molecule spectroscopy reveals that individual low-light LH2 complexes from *Rhodopseudomonas palustris* 2.1.6. Have a heterogeneous polypeptide composition”, *Biophysical Journal*, 97(5), pp. 1491–1500.

Brouers, M. and Michel-Wolwertz, M. R. (1983) “Estimation of protochlorophyll(ide) contents in plant extracts; re-evaluation of the molar absorption coefficient of protochlorophyll(ide)”, *Photosynthesis Research*, 4(1), pp. 265–270.

Bulen, W. A. and LeComte, J. R. (1966) “The nitrogenase system from Azotobacter: two-enzyme requirement for N_2 reduction, ATP-dependent H_2 evolution, and ATP hydrolysis”, *Proceedings of the National Academy of Sciences*, 56(3), pp. 979–986.

Burén, S. *et al.* (2020) “Biosynthesis of Nitrogenase Cofactors”, *Chemical Reviews*, 120(12), pp. 4921–4968.

Burén, S. and Rubio, L. M. (2018) “State of the art in eukaryotic nitrogenase engineering”, *FEMS Microbiology Letters*, 365(2), pp. 1–9.

Burke, D. H., Hearst, J. E. and Sidow, A. (1993) “Early evolution of photosynthesis: Clues from nitrogenase and chlorophyll iron proteins”, *Proceedings of the National Academy of Sciences of the United States of America*, 90(15), pp. 7134–7138.

Capdevila-Cortada, M. (2019) “Electrifying the Haber–Bosch”, *Nature Catalysis*. Springer US, 2(12), p. 1055.

Chew, A. G. M. and Bryant, D. A. (2007) “Chlorophyll biosynthesis in bacteria: The origins of structural and functional diversity”, *Annual Review of Microbiology*, 61, pp. 113–129.

Cleland, W. W. (1964) “Dithiothreitol, a New Protective Reagent for SH Groups”, *Biochemistry*, 3(4), pp. 480–482.

Cordewener, J. *et al.* (1987) “Binding of ADP and orthophosphate during the ATPase reaction of nitrogenase”, *European Journal of Biochemistry*, 162(2), pp. 265–270.

Cordewener, J. *et al.* (1988) “The role of MgATP hydrolysis in nitrogenase catalysis”,

European Journal of Biochemistry, 172(3), pp. 739–745.

Cornish, A. S. and Page, W. J. (1998) "The catecholate siderophores of *Azotobacter vinelandii*: Their affinity for iron and role in oxygen stress management", *Microbiology*, 144(7), pp. 1747–1754.

Curatti, L. *et al.* (2007) "In vitro synthesis of the iron-molybdenum cofactor of nitrogenase from iron, sulfur, molybdenum, and homocitrate using purified proteins", *Proceedings of the National Academy of Sciences of the United States of America*, 104(45), pp. 17626–17631.

Ding, J. *et al.* (2019) "Viologen-inspired functional materials: Synthetic strategies and applications", *Journal of Materials Chemistry A*, 7(41), pp. 23337–23360.

Dingler, C. and Oelze, J. (1987) "Superoxide dismutase and catalase in *Azotobacter vinelandii* grown in continuous culture at different dissolved oxygen concentrations", *Archives of Microbiology*, 147(3), pp. 291–294.

Eady, R. R. (1996) "Structure-function relationships of alternative nitrogenases", *Chemical Reviews*, 96(7), pp. 3013–3030.

Einsle, O. and Rees, D. C. (2020) "Structural Enzymology of Nitrogenase Enzymes", *Chemical Reviews*, 120(12), pp. 4969–5004.

Emerich, D. W. and Burris, R. H. (1978) "Complementary functioning of the component proteins of nitrogenase from several bacteria", *Journal of Bacteriology*, 134(3), pp. 936–943.

Erisman, J. W. *et al.* (2008) "How a century of ammonia synthesis changed the world", *Nature Geoscience*, 1(10), pp. 636–639.

Erisman, J. W. *et al.* (2015) "Nitrogen: Too much of a vital resource", *Science Brief*.

Fortune, W. B. and Mellon, M. G. (1938) "Determination of Iron with *o*-Phenanthroline: A Spectrophotometric Study", *Industrial and Engineering Chemistry - Analytical Edition*, 10(2), pp. 60–64.

Frankenberg, N., Moser, J. and Jahn, D. (2003) "Bacterial heme biosynthesis and its biotechnological application", *Applied Microbiology and Biotechnology*, 63(2), pp. 115–127.

Freibert, S.-A. *et al.* (2015) “Anaerobic MicroScale Thermophoresis reveals the Redox dependency of ferredoxin in mitochondrial Fe/S biogenesis”, *Application Note NT-MO-026 (NanoTemper)*.

Freibert, S. A. *et al.* (2017) “Evolutionary conservation and in vitro reconstitution of microsporidian iron-sulfur cluster biosynthesis”, *Nature Communications*, 8.

Fujita, Y. and Bauer, C. E. (2000) “Reconstitution of light-independent protochlorophyllide reductase from purified Bchl and BchN-BchB subunits: In vitro confirmation of nitrogenase-like features of a bacteriochlorophyll biosynthesis enzyme”, *Journal of Biological Chemistry*, 275(31), pp. 23583–23588.

Galloway, J. N. *et al.* (2008) “Transformation of the Nitrogen Cycle: Recent Trends, Questions, and Potential Solutions”, *Science*, 320, pp. 889–892.

Ganskow, S. (2006) *Diplomarbeit: Heterologe Expression und Charakterisierung der lichtunabhängigen Protochlorophyllid-Oxidoreduktase aus Chlorobium tepidum*. TU Braunschweig.

Gavira, J. A. (2016) “Current trends in protein crystallization”, *Archives of Biochemistry and Biophysics*, 602, pp. 3–11.

Goldschmidt, L. *et al.* (2007) “Toward rational protein crystallization: A Web server for the design of crystallizable protein variants”, *Protein Science*, 16(8), pp. 1569–1576.

Gruber, N. and Galloway, J. N. (2008) “An Earth-system perspective of the global nitrogen cycle”, *Nature*, 451(7176), pp. 293–296.

Hallenbeck, P. C. (2017) *Modern Topics in the Phototrophic Prokaryotes*. Springer.

Harada, J. *et al.* (2014) “Chlorophyllide *a* oxidoreductase works as one of the divinyl reductases specifically involved in bacteriochlorophyll *a* biosynthesis”, *Journal of Biological Chemistry*, 289(18), pp. 12716–12726.

Heinemann, I. U., Jahn, M. and Jahn, D. (2008) “The biochemistry of heme biosynthesis”, *Archives of Biochemistry and Biophysics*, 474(2), pp. 238–251.

Heinnickel, M. and Golbeck, J. H. (2007) “Heliobacterial photosynthesis”, *Photosynthesis Research*, 92(1), pp. 35–53.

Heyes, D. J. *et al.* (2002) “Enzymology below 200 K: The kinetics and thermodynamics

of the photochemistry catalyzed by protochlorophyllide oxidoreductase", *Proceedings of the National Academy of Sciences*, 99(17), pp. 11145–11150.

Heyrovský, M. (1987) "The electroreduction of methyl viologen", *Journal of the Chemical Society, Chemical Communications*, 20(24), pp. 1856–1857.

Howard, J. B. and Rees, D. C. (1994) "Nitrogenase: A Nucleotide-Dependent Molecular Switch", *Annual Review of Biochemistry*, 63(1), pp. 235–264.

Howarth, R. W. (2008) "Coastal nitrogen pollution: A review of sources and trends globally and regionally", *Harmful Algae*, 8(1), pp. 14–20.

Hu, Y. *et al.* (2009) "Catalytic activities of NifEN: Implications for nitrogenase evolution and mechanism", *Proceedings of the National Academy of Sciences*, 106(40), pp. 16962–16966.

Imam, S. and Eady, R. R. (1980) "Nitrogenase of *Klebsiella pneumoniae*: Reductant-independent ATP hydrolysis and the effect of pH on the efficiency of coupling of ATP hydrolysis to substrate reduction", *FEBS Letters*, 110(1), pp. 35–38.

Ito, H. *et al.* (2008) "Identification of a novel vinyl reductase gene essential for the biosynthesis of monovinyl chlorophyll in Synechocystis sp. PCC6803", *Journal of Biological Chemistry*, 283(14), pp. 9002–9011.

Jahn, M., Jahn, D. and Warren, M. J. (2021) "Heme Synthesis Three Ways", in *Reference Module in Life Sciences*. Elsevier.

Jasniewski, A. J. *et al.* (2018) "The Fe Protein: An Unsung Hero of Nitrogenase", *Inorganics*, 6(1), p. 25.

Jasper, J. *et al.* (2020) "Chimeric Interaction of Nitrogenase-Like Reductases with the MoFe Protein of Nitrogenase", *ChemBioChem*, 21, pp. 1733 –1741.

Jerabek-Willemsen, M. *et al.* (2014) "MicroScale Thermophoresis: Interaction analysis and beyond", *Journal of Molecular Structure*, 1077, pp. 101–113.

Kiesel, S. *et al.* (2015) "Iron-sulfur cluster-dependent catalysis of chlorophyllide *a* oxidoreductase from *Roseobacter denitrificans*", *Journal of Biological Chemistry*, 290(2), pp. 1141–1154.

Kuypers, M. M. M., Marchant, H. K. and Kartal, B. (2018) "The microbial nitrogen-

cycling network", *Nature Reviews Microbiology*, 16(5), pp. 263–276.

Laemmli, U. K. (1970) "Cleavage of structural proteins during the assembly of the head of bacteriophage T4", *Nature*, 227(5259), pp. 680–685.

Larsen, C., Christensen, S. and Watt, G. D. (1995) "Reductant-independent ATP hydrolysis catalyzed by homologous nitrogenase proteins from *Azotobacter vinelandii* and heterologous crosses with *Clostridium pasteuranium*", *Archives of Biochemistry and Biophysics*, 323(2), pp. 215–222.

Liu, H. and Lee, W. (2019) "The XFEL protein crystallography: Developments and perspectives", *International Journal of Molecular Sciences*, 20(14).

Ljones, T. and Burris, R. H. (1972) "ATP hydrolysis and electron transfer in the nitrogenase reaction with different combinations of the iron protein and the molybdenum-iron protein", *Biochimica et Biophysica Acta*, 275(1), pp. 93–101.

López-Méndez, B. *et al.* (2021) "Microscale Thermophoresis and additional effects measured in NanoTemper Monolith instruments", *European Biophysics Journal*.

Lovenberg, W., Buchanan, B. B. and Rabinowitz, J. C. (1963) "Studies on the Chemical Nature of Clostridial Ferredoxin", *Journal of Biological Chemistry*, 238(12), pp. 3899–3913.

Massmig, M. *et al.* (2020) "Carnitine metabolism in the human gut: characterization of the two-component carnitine monooxygenase CntAB from *Acinetobacter baumannii*", *Journal of Biological Chemistry*, 295(37), pp. 13065–13078.

Masuda, T. (2008) "Recent overview of the Mg branch of the tetrapyrrole biosynthesis leading to chlorophylls", *Photosynthesis Research*, 96(2), pp. 121–143.

Mayhew, S. G. (1978) "The Redox Potential of Dithionite and SO_2^- from Equilibrium Reactions with Flavodoxins, Methyl Viologen and Hydrogen plus Hydrogenase", *European Journal of Biochemistry*, 85(2), pp. 535–547.

McFeeters, R. F., Chichester, C. O. and Whitaker, J. R. (1971) "Purification and Properties of Chlorophyllase from *Ailanthus altissima* (Tree-of-Heaven)", *Plant Physiology*, 47, pp. 609–618.

Moore, S. J. *et al.* (2017) "Elucidation of the biosynthesis of the methane catalyst

coenzyme F_{430}", *Nature*, 543(7643), pp. 78–82.

Moser, J. *et al.* (2013) "Structure of ADP-aluminium fluoride-stabilized protochlorophyllide oxidoreductase complex", *Proceedings of the National Academy of Sciences*, 110(6), pp. 2094–8.

Moser, J. *et al.* (2019) "Expression, Purification, and Activity Analysis of Chlorophyllide Oxidoreductase and Ni^{2+}-Sirohydrochlorin *a*,*c*-Diamide Reductase", in Hu, Y. (ed.) *Metalloproteins: Methods and Protocols*. Humana Press.

Moser, J. and Bröcker, M. J. (2011) "Methods for Nitrogenase-Like Dark Operative Protochlorophyllide Oxidoreductase", in Ribbe, M. (ed.) *Nitrogen Fixation. Methods in Molecular Biology: Methods and Protocols*. Humana Press.

Mülhardt, C. (2009) *Der Experimentator: Molekularbiologie/Genomics*. 6. Auflage. Spektrum Akademischer Verlag.

Müller, A. H. *et al.* (2011) "Methods for the preparation of chlorophyllide *a*: An intermediate of the chlorophyll biosynthetic pathway", *Analytical Biochemistry*, 419(2), pp. 271–276.

Muraki, N. *et al.* (2010) "X-ray crystal structure of the light-independent protochlorophyllide reductase", *Nature*. Nature Publishing Group, 465(7294), pp. 110–114.

Nakamura, M., Saeki, K. and Takahashi, Y. (1999) "Hyperproduction of recombinant ferredoxins in Escherichia coli by coexpression of the ORF1-ORF2-*iscS-iscU-iscA-hscB-hscA-fdx*-ORF3 gene cluster", *Journal of Biochemistry*, 126(1), pp. 10–18.

Noar, J. D. and Bruno-Bárcena, J. M. (2018) "*Azotobacter vinelandii*: The source of 100 years of discoveries and many more to come", *Microbiology*, 164(4), pp. 421–436.

Nomata, J. *et al.* (2005) "Overexpression and characterization of dark-operative protochlorophyllide reductase from *Rhodobacter capsulatus*", *Biochimica et Biophysica Acta*, 1708(2), pp. 229–237.

Nomata, J. *et al.* (2006) "A second nitrogenase-like enzyme for bacteriochlorophyll biosynthesis: Reconstitution of chlorophyllide a reductase with purified X-protein (BchX) and YZ-protein (BchY-BchZ) from *Rhodobacter capsulatus*", *Journal of Biological Chemistry*, 281(21), pp. 15021–15028.

Papenbrock, J. and Grimm, B. (2001) “Regulatory network of tetrapyrrole biosynthesis - Studies of intracellular signalling involved in metabolic and developmental control of plastids”, *Planta*, 213(5), pp. 667–681.

Pence, N. K. (2020) *Dissertation: Mechanisms of Gating Nucleotide-Driven Electron Transfer in Nitrogenase*. Montana State University.

Ribbe, M. W. (2015) “Nitrogenase and Homologs”, *Journal of Biological Inorganic Chemistry*, 20(2), pp. 435–445.

Rutledge, H. L. and Tezcan, F. A. (2020) “Electron Transfer in Nitrogenase”, *Chemical Reviews*, 120(12), pp. 5158–5193.

Ryle, M. J. and Seefeldt, L. C. (1996) “Elucidation of a MgATP signal transduction pathway in the nitrogenase iron protein: Formation of a conformation resembling the MgATP-bound state by protein engineering”, *Biochemistry*, 35(15), pp. 4766–4775.

Sabra, W. *et al.* (2000) “Effect of oxygen on formation and structure of *Azotobacter vinelandii* alginate and its role in protecting nitrogenase”, *Applied and Environmental Microbiology*, 66(9), pp. 4037–4044.

Sarma, R. *et al.* (2008) “Crystal structure of the L protein of *Rhodobacter sphaeroides* light-independent protochlorophyllide reductase with MgADP bound: A homologue of the nitrogenase Fe protein”, *Biochemistry*, 47(49), pp. 13004–13015.

Saywell, L. G. and Cunningham, B. B. (1937) “Determination of Iron: Colorimetric *o*-Phenanthroline Method”, *Industrial and Engineering Chemistry - Analytical Edition*, 9(2), pp. 67–69.

Scherings, G. *et al.* (1983) “On the formation of an oxygen-tolerant three-component nitrogenase complex from *Azotobacter vinelandii*”, *European Journal of Biochemistry*, 135(3), pp. 591–599.

Schindelin, H. *et al.* (1997) “Structure of ADP·AlF_4^--stabilized nitrogenase complex and its implications for signal transduction”, *Nature*, 387(6631), pp. 370–376.

Schrödinger LCC (2021) “The PyMOL Molecular Graphics System”

Scott, G. R. and Cheviron, Z. A. (2016) “The biosynthetic pathway of coenzyme F_{430} in methanogenic and methanotrophic archaea”, *Science*, 354(6310), pp. 339–342.

Seefeldt, L. C., Peters, J. W., *et al.* (2018) “Control of electron transfer in nitrogenase”, *Current Opinion in Chemical Biology*, 47, pp. 54–59.

Seefeldt, L. C., Hoffman, B. M., *et al.* (2018) “Energy Transduction in Nitrogenase”, *Accounts of Chemical Research*, 51(9), pp. 2179–2186.

Seefeldt, L. C. and Dean, D. R. (1997) “Role of Nucleotides in Nitrogenase Catalysis”, *Accounts of Chemical Research*, 30(6), pp. 260–266.

Seidel, S. A. I. *et al.* (2013) “Microscale thermophoresis quantifies biomolecular interactions under previously challenging conditions”, *Methods*, 59(3), pp. 301–315.

Sievers, F. *et al.* (2011) “Fast, scalable generation of high-quality protein multiple sequence alignments using Clustal Omega”, *Molecular Systems Biology*, 7(539).

Spatzal, T. *et al.* (2011) “Evidence for interstitial carbon in nitrogenase FeMo cofactor”, *Science*, 334(6058), p. 940.

Stroz, S. (2018) *Bachelorarbeit: Chlorophyllid a Oxidoreduktase aus Heliobacterium modesticaldum und Rhodopseudomonas palustris : Biochemische Untersuchungen und Kristallisationsversuche*. TU Braunschweig.

Suzuki, J. Y., Bollivar, D. W. and Bauer, C. E. (1997) “Genetic Analysis of Chlorophyll Biosynthesis”, *Annual Review of Genetics*, 31, pp. 61–89.

Terry, M. J. (2003) *Biosynthesis and Analysis of Bilins*. Humana Press.

Tezcan, F. A. *et al.* (2005) “Nitrogenase Complexes: Multiple Docking Sites for a Nucleotide Switch Protein”, *Science*, 309(5739), pp. 1377–1380.

Tsukatani, Y., Yamamoto, H., Harada, J., *et al.* (2013a) “An unexpectedly branched biosynthetic pathway for bacteriochlorophyll *b* capable of absorbing near-infrared light”, *Scientific Reports*, 3(1217), pp. 1–7.

Tsukatani, Y., Yamamoto, H., Mizoguchi, T., *et al.* (2013b) “Completion of biosynthetic pathways for bacteriochlorophyll g in *Heliobacterium modesticaldum* : The C8-ethylidene group formation”, *Biochimica et Biophysica Acta*, 1827(10), pp. 1200–1204.

Uliczka, F. (2007) *Diplomarbeit: Überproduktion und Charakterisierung der lichtunabhängigen Protochlorophyllid Oxidoreduktase aus Thermosynechococcus elongatus und Prochlorococcus marinus*. TU Braunschweig.

Vavilin, D. V. and Vermaas, W. F. J. (2002) "Regulation of the tetrapyrrole biosynthetic pathway leading to heme and chlorophyll in plants and cyanobacteria", *Physiologia Plantarum*, 115(1), pp. 9–24.

Walls, D. and Loughran, S. T. (2017) *Protein Chromatography: Methods and Protocols*. Humana Press.

Waterhouse, A. M. *et al.* (2009) "Jalview Version 2-A multiple sequence alignment editor and analysis workbench", *Bioinformatics*, 25(9), pp. 1189–1191.

Wätzlich, D. *et al.* (2009) "Chimeric Nitrogenase-like enzymes of (bacterio)chlorophyll biosynthesis", *Journal of Biological Chemistry*, 284(23), pp. 15530–15540.

Weaver, P. F., Wall, J. D. and Gest, H. (1975) "Characterization of *Rhodopseudomonas capsulata*", *Archives of Microbiology*, 105, pp. 207–216.

Webert, H. *et al.* (2014) "Functional reconstitution of mitochondrial Fe/S cluster synthesis on Isu1 reveals the involvement of ferredoxin", *Nature Communications*, 5(5013).

Wienken, C. J. *et al.* (2010) "Protein-binding assays in biological liquids using microscale thermophoresis", *Nature Communications*, 1(7).

Willows, R. D. (2003) "Biosynthesis of chlorophylls from protoporphyrin IX", *Natural Product Reports*, 20(3), pp. 327–341.

Wongnate, T. and Ragsdale, S. W. (2015) "The reaction mechanism of methyl-coenzyme M reductase", *Journal of Biological Chemistry*, 290(15), pp. 9322–9334.

Yamamoto, H. *et al.* (2020) "Chlorophyllide *a* oxidoreductase Preferentially Catalyzes 8-Vinyl Reduction over B-Ring Reduction of 8-Vinyl Chlorophyllide *a* in the Late Steps of Bacteriochlorophyll Biosynthesis", *ChemBioChem*, 21(12), pp. 1760–1766.

Yang, Z. M. and Bauer, C. E. (1990) "*Rhodobacter capsulatus* genes involved in early steps of the bacteriochlorophyll biosynthetic pathway", *Journal of Bacteriology*, 172(9), pp. 5001–10.

Yin, L. and Bauer, C. E. (2013) "Controlling the delicate balance of tetrapyrrole biosynthesis", *Philosophical Transactions of the Royal Society B: Biological Sciences*, 368(1627)

Yip, K. M. *et al.* (2020) "Atomic-resolution protein structure determination by cryo-EM", *Nature*, 587(7832), pp. 157–161.

Young, D. A. *et al.* (1989) "Genetic evidence for superoperonal organization of genes for photosynthetic pigments and pigment-binding proteins in *Rhodobacter capsulatus*", *Molecular Genetics and Genomics*, 218, pp. 1–12.

Yu, L. and Wolin, M. J. (1969) "Hydrogenase measurement with photochemically reduced methyl viologen", *Journal of Bacteriology*, 98(1), pp. 51–55.

Zhu, B. *et al.* (2007) "Short Technical Reports In-Fusion TM assembly: seamless engineering of multidomain fusion proteins, modular vectors, and mutations", *BioTechniques*, 43(3), pp. 354–359.

7. Appendix

7.1 Synthetic genes

Table 20 summarizes the synthetic genes used to produce the chimeric $(ChlL)_2$ proteins CLmax and CLmin and the COR enzymes from *H. modesticaldum* and *R. palustris*.

Table 20: Synthetic genes used in this work.
The In-Fusion cloning 15 base overlap is highlighted in bold font. Restriction sites are underlined. Blue marked nucleotides were added to preserve the restriction site. Inserted stop codons are highlighted red and inserted ribosome binding sites are highlighted green. Hm: *H. modesticaldum*, Rp: *R. palustris*, *cLmax/cLmin*: chimeric *chlL*.

Gene	Sequence 5´-3´
bchX Hm	**GGGATCCCCGGAATTC**ATGAGCGAGAAAAACTTCTATGCCGTGTATGGTAAAGGTGGTAGCGGTAAAAGCTTTGT GATTAGCAATCTGAGCAATGCAACCGCACGTCTGGGTAAACGTGTTCTGCAGATTGGTTGTGATCCGAAACATGA TAGCACCGTGATTCTGTTTAATGGTGTTAATCCGCCTACACTGCTGGAATATTGGGCAGAACTGAATGAACATAG TGATGAAGTTGAACCGACACCGCGTGTTGAAGATATTATCTTTAAAGGCAAAGGTGTGTACGCCCTGGAAATTGG TGGTCCGGAAGTTGCAATTGGTTGCGGTGGTCGTGGTATTAGCCTGGGTTTTGAAGTTCTGGAAAAAATGGGTCT GTACAAATGGGATTTCGATTATGTGTTTCTGGATTTCCTGGGTGATGTTGTTTGTGGTGGTTTTGGTGTTCCGAT TAGCAAAAGCATTGCCAAAAGTATTATTCTGGTGGCAGGTAATGATCACCAGAGCCTGTATGTTGCAAATAACAT TTGTAGCGCAGTTGCAAGCTTTGCACGTTTAGGTGGTAAAAGCCGTATTCTGGGTATGATCATCAATAAAGATGA TGGTAGTGGTTATGCCGAACAGTTTTGTGATACCGTTGGTATTAAAGTGCTGGCCAAAATTCCGAATAATCCGGA AGTGGCCAAACTGAATGCACTGTTTCAGCTGGTTAGCGATATTCCGCCTTATGATAAACTGTTCCAGGATCTGGT TCAGCGTCTGCCGGAAGAAACCGGTGTTCTGCCGAAACCGATGGATTTTGAAGCATTCAGCAAAATCTATCGTGA TATCCCGCAGGTTCATCTGGAACGTGTTACCGCAGAAGAAATGTTTCAGCGTTAACTCGAGCGGCCGCATC
bchX *Rp*	**GGGATCCCCGGAATTC**ATGAATGTTGTTCCGCAGATTAGCCTGCAGGATGCACAGCTGCGTGCAGAAGCAAGCGT TGAACCGGATGCACCGGTGACCACACCGGTTACCAAAGAAACCCAGATTATTGCCATTTATGGCAAAGGTGGTAT CGGCAAAAGCTTTACCCTGGCAAATCTGAGCTACATGATGGCACAGCAGGGTAAAAAAGTTCTGCTGATTGGTTG TGATCCGAAAAGCGATACCACAAGCCTGCTGTTTGGTGGTAAAGCAACCCCGACCATTATTGAAACCAGCAGCAA AAAAAAGCTGGCAGGCGAAGAGGTTACCATTAGTGATGTTTGTTTTAAACGTGATGGCGTGTTTGCCATGGAATT AGGTGGTCCGGAAGTTGGTCGTGGTTGTGGTGGTCGCGGTATTATTCATGGTTTTGAAACCCTGGAAAAACTGGG CTTTCATGAATGGGGTTTTGATTATGTTCTGCTGGATTTTCTGGGTGATGTTGTTTGCGGTGGTTTTGGTCTGCC GATTGCACGTGATATGTGTCAGAAAGTTATTATTGTGGGCAGCAATGATCTGCAGAGCCTGTATGTTGCAAATAA TGTTTGTAGCGCAGTGGAATACTTTCGCAAATTAGGCGGTAATGTTGGTGTTGCAGGTATGGTGATTAACAAAGA TGATGGTACAGGTGAAGCACAGGCATTTGCAAAAGCAGCAGGTATTCCGGTTCTGAGCGCAATTCCGGCAGATGA AGGTATTCGTCGTAAAAGCGCAAACTATGAAATTGTGGGTCTGCCGGATGGTCAGTGGGGTCCGCTGTTTGCAAC CCTGGCAGAAAATGTTGCAACCGCACCGCCTGTTCGTCCGAAACCGCTGACACAGGATGGTCTGCTGGGTCTGTT TAGCAGTGATGTTACCGGTCGTGATGTGGTTCTGGAACCGGCAACCATGGCCGATATGTGTGGTGCAGCAGTTCT GAATAAACCGAGCCTGGAAGTTATTTATGATGAAGTGTAACTCGAGCGGCCGCATC
bchY Hm	**GGGATCCCCGGAATTC**ATGGAACCGATCAAAAGCATTAAACTGGCAACCCAGAGTCCGTGTCCGGCATTTGGTGC ACTGCGTATTCTGACCCGTCTGGAAGGTTTTCTGCCGATTCTGCTGGGTAATCATGGTTGTTATTATGGCCTGAA TTTTCTGGCCCATTTTTATGCAGCACGCAAAAGTATTTATGCACCGCTGCTGTATAGCATCGATTTCACCGATAA AAACCTGCATCATAAACTGCTGGATGCCATCAAAGAAATCATCAAAGAGGAAAAGCCGGAATTTGTTCCGGTTAT TAATCTGTGTGTTGCAACCACCGTTGGCATTGATATTGATGAAATGGCACGTGAACTGCCGGAAATTATTCCGCT GCGTGTTACCGGTTTTGGCACCCGTAGCCATGCCGAAGCAAAAGATGTTGCAATGGAAGGCATTTTCAAAAAACT GCGTCAGTTTGGTGATCATAAGCTGCGTGAACCGAAAGCAGTTGCAAGCATTGGTGAAGTTTTTCCAGCAGATAC CATTGCACTGGAAAACCTGTTAGAAAAAATGGGTCTGAAACTGCGTGCACATGTTCCGAGCAAAGATATTAATGA TTTTCGCAAAGCCCTGAACGTTAGCACCATGGCATGTCTGCATCCGTTTTATACCCGCACCATGCGCCAGTTTGG CGAACTGGGTATTCCGCATATTACCGGTGGTCCGGCAGGCGCAGAAATGACCTATGCATGGATTAAAGCAATTGC AGAAAGTACCGGTGCAGATATGGGTTTAGCAGAGCAGATTGCACAAGAGGAACGTGATGCAGTTCAGAAAGTTCT GGATGGTCCGCTGAATCTGCGTGGTGTTCGTATTGCAGTTGCAGGTTATGAAGGTATTGAATTTCTGGTTGGTCG TATTCTGGTTGAAGCGGGTGCCGATGTTCCGTATCTGAGCACCAGCATTGGTAAAAGTCCGCTGTGTGAAGCAGA TGTTGCCTGGTTTCAGGCACGTGGCACCGAAGTTAAATTTCGTAAAAGCGCAGCAGATGATCTGGTTGCAGTGAA AAAATACAAACCGGATATTGCCCTGGCAGCAACCGATGTTGCAGGTATGGGTAAAGAACTGGGTTCAGCAAGCGT GTATTTTACAAATCTGATTGCAGCACGTCCGCTGTTTCTGGCACACGGTGCAGAAAATATTCTGAGCCTGATGCA CCATCTGCTGAAAGCCCGTCCGAGCATTAATCGTGTTCGTAGCTTTTTTCAGGACGTTGAAATGGAACGTAGCAT TGCAATTAGCGAAGTGAAAGCACATCTGGGTGATGCATTTGCATGTGGTTGGGGTGCACCGGTTTGGGGTGGTTG TAGCGCAGAAGAAGCAGCAGCCGCAAGCGATTGTGGTTGTGGTGATGCAATGGATGGTGCAGCATGTTTTGGTGG TGATACCGGTGCCGGTGCAAGCGCAATGAATTGTGCACCGGGTTGTGCAATTGCGGGTTGTCCGGCAGCCGGTGG CCAGAATAGCCGTGAAGCAAAATAACTCGACTCGAGCGGCC

bchZ Hm

AGCAAAATAAGTCGACTCAATTTCACACAGGAAACAGTATTCATGCAGATGATGCGTGATGTTGATCTGACCAAT
GGTTATTGGGGTGCACTGTATGTTCTGGCACCGATGCGTGGTAATTTTTGCGTTATTGTTGATGGTCCGATTGGC
TGTCATTATGTTCCGATTGATAGCGCACTGAATTATACCGATGCAATTCCGTATCTGCAGAATGTTTATGCAACC
CATATTCTGGAAGGTGATGTTGCACTGGATGGCACCCTGCATAAACTGCGTAAACTGTGTGGTGAACTGATTGAT
CGCTATGAGAACATTTTTATCCTGAGCTGTGCAGAAAGCGAAATTATCAGCAGCGAAGGTGCAATGCTGGAAGCA
GAAATTGATGGTCGTCGTATCTGGTATATTCATACCCGTAGCCTGGATGTTGATGATCTGACAGCACGTGATGAT
ATTATGCTGTATCTGTATGAACATGTGGTGCCGAAAATGCCTCGTCTGCCGAAAAAAGCAAGCGCAAAACCGCTG
GTTAATATTCTGGGTCCGACCTATGGTAACTTTAACCATTATGCAGATTTCGCCGAAATTAAGCGTCTGATTGAA
GGTATTGGTGCGGAAGTTAATGTTGCCTTTCCGTTTGATTGTGAACTGGGTGATATTACCCGTCTGGATGATGCA
GATGCAAATGTTCTGCTGTATCAAGAATATGGTCAGAAACTGGGTAAAGCCCTGGGTAAACCGCTGTTTTTTGGT
CCGATCGGTCTGCAGGCAACCACCGCATTTCTGTTAGGTCTGGGTGATGCGCTGGGTCTGCGTGCAGAAGCAGAA
GCATTTATTGCAAAAGAAAAACGTACCACGCTGCAAGGTTTTTGGGATGTTTGGCGTAGTCCGCATCAGGATATT
TTTCGTACCAATAGCTTTGGTGTGTATGCCCATAAAACCTATGCCGAAGGTCTGGTGAATTTTCTGCGTGATGAA
CTGGGCTTTGAAGCATATGCATGTGGTGTTAAAACCGATCGTTGGCGTAGCAAAAAAGCCATGGATATTGAAGCA
GCACTGCTGGAAAATCCGCCTACACTGTTTTTCGGTAGCATCAACGAAAAAATCTATATCACCGAACATATTCTG
CCGACGCGTTTTATTGCAGCAGCAACCCCGATGCCGATTGTTTGTCGTAGCACCGGTACACCGTTTATGGGTTAT
AATGGTGTTGTTTATCTGACCCAGCTGGTTAGCAATGAACTGTTTGATATTCTGTATAGCCACATCCACATTGAG
TATGCACCGGAAAAAGATAAACGTCGTCGTGAACGTGATGCAGCACGTAAAGAATGGGAAGCACAGCTGAAAGGT
AGCATTGTTATTCGTGAAGTTCGTTGGCCTGAAGAAACCGTTGCACATATGGAAAAAGTGCTGAAAAAAGTGCCG
TTTTTTGTTCGTGTTAGCGCAAGCAAAATGCTGCGTGTTGAAAGTGAAAAACTGGCAAAAGAACAGCTGCGTGAT
TATGTTACCACCGATGATGTGGATCAGGTGTATAATCGTTTTAAGCGC**TAAGCGGCCGCATCGTGACT**

bchY Rp

GGGATCCCCGGAATTCATGAGCGTTATGAGCCGTTATAGCGGTCCGGTTGCAGGTAGCATTGTTGATGATGCAGC
AGAATTTAGTGATGTGGATACCACCAGTATTAATCAGGCAGCAACCAAAAATGATGGTCTGGGTTGTCATGCCGG
TGCAGCACAGATGAAAGCAGCAGCAGAAGCAGCAGGTAAATCAGATGTTCTGGAACGTTATGCCGCAGATTATCC
GAAAGGTCCGCATGATCAGCCGCAGAGCATGTGTCCGGCATTTGGTAGCCTGCGTGTTGGTCTGCGTATGCGTCG
TACCGCAACCGTTCTGAGCGGTAGCGCATGTTGTGTTTATGGTCTGACCTTTGTGAGCCATTTTTATGGTGCACG
TCGCACCGTTGGTTATGTTCCGTTTAGCAGCGAAACCCTGGTGACCGGTAAACTGTTTGAAGATATTCGTGAAGC
CGTGTATAAACTGGCAGATCCGAGCCAGTATGATACCATTATTATCACCAATCTGTGTGTTCCGACCGCAAGCGG
TGTTCCGCTGGATCTGCTGCCGAAAGAAATTAATGGTGTTCGCATTATTGGCATTGATGTGCCTGGTTTTGGTGT
GCCGACGCATGCCGAAGCAAAAGATGTGCTGGCAGGCGCAATGCTGGAATATGCACGTAAAGAAGCAGAACAGGG
TCCTGTTCAGGCACCGCGTGGTGGTCGTAGCGAACGTCCGACCGTTACACTGCTGGGTGAAATGTTTCCGGCTGA
TCCGGTTGGTATTAATCTGATGCTGGACCCGCTGGGTTTAGCAGTTGGTCCGGTGGTTCCGACACGTGAATGGCG
TGAACTGTATGCAGCACTGGATTGTCAGGTTGTTGCAGCAATTCATCCGTTCTATAAAAGCTGCATTCGTCAGTT
TGATCTGGCAGGTCGTAAAGTTGTTGGTAGCGCACCGGTTGGTCATGATGGCACCGAAGCATGGCTGGAAGCAAT
TGGCACCGCATGTAATGTTGAACGTAGCAAAATTGATGCAGCCAAAAATCGTTTTCTGCCTGCAATTAAAGCAGC
CCTGGCAGCAAAACCGATTAATGCACGTATTACCGTTAGCGGTTATGAAGGTAGCGAACTGCTGGTTGCACGTCT
GCTGATTGAAAGCGGTGCAAATGTTCCGTATGTTGGTACAGCAGTTCCGCGTACACAGTGGTCAGATCCTGATCG
TGAATGGTTAGAAGCCAAAGGTGTTCGTGTTCAGTATCGTGCAAGCCTGGAACAGGATTTTGCAGCAGTTGATGA
ATTTATGCCGGATCTGGCCATTGGCACCACACCGGTTGTTCAGAAAGCAAAAACCATGAGCATTCCGGCACTGTA
TTTTACCAATCTGATTAGCGCACGTCCGCTGTTTGGTCCTGCCGGTGCCGGTAGCCTGGCACAGGTTATTAATGC
CGCACTGGGTAATAAAGCACGCTTTGATGAAATGAAAGAGTTCTTTGGCGACGTTGGTCAGGGTTATGCAGCCGG
TGTTTGGGAAGATACCCCGAAAGATGTTCCGGCATATCGTGAAAAATACAAAAAGCAGATTGAAGCCGCAGCCAA
GAAACGTAAAGCAGAAGAAATGATC**TAAGTCGACTCGAGCGGCC**

bchZ *Rp*

AATGATCTAAGTCGACTCAATTTCACACAGGAAACAGTATTC**A**TGCTGGTTCTGGATCATGACCGTGCCGGTGGT
TATTGGGGTGCAGTTTATGCATTTACCGCAGTTAAAGGTCTGCAGGTTATTATTGATGGTCCGGTTGGTTGTGAA
AATCTGCCGGTTACCAGCGTTCTGCATTATACCGATGCACTGCCTCCGCATGAACTGCCGATTGTTGTTACCGGT
CTGGGTGAAGAAGAACTGGGTAAACTGGGCACCGAAGGTGCAATGCATCGTGCACATAAAGCACTGGACCCGTAT
CTGCCTGCAGTTGTGGTGACCGGTAGCATTGCAGAAATGATTGGTGGTGGTGTTACACCGGAAGGCACCGGTATT
AAACGTTTTCTGCCTCGTACCATTGATGAAGATCAGTGGCAGAGCGCAGATCGTGCAATTAGCTGGCTGTGGAAA
GAATATGGTCCGAAAAAAATCCCGGAACGCAAACGTAAAGATGGTGAAAAACCGCGTGTTAACATTATCGGTCCG
ATTTATGGCACCTTTAATATGCCGAGCGATCTGGCAGAAATTCGTCGTCTGATTGAAGGTATTGGTGCCGAAGTT
AATATGGTTTTTCCGCTGGGCACCCATCTGGCCGATATTCCGAAACTGGTTAATGCAGATGTTAACGTGTGTATG
TATCGTGAATTTGGTCGTCTGCTGTGTGAAAGCCTGGAACGTCCTTATCTGCAGGCACCGATTGGTCTGCATAGC
ACAACCCGCTTTCTGCGCAAACTGGGCGAACTGACCGGTTTAGATCCGGAACCGTTTATTGAACGTGAAAAAAAC
ACCACGATTAAACCGCTGTGGGATCTGTGGCGTAGCGTTACCCAGGATTTTTTCGGCACCGCAAGCTTTGCAGTT
GTTGCAACCGATACCTATGCACGTGGTGTTCGTCATTTTCTGGAAGATGAAATGGGTCTGCCGTGTACCTTTGCC
GTTAGCCGTTGTGTTGGTAAAAAAACGGATAATGAAGCAGTTCGTGCAGCAATTCGTCAGACCCCTCCGCTGATT
ATGTTTGGTAGCTATAATGAACGTATGTACCTGGCCGAAACCGGTGGTCGTGCCGTTTATATTCCGGCAAGCTTT
CCGGGTGCCGTTATTCGTCGCCATACCGGTACACCGTTTATGGGTTATAGCGGTGCAACCTATCTGGTTCAAGAA
GTTTGTAACGCACTGTTTGATGCCCTGTTTAACATTCTGCCGCTGGGTAGTGATCTGGATCGTGTTGATCCGACT
CCGGCACGTCGTCATGAAGAACTGCTGTGGTCAGATGAAGCAAAAGCACTGCTGGATGAAGTTCTGGAACAGCAT
CCGGTTCTGGTTCGTATTAGCGCAGCAAAACGTCTGCGTGATGCAGCAGAAAATTCAGCACGTCGTGCAGGTCAA
GAAAAAGTTACCACCGAATTTGTTAGCAAAGCACGTGCAGCCCTGCTGGACGGTCAGAGCGTT**TAAGCGGCCGCA**
TCGTGACT

cLmax

GGGATCCCCGGAATTCATGACCACCACACTGGCAAATCGTCCGGATGGTGAAGGTAGCGTTCAGGTTAAACTGGA
CCCGAAAGTTAATATTGAAGAAGGTGCACTGGTTATTGCCGTGTATGGTAAAGGTGGTATTGGTAAAAGCACCAC
CAGTAGCAATCTGAGCGCAGCATTTAGCAAACTGGGTAAAAAAGTTCTGCAGATTGGTTGCGATCCGAAACATGA
TAGCACCTTTACACTGACCCATAAAATGGTTCCGACCGTTATGGAAATTGCAGCAGAAGCAGGCACCGTTGAAGA
TCTGCGTCCGCAGGATTTTATGTTTGAAGGTTTTAATGGTGTGCAGTGCGTTGAAAGCGGTGGTCCGGAACCTGG
TGTTGGTTGCGGTGGTCGTGGCACCATTACCACCGTTAATCTGCTGAAAGAACATCATCTGCTGGAAGATACCGA
TGTGGTTATTTTTGATGTTCTGGGTGATGTTGTTTGTGGTGGTTTTGCAGCACCGCTGCGTGAAAATCATGCAAA
TTATTGTCTGATTGTGACCGCCAACGATTTCGATAGCATTTTTGCAATGAATCGTATTGTGGCAGCCATCAACAA
ATATGCCAATAGCGGTAAAGTTCGTTTAGGTGGTGTTATTGCAAATCGTAGCGCAGAACTGGATCAGATCGAAAA
ATTCAATGAAAAAACCGGTCTGAAAACCATGGCGCATTTTCGTAATGTTGATGCAATTCGTCGTAGCCGTCTGAA
AAAATGCACCATTTTTGAAATGGACCCGGAAGAAGAAGGCGTTCTGGAAGTTCAGAATGAATATCTGAGCCTGGC
CAAAAAAATGATCGATAATGTTGAACCGCTGGAAGCAGAACCGCTGAAAGATCGTGAAATCTTTGATCTGCTGGG
CTTCGATTAACTCGAGCGGCCGCATC

cLmin

GGGATCCCCGGAATTCATGACCACCACACTGGCAAATCGTCCGGATGGTGAAGGTAGCGTTCAGGTTAAACTGGA
CCCGAAAGTTAATATTGAAGAAGGTGCACTGGTTATTGCCGTGTATGGTAAAGGTGGTATTGGTAAAAGCACCAC
CAGTAGCAATCTGAGCGCAGCATTTAGCAAACTGGGTAAAAAAGTTCTGCAGATTGGTTGCGATCCGAAACATGA
TAGCACCTTTACACTGACCCATAAAATGGTTCCGACCGTGATTGATATTCTGGAAGAAGTTGATTTTCACAGCGA
AGAACTGCGTCCGCAGGATTTTATGTTTGAAGGTTTTAATGGTGTGCAGTGCGTTGAAAGCGGTGGTCCGGAACC
TGGTGTTGGTTGCGGTGGTCGTGGCACCATTACCACCGTTAATCTGCTGAAAGAACATCATCTGCTGGAAGATAC
CGATGTGGTTATTTTTGATGTTCTGGGTGATGTTGTTTGTGGTGGTTTTGCAGCACCGCTGCAGCATGCAAATTA
TTGTCTGATTGTTACCGCCAACGATTTCGATAGCATTTTTGCCATGAATCGTATTGTGGCAGCCATTAATGCAAA
AGCCAAAAACTATAAAGTGCGCTTAGGTGGTGTTATTGCAAATCGTAGCGCAGAACTGGATCAGATCGAAAAATT
CAATGAAAAAACCGGTCTGAAAACCATGGCGCATTTTCGTAATGTTGATGCAATTCGTCGTAGCCGTCTGAAAAA
ATGCACCATTTTTGAAATGGACCCGGAAGAAGAAGGCGTTCTGGAAGTTCAGAATGAATATCTGAGCCTGGCCAA
AAAAATGATCGATAATGTTGAACCGCTGGAAGCAGAACCGCTGAAAGATCGTGAAATCTTTGATCTGCTGGGCTT
CGATTAACTCGAGCGGCCGCATC

7.2 $(CfbD)_2$ interaction-assays

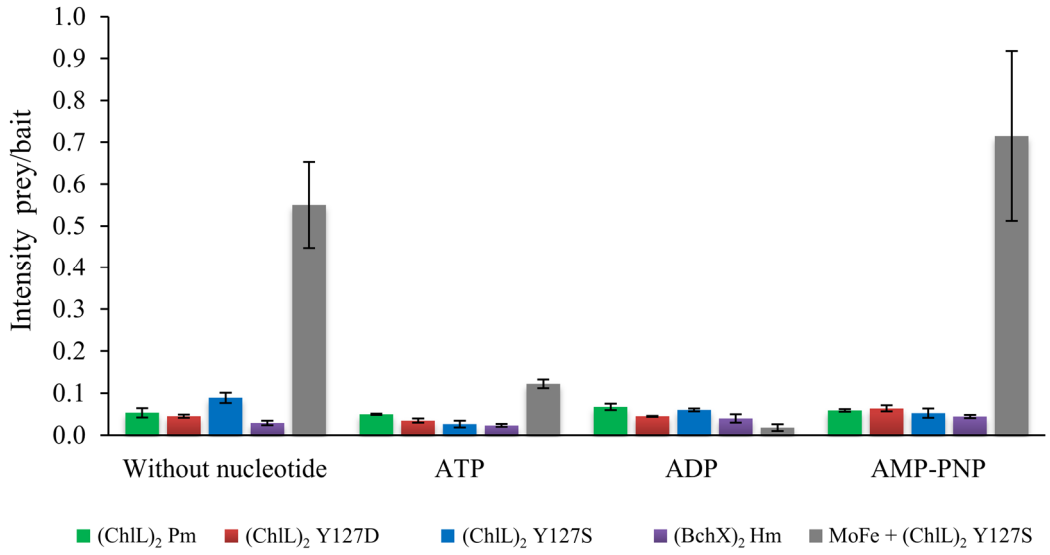

Figure 28: Interaction of $(CfbD)_2$ with nitrogenase-like reductases compared to the interaction of MoFe with $(ChlL)_2$ variant $(ChlL)_2$ Y127S.
The interaction-assays with $(CfbD)_2$ as prey protein and nitrogenase-like reductases as bait proteins were performed in the presence of different nucleotides as described in the materials and methods section (compare section 2.10). Band intensities after SDS-PAGE were analyzed using GelQuant.NET software to calculate the prey/bait intensity ratios. Binding experiments of $(CfbD)_2$ with $(ChlL)_2$ (green), $(ChlL)_2$ Y127D (red), $(ChlL)_2$ Y127S (blue) and $(BchX)_2$ Hm (purple) are compared against the binding experiment MoFe (prey) + $(ChlL)_2$ Y127S (bait) shown in grey (Jasper *et al.*, 2020). Hm: *H. modesticaldum*, Pm: *P. marinus*.

7.3 UV-Vis spectra of reduced and oxidized methyl viologen

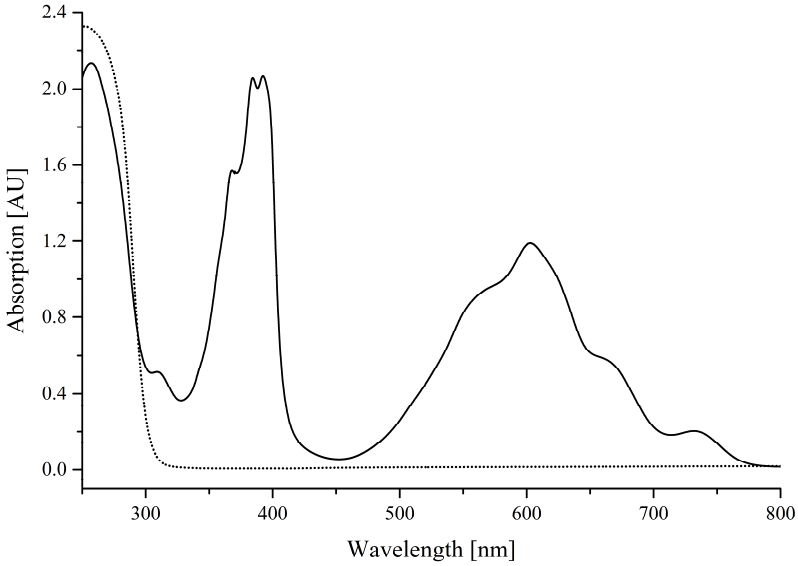

Figure 29: UV-Vis spectra of reduced and oxidized methyl viologen (MV).
MV was reduced in 1 mL anoxic 0.1 M Na_2CO_3 supplemented with 10 mg glucose and 5 mg MV-dichloride. After incubation for 1 h at 50 °C under anoxic conditions, the colorless MV-dichloride turned violet-blue, indicating the presence of the MV cation radical ($MV^{+\cdot}$). 1.56 µL of the sample was added to a total volume of 250 µL (100 mM HEPES pH 7.5, 150 mM NaCl, 10 mM $MgCl_2$) for UV-Vis analysis in a rubber-sealed cuvette (black line). Subsequently, the sample was exposed to air and mixed by pipetting (20 s). A rapid loss of color was observed, indicating the oxidation of $MV^{+\cdot}$ (black dotted line).

7.4 Interaction between *P. marinus* DPOR subcomplexes $(ChlNB)_2$ and $(ChlL)_2$ or $(ChlL)_2$ variants Y127D and Y127S

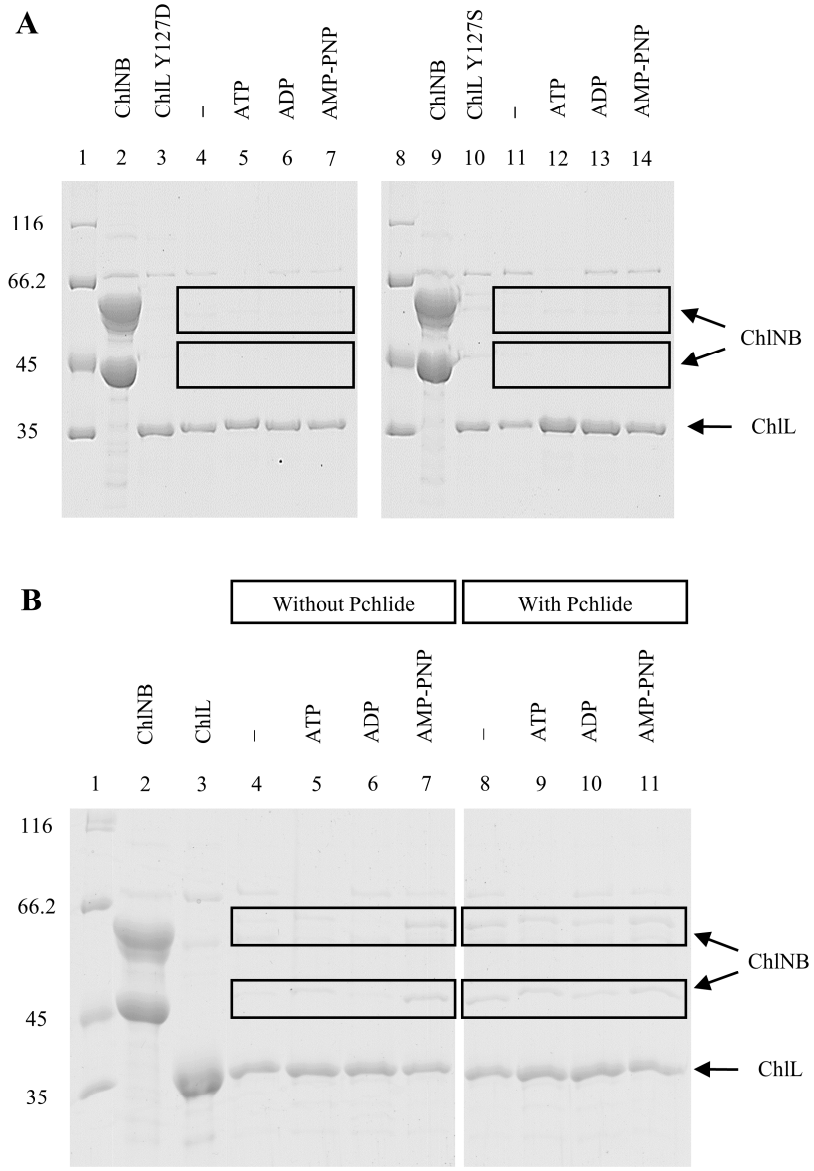

Figure 30: SDS-PAGE analysis of elution fractions from the interaction-assay between *P. marinus* DPOR subcomplexes $(ChlNB)_2$ and $(ChlL)_2$ or $(ChlL)_2$ variants Y127D and Y127S.
The interaction-assays with subcomplex $(ChlNB)_2$ as prey protein and $(ChlL)_2$ or $(ChlL)_2$ variants Y127D and Y127S as bait proteins were performed in the absence and presence of different nucleotides as described in the materials and methods section (compare section 2.10). **A**: SDS-PAGE analysis of interaction-assay samples indicating no complex formation between subcomplexes $(ChlNB)_2$ and $(ChlL)_2$ Y127D or $(ChlL)_2$ Y127S. *Lanes 1 and 8*: Molecular mass marker, relative molecular masses (x 1'000) are indicated. *Lanes 2 and 9*: Purified $(ChlNB)_2$. *Lane 3*: Purified $(ChlL)_2$ Y127D. *Lanes 4-7*: Interaction of $(ChlL)_2$ Y127D with $(ChlNB)_2$ in the absence and presence of ATP, ADP or AMP-PNP, respectively. *Lane 10*: Purified $(ChlL)_2$ Y127S. *Lanes 11-14*: Interaction of $(ChlL)_2$ Y127S with $(ChlNB)_2$ in the absence and presence of ATP, ADP or AMP-PNP, respectively. Co-elution of $(ChlNB)_2$ (black boxes) was not observed. **B**: SDS-PAGE analysis of interaction-assay samples indicating a weak interaction between subcomplexes $(ChlNB)_2$ and $(ChlL)_2$. Experiments were performed in the absence and presence of Pchlide. *Lane 1*: Molecular mass marker, relative molecular masses (x 1'000) are indicated. *Lane 2*: Purified $(ChlNB)_2$. *Lane 3*: Purified $(ChlL)_2$. *Lanes 4-7*: Interaction of $(ChlL)_2$ with $(ChlNB)_2$ in the absence and presence of ATP, ADP or AMP-PNP, respectively. *Lanes 8-11*: $(ChlNB)_2$ was incubated with Pchlide prior to the interaction assay. The presence of Pchlide increases the affinity between $(ChlL)_2$ and $(ChlNB)_2$ (black boxes).

Danksagung

Abschließend möchte ich mich bei den vielen Personen bedanken, die in den letzten Jahren alle auf unterschiedlicher Art und Weise zum Gelingen dieser Arbeit beigetragen und mich unterstützt haben.

Ich möchte mich besonders beim Mentor Prof. Dr. Dieter Jahn und meinem Arbeitsgruppenleiter Dr. Jürgen Moser für die Möglichkeit bedanken, am Institut für Mikrobiologie nach meiner Masterarbeit auch die Promotion durchführen zu können. Das Projekt *Nitrogenase-like Biosynthesis of (Bacterio)chlorophylls* und die Einbindung in das *Iron - Sulfur for Life* Programm eröffneten mir einen guten Weg, mich sowohl fachlich als auch persönlich weiterzuentwickeln. Ich bedanke mich für die gute Betreuung, Motivation, hilfreichen Diskussionen und Johnnys unerschütterliche, ruhige und freundliche Art im Umgang mit seinen Leuten. Vielen Dank für die Unterstützung bei den Höhen und Tiefen des gesamten Projekts.

Weiterhin danke ich Prof. Dr. Gunhild Layer als zweite Referentin der Arbeit und apl. Prof. Dr. Simone Bergmann für die Übernahme des Prüfungsvorsitzes. Vielen Dank für das Interesse an meiner Arbeit.

Mein Dank für die zahlreichen kleinen Dinge im Laboralltag gilt den derzeitigen und auch den vielen ehemaligen Mitgliedern der AG Moser. Simone, Steffi, Marco, Milan und die vielen Studenten und Gäste der Arbeitsgruppe - vielen Dank für die angenehme Atmosphäre, die Gespräche, eure Hilfsbereitschaft und unsere gemeinsamen Aktivitäten. Mein besonderer Dank gilt auch allen Studenten, die in meinem Projekt mitgewirkt haben: Maika, Sylvia, Dorina, Lena, Stephanie, Marc, Kevin, Carolin K. und Carolin M. – vielen Dank für euren Beitrag zu dieser Arbeit.

Ich möchte mich an dieser Stelle auch allgemein bei allen Mitarbeitern der Mibi für den netten Umgang und die Hilfsbereitschaft über die letzten Jahre bedanken. Stefan, Lisa, Martina, Elli, Anja, AG Steinert, Christina, Gunhild, Daniela, Dagmar und Barbara – vielen Dank für eure Unterstützung.

Hier möchte ich auch unbedingt die internationalen Mitglieder und Gäste des Instituts erwähnen. Danke an Dunya, José, Hao, Dave und Dong – dank euch ist mein Englisch sicher nicht schlechter geworden.

Ich möchte der AG Layer und AG Einsle aus Freiburg, besonders José Vazquez Ramos und Christian Trncik, für die Kooperation und Hilfe bei der Erstellung unseres Papers danken.

Dr. Edward Reijerse und Marco danke ich außerdem für ihre Unterstützung bei den EPR Experimenten.

Bei Dr. Peer Lukat und Dr. Jörn Krausze möchte ich mich für die Hilfe bei der Proteinkristallisation bedanken. Leider wurden wir nicht mit Erfolg belohnt. Dr. Peer Lukat danke ich außerdem für die Einführung in die MST Methodik. Beate Jaschok-Kentner möchte ich für die Hilfe bei der N-terminalen Sequenzierung danken.

Prof. Kylie Vincent, Dr. Patricia Rodríguez Macía und Yu Sun danke ich für ihr Interesse an meiner Arbeit und für die ersten interessanten Einblicke aus ihren elektrochemischen Experimenten.

Am Schluss möchte ich mich für die positive Energie bedanken, die ich von meiner Familie erhalten habe. Danke, dass ihr immer an mich geglaubt und mich unterstützt habt. Ohne diese Unterstützung wäre diese Arbeit nicht möglich gewesen.